Multiphoton Ionization and Recombination Dynamics in Liquid-to-Supercritical Ammonia

Dissertation
zur
Erlangung des Doktorgrades (Dr. rer. nat.)
der
Mathematisch-Naturwissenschaftlichen Fakultät
der
Rheinischen Friedrich-Wilhelms-Universität Bonn

vorgelegt von
Janus Urbanek
aus Nikolai

Bonn Januar, 2014

Angefertigt mit Genehmigung der Mathematisch-Naturwissenschaftlichen
Fakultät der Rheinischen Friedrich-Wilhelms-Universität Bonn

1. Gutachter: Prof. Dr. Peter Vöhringer
2. Gutachter: Priv. Doz. Dr. Andreas-Neil Unterreiner

Tag der Promotion: 07.04.2014
Erscheinungsjahr: 2014

ABSTRACT

This thesis reports on the first-ever femtosecond transient absorption study of solvated electrons that were produced by multiphoton excitation of neat fluid ammonia. To obtain insight into the ionization mechanism below and above the optical valence-to-conduction band gap of the solvent, the initial ultrafast ionization was carried out with a 400 nm, respectively a 266 nm laser pulse, both of which were found to require two photons corresponding to a total excitation energy of 6.2 eV, respectively 9.3 eV. Subsequently, the solvated electron was monitored with femtosecond probe pulses that was resonant with its characteristic near-infrared absorption band around 1700 nm.

A primary goal of the experiments was to explore the role of structural and electronic properties of the solvent network in the photoionization pathways below and above the band-gap. For this purpose, the ammoniated electron's geminate recombination dynamics was systematically studied over wide ranges of temperature (227 K $\leq T \leq$ 489 K) and density (0.17 g cm^{-3} $\leq \rho \leq$ 0.71 g cm^{-3}), thereby covering the dense liquid and the dilute supercritical phase of the solvent. A kinetic analysis of the electron's survival probability was carried out to determine the temperature and density-dependent average thermalization distance of the solvated electron from its primary ionization site, $\langle r_0 \rangle$, which offers insight into the nature of the electronic state of the liquid from which the electron is initially injected.

i) At 9.3 eV total excitation energy, vertical ionization was found to initially produce highly mobile electrons in the conduction band of the liquid which only subsequently become localized by the solvent. A pronounced dependence of $\langle r_0 \rangle$ on the thermodynamic state variables T, ρ was related to a T, ρ-induced energy level shift of the valence-to-conduction band-gap which gives rise to a variation of the energy initially imparted on the photo-ejected electron. ii) A total excitation energy of 6.2 eV is about 2 eV below the optical band-gap band in liquid ammonia, hence, an ionization of the neat fluid requires solvent nuclear rearrangement. The solvated electron's geminate recombination is strongly accelerated compared to the data at 9.3 eV and indicates that the majority of electrons is injected into suitable trapping sites located between the first and second solvation shell of the initially ionized ammonia molecules. Such configurations can be considered as instantly reactive and facilitate an ultrafast barrierless electron annihilation.

CONTENTS

Part I

Introduction and Experimental Details

1

INTRODUCTION

The solvated electron is a ubiquitous transient species found in molecular liquids exposed to high energy radiation[1] and crucial to the understanding of a wide variety of biological, physicochemical and environmental issues in the chemistry of condensed phases.[2–4] Due to their implication in topics such as radiation-induced DNA damage,[5,6] hazardous waste treatment[7,8] or electron-transfer reactions in solution,[9–11] the hydrated and the ammoniated electron, i.e. the solvated electron in water and ammonia, respectively, are of particular importance. Historically, the latter representative was discovered first over 200 years ago as a metastable reaction product in solutions of alkali metals in ammonia.[12,13] However, the recent interest in these species was mainly stimulated by the observation of the hydrated electron as a transient species upon irradiation of water with fast electrons in 1962[14,15] and only a few years later upon photolysis of aqueous solutions of various inorganic ions (e.g. OH^-, $Fe(CN)_6^{4-}$ or halide anions)[16] and of pure water.[17] Since then a considerable number of both experimental and theoretical studies was carried out to obtain a comprehensive understanding of the structure, the reactivity and the dynamics of these species with research in particular focusing on the hydrated electron.[18–28] Substantial attention was devoted to the photoionization of pure liquid water which is, when compared to the gas phase, a highly complex many body process and still not fully understood.[29–34] It is well established that the formation of the hydrated electron involves several competing ionization mechanisms, all of which are still subject to ongoing discussions[35–39] which clearly reveal the need for further investigations of the electronic structure of polar and protic liquids.[40–43]

With the availability of high-power ultrashort-pulse laser systems the solvated electron gained increasing attention as a unique and highly sensitive probe for the microscopic properties of the solvent network itself. Having only electronic degrees of freedom, the solvated electron is in fact the most fundamental quantum solute and spin-center in the condensed phase. Thus it

is ideally suited to address elementary processes in solution chemistry, which are prerequisite to a molecular level understanding of chemical reactivity in solution chemistry, like for example the dynamic solvent response to changes of the electronic structure of reactants. Topics that were addressed using ultrafast optical absorption spectroscopy of the solvated electron include, for example, charge localization and delocalization processes following electron injection into the bulk or the relaxation of a non-equilibrium solvent configuration.[44–48] Moreover, solvated electrons produced by femtosecond multi-photon excitation of the neat solvent carry important information about the primary matter-field interaction and the ionization mechanism in the liquid.[10,49] Unlike in the gas phase, the electronic structure of the fluid results from a complex interaction between the individual solvent molecules forming a network and is currently only poorly understood. Resolving the correlation between electronic structure and a structural inhomogeneity of a liquid, including the potential role of a hydrogen-bond network in polar and protic media, is highly desirable and an active field of research.[50–54]

The aim of the work presented in this thesis is to provide new experimental insight into the femtosecond multi-photon ionization of polar and protic liquids by exploring, in particular, the role of structural and electronic properties of the solvent network on the ionization mechanism in neat fluid ammonia, which is an important reaction medium and the prototype basic water-like solvent.[55] The following introduction starts with an overview of the different preparation methods of solvated electrons in order to rationalize their specific potential and applicability in scientific research. Next, the dynamics of solvated electrons are explained prior to addressing in detail the photoionization of neat polar and protic liquids. The most complete picture of the underlying processes is available for liquid water. The data will be compared with that of ammonia as the solvent, where the knowledge regarding these topics is relatively scarce.

1.1 The Solvated Electron in Water and Fluid Ammonia

The number of methods available for the generation of solvated electrons is similarly diverse as their appearance in a large variety of condensed host media like ammonia, water, alcohols, ethers or even cement.[1,56,57] Of particular relevance are chemical synthesis, radiolysis, photolysis and electrochemistry,

which have contributed to our current understanding of the nature of the solvated electron in ammonia and water in numerous experimental studies over the last 100 years.[1,2,10,58] New results, like those presented in this thesis, have to be interpreted as an integral contribution to the existing picture obtained through the various generation techniques. It is therefore important to briefly review the different ways to produce solvated electrons and their inherent limitations regarding the physicochemical properties of these species and their host medium that can be addressed. Additionally the stationary optical absorption spectroscopy of the ammoniated and hydrated electron is discussed to establish these species as versatile and highly sensitive probes of their local solvation environment.

1.1.1 Generation Methods and their Role in Research

Chemical Synthesis. Historically, it was Sir Humphry Davy who isolated metallic potassium and sodium in 1807 and only one year later recorded the following observation in his laboratory notebook: "When 8 grains of potassium were heated in ammoniacal gas – it assumed a beautiful metallic appearance & gradually became of a fine blue colour". Today this note is recognized as the first documented observation of the solvated electron in ammonia.[12] It was however not until 1863 that Weyl rediscovered these species,[59] 1914 that Kraus related the electrolytic conductivity of dilute sodium-ammonia solutions to negative charge carriers[60] and shortly after the term solvated electron was introduced by Gibson and Argo.[61] Today it is common knowledge to every chemistry student that all alkaline metals, the alkaline earth metals Ca, Sr, Ba and Ra as well as the lanthanides Eu and Yb spontaneously dissolve in liquefied, anhydrous ammonia without the evolution of hydrogen, transferring their valence electrons into the bulk liquid where they are rapidly solvated forming the ammoniated electron, e^-_{am},[58] e.g. in the case of sodium

$$\mathrm{Na} \xrightarrow{\mathrm{NH_3,\, T < 240\, K}} \mathrm{Na^+_{am}} + \mathrm{e^-_{am}}. \tag{1.1}$$

Fully solvated electrons and metal cations only exist in highly dilute ammoniacal solutions which are of brilliant blue color. As the metal concentration is increased the electrostatic interaction of these species with one another gives rise to the formation of paramagnetic ion-pairs ($Na^+ \cdot e^-_{am}$) as well as diamagnetic, spin-paired multimers like ($e^-_{am} \cdot Na^+ \cdot e^-_{am}$) or ($e^-_{am} \cdot Na^+ \cdot e^-_{am} \cdot Na^+$),

the latter of which are also referred to as bipolarons.[58] All of these species coexist in a complex chemical equilibrium whereas already at 0.5 mol% metal concentration more than 90% of the electrons exist in a spin-paired state. Interestingly, increasing the concentration further above 1 mol% metal results in a transition of the solution into a genuinely metallic state that is characterized by a golden bronze color. Saturated solutions behave like liquid metals and exhibit for example an atomic conductance which is higher than that of liquid mercury indicating a delocalization of the solvated electrons.[13]

From a chemist's point of view it is not surprising that the blue metal-ammonia solutions are strong reducing agents and for example utilized in organic synthesis in the Birch reaction to convert the benzoid ring of aromatic compounds into 1,4-cyclohexadiene products.[62] Ammoniated electrons produced chemically are perfectly stable and have a lifetime of several weeks or more if no contaminations like metal oxides or finely divided metals are present which catalyze a decomposition under liberation of hydrogen yielding amide solutions

$$\mathrm{e^-_{am}} + \mathrm{NH_3} \overset{\text{catalyst}}{\rightleftharpoons} \mathrm{NH_2^-} + \tfrac{1}{2}\mathrm{H_2}. \tag{1.2}$$

The reaction is reversible with an equilibrium constant of $5 \times 10^4 \ \sqrt{\mathrm{dm^3/mol}}$ at 298 K,[63] i.e. solvated electrons in ammonia can also be prepared from metal amide solutions by introducing hydrogen gas under high pressure.[64] The broad application of these systems in research is hindered by the preparative challenges involved with obtaining highly dilute solutions that have a defined composition and an optical density that is suitable for optical absorption spectroscopy. Furthermore, the decomposition according to reaction 1.2 is autocatalytic, i.e. accelerated by amide salts.[55] As a consequence the chemical preparation of solvated electrons in liquefied ammonia at temperatures below the boiling point or at elevated pressure is not widespread for spectroscopic investigations.

RADIOLYSIS. Unlike in ammonia, dissolving alkaline metals in highly purified water rapidly yields metal hydroxide solutions in complete analogy to the products of reaction 1.2 releasing hydrogen gas.[65] Thus, it was not until 1962 that Hart and Boag,[14,15] and Keene[66] independently discovered the hydrated electron through its absorption spectrum as a primary intermediate produced

by the interaction between ionizing radiation and water or aqueous solutions. The first experimental evidence of the ammoniated electron's companion marked an important accomplishment in radiation chemistry and stimulated numerous theoretical and experimental studies addressing topics like the radiation induced damage in biological systems[67,68] or the performance of water-cooled nuclear power reactors under operating conditions.[69,70] A prerequisite to a fundamental understanding of these processes is of course a detailed knowledge of the chemical transformations induced by high-energy radiation in condensed phases as well as the subsequent chemistry of these systems, both of which are an active field of research.[71]

A method commonly employed in these studies is pulse radiolysis using short-pulse beams of electrons (which are usually accelerated to a kinetic energy ranging from a few MeV to a few tens of MeV) as irradiation source for the generation of solvated electrons.[72] To provide a basis for orientation about the degree of excitation, the ionization potential of liquid water is 11.1 eV,[39,73] i.e. this value is exceeded by several orders of magnitude in these experiments. Due to the high excitation energies, the ionization process is largely unselective and very complex. In aqueous solution rapid reorganization and thermalization of the nascent products within the first few picoseconds after irradiation gives rise to a considerable number of highly reactive species including the hydrated electron e^-_{aq} and the molecular species H_3O^+, OH^-, OH, H, H_2, H_2O_2, O_2^- and O.[74] The exact composition of the produced systems is at least equally complex as their ensuing chemistry which is mainly governed by the initial spatial distribution of free radicals and molecular fragments. Energetic electrons traveling through the sample induce a series of excitation and ionization events along their tracks which result in the formation of small volumes (so called spurs) containing a high density of radiolysis products.[75] At modest radiation dose, the different spurs are well separated when compared to the separation between reactive particles within a spur. Due to the highly nonhomogeneous spatial distribution, the ensuing chemistry can be separated into two stages which take place on characteristic timescales.[76,77] As the system propagates in time, the radiolytic products diffuse from their original positions and initially either meet and react with other species within the same spur or they escape into the bulk. The initial stage of nonhomogeneous spur kinetics in ambient water is typically completed within 10^{-7} s to 10^{-6} s after the action of the radiolysis pulse. This time window simultane-

ously marks a changeover of the kinetics as now the original spur structure is dissipated and the remaining reactants are distributed homogeneously and become annihilated on a slower timescale within microseconds.[78] In other words, the time-dependent yield of the solvated electron (which is usually employed as an observable in such experiments) during the nonhomogeneous stage contains important information about the initial distribution of products within the spurs which in turn provides a window into the ionization process itself. Through recent technological developments, like the compression of the electron bunch used for excitation to the femtosecond time domain, pulse radiolysis experiments are now capable to achieve time resolutions on the subpicosecond time-scale allowing the study of ultrafast dynamics in real time.[72]

Considering the number of different reactants, their yields and their relative spatial distributions within the spurs, it is not surprising at all, that the interpretation of spur kinetics is a challenging task. A detailed description of the available models is beyond the scope of this introduction and the interested reader is referred to ref 79 and 80. Briefly, the analysis usually involves stochastic computer simulations starting with the development of a computationally large number of isolated spurs by modeling the excitation and ionization events induced by energetic electrons in the solvent. The results provide the initial relative positions of the thermalized radiolysis products representative of the situation a few picoseconds after the action of the electron pulse. Subsequently, nonhomogeneous kinetics are implemented by propagating the individual spurs in time. To this end, the trajectories of motion are calculated for each reactive particle, whereas chemical reactions are accounted for by testing the inter-particle separations against pre-defined reaction distances. A realistic simulation of the kinetics is ultimately bound to an accurate parametrization of the underlying model which requires a detailed knowledge of the individual reactants' properties as well as their interactions, e.g. diffusion coefficients, the nature of mutual electrostatic interactions and rate constants as well as activation energies for all possible reactions in the system.[80] Although more computation-time efficient realizations of these simulations have been developed in the recent years,[81–83] the evaluation of radiolysis data is quite complex and remains an active field of research.[71,74,75]

PHOTOLYSIS. The discovery of the hydrated electron upon bombardment of ambient water with highly energetic electrons stimulated numerous investigations in the field. Among others, experiments employing milder excitation conditions like photoionization of the neat solvent or photodetachment from dissolved anions were performed. Thus only a few years later in 1969 the generation of the solvated electron was also reported in a flash photolysis study upon exposure of liquid water to ultraviolet (UV) light.[17] Moreover, it is well established, that electrons can be photo-injected into the bulk through a charge-transfer-to-solvent (CTTS) transition from dissolved anions like ferrocyanide[84] or hydroxide[85] where they become rapidly localized due to solvation by the abundant solvent molecules. In the recent decades the development of ultrashort-pulse laser systems and ultrafast spectroscopic techniques has provided the possibility to investigate the dynamics of the solvated electron on a femtosecond timescale in real time.[10,29,30,45,86–98] The majority of these investigations was unequivocally devoted to unraveling the properties of the electron in liquid water so that over the years a coherent picture of its localization and delocalization dynamics following photo-injection as well as its interaction with the solvent leading to solvation and thermalization emerged, which is unavailable for any other solvent system.[10,21,47] Furthermore, the quality of the solvated electron as a highly sensitive probe of the local properties of the solvent network has been established in several femtosecond photoionization studies on pure water[29,30,34,39,99] thereby providing a unique window into the dynamic and electronic properties of the liquid phase.[10] The current state of knowledge on these topics is vital to the understanding of new contributions on the solvated electron in anhydrous fluid ammonia presented in this thesis and is discussed in detail in the following section.

ELECTROCHEMISTRY. To complete the overview on the most important generation methods it should be noted that solvated electrons can also be generated electrochemically by cathodic reduction of electrolyte solutions such as alkali metal salts dissolved in anhydrous ammonia which are stable towards the generation conditions. Due to the high overpotential of hydrogen at many electrode materials (e.g. silver), the thermodynamically favored formation of hydrogen is inhibited and the generation of ammoniated electrons is indicated by the characteristic blue coloration of the solution.[100,101] The electrolysis of

aqueous electrolytes, however, leads to the evolution of hydrogen at the cathode whereat the hydrated electron is discussed as a highly reactive precursor during this process.[101,102]

Measurements of the electromotoric force of equilibrium reactions of solvated electrons in metal-ammonia solutions contributed to a basic understanding of the thermodynamic properties of these systems and were carried out mostly by Schindewolf and coworkers.[103–106] One of the questions addressed was, why the ammoniated electron in metal-ammonia solutions is virtually indefinitely stable whereas its hydrated companion is only known as a transient species with a lifetime of less than one millisecond. Assuming that the dissolution of alkali metals in water indeed leads to the intermediate formation of hydrated electrons, its primary reducible reaction partners are the abundant number of surrounding H_2O solvent molecules. With respect to the hydrated electron a pseudo monomolecular and pseudo bimolecular reaction can be distinguished. The latter transformation taking place under liberation of molecular hydrogen according to

$$2\,e^-_{aq} + 2\,H_2O \longrightarrow 2\,OH^- + H_2 \tag{1.3}$$

is strongly exothermic ($\Delta H^\circ = -397\,\mathrm{kJ/mol}$) at room temperature and involves only a small, negative reaction entropy of $\Delta S^\circ = -12\,\mathrm{J/(mol\,K)}$. Thus, this decay is strongly exergonic ($\Delta G^\circ = -393\,\mathrm{kJ/mol}$) and therefore is expected to be an efficient decay channel at ambient conditions.[107,108] The pseudo monomolecular annihilation of the hydrated electron

$$e^-_{aq} + H_2O \longrightarrow OH^- + H \tag{1.4}$$

producing atomic hydrogen is thermodynamically slightly unfavorable with $\Delta H^\circ = 10\,\mathrm{kJ/mol}$ and $\Delta S^\circ = -48\,\mathrm{J/(mol\,K)}$. It is however driven by a subsequent, strongly exergonic hydrogen atom combination, making the sequential variation of equation 1.3 a thermodynamically and kinetically feasible decay mechanism as well.[107,108] Additionally water is dissociated due to autoprotolysis according to $2\,H_2O \rightleftharpoons H_3O^+ + OH^-$ with an ion product of $10^{-14}\,M^2$ at 298 K.[109] Though the equilibrium concentration of the hydronium ions, H_3O^+, is low, these species are possible reaction partners for the solvated electron

$$e^-_{aq} + H_3O^+ \longrightarrow H_2O + H. \tag{1.5}$$

The electronic charge annihilation is exergonic ($\Delta G^\circ = -35\,\mathrm{kJ/mol}$) and known to be thermally activated with an energetic barrier of 14.5 kJ/mol thereby adding another electron loss pathway.[107,110]

In the case of metal-ammonia solutions the analogue reactions have to be considered, this time however to account for their stability. Firstly, a reduction of the solvent involving hydrogen atom abstraction, i.e.

$$\mathrm{e^-_{am}} + \mathrm{NH_3} \longrightarrow \mathrm{NH_2^-} + \mathrm{H} \tag{1.6}$$

is associated with a reaction enthalpy of $\Delta H^\circ = 125\,\mathrm{kJ/mol}$ and an entropy change of $\Delta S^\circ = -272\,\mathrm{J/(mol\,K)}$ at 233 K. Hence the reaction is not only endothermic, but also strongly endergonic by $\Delta G^\circ = 188\,\mathrm{kJ/mol}$.[107] Secondly, the thermodynamically favored decay under liberation of molecular hydrogen

$$2\,\mathrm{e^-_{am}} + 2\,\mathrm{NH_3} \longrightarrow 2\,\mathrm{NH_2^-} + \mathrm{H_2} \tag{1.7}$$

is exothermic ($\Delta H^\circ = -168\,\mathrm{kJ/mol}$), but involves a strongly negative entropy of reaction of $\Delta S^\circ = -466\,\mathrm{J/(mol\,K)}$. The latter is mainly attributed to the loss of the very positive entropy of the ammoniated electron of $S^\circ = 169\,\mathrm{J/(mol\,K)}$ (for reference that of the solvated electron in water is only $S^\circ = 13\,\mathrm{J/(mol\,K)}$).[108,111] Accordingly a large, negative activation entropy is expected as it is reflected by an estimated reaction rate constant smaller than $k = 10^{-7}\,\mathrm{M^{-1}\,s^{-1}}$,[107] thereby confirming the experimentally observed kinetic stability of metal-ammonia solutions. Finally a reaction with ammonium cations, $\mathrm{NH_4^+}$, that are produced by the autoprotolytic dissociation of ammonia

$$\mathrm{e^-_{am}} + \mathrm{NH_4^+} \longrightarrow \mathrm{NH_3} + \mathrm{H} \tag{1.8}$$

is negligible for two reasons. On one hand the concentration of $\mathrm{NH_4^+}$ in the neat liquid is insignificant as indicated by an ion product on the order of $10^{-35}\,\mathrm{M^2}$ at 233 K, i.e. the equilibrium of the autoprotolysis $2\,\mathrm{NH_3} \rightleftharpoons \mathrm{NH_4^+} + \mathrm{NH_2^-}$ is shifted completely to the left side owing to the strong basicity of the amide ion, $\mathrm{NH_2^-}$.[104] On the other hand, the charge neutralization reaction (1.8) is endothermic ($\Delta H^\circ = 30\,\mathrm{kJ/mol}$) and involves a negative reaction entropy ($\Delta S^\circ = -12\,\mathrm{J/(mol\,K)}$). Thus it is endergonic by about $\Delta G^\circ = 33\,\mathrm{kJ/mol}$ and can be excluded as a decay pathway for the solvated electron in ammonia.[107,112]

1.1.2 Linear Spectroscopy

The solvated electron in polar and protic solvents like ammonia or water has spectroscopic properties which allow its optical detection in highly diluted solutions and make it an excellent model system to study coupled electron-solvent dynamics and ultrafast reactions in the condensed phase.[65] The absorption spectra of these species are characterized by a several hundred wavenumbers broad and featureless band located in the visible (Vis) to near-infrared (NIR) region depending on the solvent medium.[56,113–115] For example, the maximum resonance peaks at 720 nm in ambient water[116] and is found redshifted to 1545 nm in liquefied ammonia at the boiling point of 240 K and 1 atm.[117,118] The intense blue color of dilute metal-ammonia solutions is attributed to an extension of the high frequency tail of the absorption band into the Vis spectral region and indicates that the extinction coefficient of these species is large. More precisely it is $4.9 \times 10^4\,\mathrm{M^{-1}\,cm^{-1}}$ for the ammoniated electron at 203 K[117,119] or $2.3 \times 10^4\,\mathrm{M^{-1}\,cm^{-1}}$ for the hydrated electron at 293 K.[120] Accordingly, apart from a few exceptions[37,98] usually experiments are performed, in which the absorption of the solvated electron is optically probed following the dynamics ensuing photoexcitation of the neat liquid.[30,34,39,43,47,97,99,121] It should be noted that the absorption of the hydrated electron in the Vis to NIR is not perturbed by the molecular photolysis fragments H_3O^+ and OH which absorb spectrally well-separated in the UV region.[37] The same holds true for the photolysis of ammonia assuming that the excitation process produces analogue to reaction 1.10 the ammonium cation NH_4^+ and the aminyl radical NH_2.[122,123]

Interestingly the spectral position of the solvated electron's electronic resonance was found to sensitively depend on the thermodynamic state variables temperature, T, and density, ρ, allowing its application as a local thermometer or densimeter.[45,46] In the case of the hydrated electron isochoric cooling or isothermal compression of the solvent both give rise to a gradual shift of the stationary absorption to higher frequency whereas its spectral shape remains mainly unaffected.[116,124] In principle this qualitative correlation holds true for solvated electrons in ammonia as well.[118,125] However, unlike in water its stationary absorption is reported to be barely sensitive to the thermodynamic conditions above $T \approx 323\,\mathrm{K}$. Here, increasing the temperature well above supercritical conditions or varying the density over a wide range be-

tween 0.64 g dm^{-3} and 0.10 g dm^{-3} does not result in the expected shift of the spectral position of the resonance.[64,126–128]

1.2 Photoionization of Water

Since the discovery of the hydrated electron by Hart and Boag[15] significant advances were made in the field of ultrafast spectroscopy continuously improving the temporal resolution from the microsecond towards the femtosecond time domain.[129] Due to these efforts, nowadays it is possible to experimentally monitor almost in real time the coupled charge-solvent dynamics following photo-induced electron ejection.[21,98] It is re-emphasized at this point that solvated electrons produced by multi-photon excitation of the neat fluid are well established as sensitive probes of the primary matter-field interaction.[10] A highly intriguing aspect of the ionization mechanism in water is that the formation of solvated electrons is reported for excitation energies well below the ionization potential of the liquid, extending virtually down to the optical absorption edge of ambient water around 5.8 eV.[36,38,130] It is interesting to note that this value coincides with the calculated free enthalpy change $\Delta G = 5.8\,\mathrm{eV}$ for reaction[17]

$$2\,H_2O \longrightarrow e^-_{aq} + H_3O^+ + OH, \tag{1.9}$$

i.e. it corresponds to the minimum energy required for a photo-induced preparation of the hydrated electron. The finding of charge injection at energies as much as $\sim$5 eV below the ionization potential of the neat liquid[73] indicates that multiple ionization pathways are present in a polar and protic solvent.[39] Currently several mechanisms are debated in the scientific community which illustrates that the electronic structure of the disordered, dynamically fluctuating fluid phase is currently only incompletely understood. The leading candidates for ionization in water are depending on the excitation energy, a proton-coupled electron transfer, a hot hydrogen atom mechanism and a vertical ionization.[31]

In the following the current knowledge on the ionization pathways in liquid water is presented in detail. Moreover, it is discussed how femtosecond multi-photon ionization of the neat solvent can provide experimental insight into these processes by monitoring the solvated electron's recombination dy-

namics with complementary photolysis products. To this end it is crucial to understand the complex dynamics of photo-injected electrons on the submicrosecond timescale where a thermalization of the nascent photoproducts overlaps with their chemical recombination.

1.2.1 Early Time Dynamics

The stationary absorption spectrum of the hydrated electron in ambient water is characterized by a spectrally broad and featureless absorption spectrum with a maximum, around 720 nm, in the visible spectral region.[131] Following multi-photon ionization of the neat solvent, it is established that at early times the electron's resonance is found in the mid-to-near infrared region. The subsequently observed spectral shift can be fully explained by a non-equilibrium configuration,[21,93] i.e. immediately after electron formation, structural rearrangements and thermal cooling of the solvation shell lead to a fully localized and thermalized hydrated electron. These primary processes give rise to an ultrafast spectro-temporal blue-shift of the electronic resonance towards shorter wavelengths (i.e. the spectral position of the stationary resonance) and are essentially completed within 2 ps in liquid water at room temperature.[21]

Thus when conducting time-resolved experiments with an optical detection of the solvated electron, it is important to carefully separate the change in absorption due to the initial localization and thermalization dynamics from the overlapping geminate recombination, i.e. the change of the optical absorption due to an actual loss of solvated electrons. The details of this approach are described in detail in the experimental section in chapter 2.

1.2.2 Geminate Recombination

The total excitation energy in femtosecond multi-photon ionization experiments is usually on the order of the ionization potential of the studied solvent which is large compared to the spectral bandwidth of the excitation laser pulse.[39] Under these energetically well defined conditions the hydrated electron is produced selectively alongside the molecular fragments hydronium cation and hydroxyl radical according to

$$2\,H_2O + n\,h\nu \longrightarrow e^-_{aq} + H_3O^+ + OH, \tag{1.10}$$

where n gives the number of photons with the energy hν involved in the primary matter field interaction.[17,21,31] According to recent results the reaction is essentially completed within less than 100 fs[98,132] whereas the photo-ejected electron is fully solvated and thermalized within 2 ps after the action of the laser pulse.[21]

Similar to the pulse radiolytic generation of solvated electrons, the distribution of ionization events within the liquid phase is highly nonhomogeneous. However, in the case of photoexcitation there is no spur structure with a rather complicated configuration of reactive species,[82,133] but spatially well separated photolysis sites are present, each consisting of the three particles e^-_{aq}, H_3O^+ and OH.[29,30] The separation at which the ejected electron becomes initially solvated and thereby well-localized away from its parental ionization core is of particular interest. This quantity is usually referred to in literature as the thermalization distance or ejection length of the solvated electron, r_0. It depends on the total excitation energy and is on the order of a few nanometers, i.e. similar to the inter-particle separation in ambient water of 0.29 nm.[39,99,134] The ensuing chemistry in this system is initially governed by the nonhomogeneous spatial distribution of reactants created by the excitation laser pulse and on the submicrosecond timescale almost exclusively due to encounters between the solvated electron and its parental, i.e. geminate molecular fragments OH and H_3O^+. Thus, time-resolved data on the geminate recombination carries information on the initial thermalization distance of the solvated electron which ultimately provides insight into the properties of the ionization mechanism and the electronic structure of the liquid phase.[47]

The well defined spatial configuration and chemical composition of these systems with respect to the reactive particles facilitates an analysis of the experimentally observed loss of the solvated electron on the picosecond timescale. In particular only two elementary recombination reactions need to be considered,[30] on the one hand a charge neutralization involving the H_3O^+ cation according to equation 1.5 and on the other hand an electron-dipole annihilation according to

$$e^-_{aq} + OH \longrightarrow OH^-. \tag{1.11}$$

It should be noted that the reaction of the solvated electron with the surrounding solvent molecules is slower by several orders of magnitude and does not play a role on the relevant time frame of 1 ns.[107] At each ionization site the

fate of the solvated electron, i.e. whether it recombines geminately with its parental H_3O^+ or OH fragment according to reaction 1.5 or 1.11 or escapes into the bulk and recombines subsequently in a non-geminate fashion on a microsecond timescale, is determined by its thermalization distance. Commonly geminate recombination is characterized by the time-dependent survival probability, $\Omega(t, r_0)$, that corresponds to the fraction of solvated electrons that are still present at a time, t, subsequent to the action of the ionization pulse at $t = 0$.

It is possible to extract the thermalization distance by comparing the experimentally measured survival probability with predictions from quantitative diffusion models which take into account the relative microscopic motion of all the recombination partners in the system including their mutual reactive encounters.[49,134] As the ionization events can be considered to be on average well-separated from each other, geminate recombination is practically analyzed in terms of an ensemble of isolated, i.e. non-interacting ionization sites each consisting of three reactive particles, i.e. e^-_{aq}, H_3O^+ and OH. Interestingly it is found, that although the solvated electron is undoubtedly a quantum mechanical solute, its migration in polar and protic fluids can be treated in terms of Brownian motion analogue to classical ions.[27] For the photoionization of water, both, analytical solutions[49] as well as stochastic computer simulations,[134] have been developed to extract the relevant information on the thermalization distance. Both methods were shown to give similar results,[134] however the latter approach using Monte-Carlo simulations is particularly advantageous when it comes to adapting the diffusion model to specific properties of the reaction, like for example competing multiple recombination pathways or specific electrostatic interactions between the particles.[99]

Compared to pulse radiolysis which exposes the liquid to a high energy ($\sim$MeV) electron beam,[78] the well-defined charge-ejection process in femtosecond multi-photon ionization experiments prepares a well defined model system, that allows a systematic investigation of the solvated electron's geminate recombination as a function of the excitation energy.[35,39] These studies[34,35,37,39,43,47,99,135] thereby offer a unique spectroscopic window into the ionization process and the electronic structure of the dynamically disordered fluid phase that complements the radiochemistry of water at high excitation energies.[134] Over the past years a comprehensive microscopic mechanism for the photoionization of liquid water has emerged in which different pathways

have been identified depending on the total ionization energy provided by the incident laser radiation. Each of these pathways was found to be associated with a characteristic ejection length for the hydrated electron which in turn is reflected in different recombination kinetics.[31,34,37,39,99,135] The current state of knowledge on these processes including their correlation with the electronic properties of the liquid is discussed in the following.

1.2.3 Pathways Leading to the Hydrated Electron

The electronic properties of polar liquids like water and ammonia can be conceptually understood in terms of a lone-pair amorphous semiconductor.[136,137] Compared to the isolated gas phase molecule, in the fluid short-range orientational order gives rise to the merging of intermolecularly interacting nonbonding orbitals into a completely filled valence band. It is separated by a large energy gap from the conduction band, which according to ab initio molecular dynamic simulations, is a continuum of quasi-free electronic states that are delocalized over the interstitial space between many molecules in the solvent network.[40] Depending on whether or not the total excitation energy exceeds the band-gap energy, direct and indirect ionization mechanisms are distinguished.[31]

In bulk liquid water the most probable vertical transition energy from the valence band into the ionization continuum is reported to be 11.1 eV at ambient temperature.[39,73] At and above this energy the optical excitation directly promotes an electron into the conduction band of the solvent. The vertical transition or ionization initially produces a nonthermal conduction band electron, e^-_{CB}, and a cationic hole, H_2O^+, whose geometry is unchanged compared to the neutral H_2O molecule, i.e.

$$H_2O + n\ h\nu \longrightarrow e^-_{CB} + H_2O^+. \tag{1.12}$$

In a polar and protic solvent these nascent products do not represent the final fully equilibrated chemical species. In the case of above-band-gap excitation it is important to emphasize that the relaxation of the cationic hole and the photoejected electron are mainly decoupled from each other.[138] The H_2O^+ cation is known to be highly unstable and decomposes involving a proton-

transfer onto a neighboring water molecule according to

$$H_2O^+ + H_2O \longrightarrow OH + H_3O^+. \tag{1.13}$$

Recent ab initio molecular dynamics simulations and transient absorption measurements by Marsalek et al. indicate that the decay is essentially completed within less than 40 fs.[98] The delocalization of the electron is reported to take place on a time scale of less than 500 as.[132] Subsequently it becomes trapped at asymmetric or broken hydrogen-bond geometries in the water network which serve as precursors to the fully solvated and localized hydrated electron,[132] i.e.

$$e^-_{CB} \longrightarrow e^-_{aq}. \tag{1.14}$$

Consistent with the quasi-free nature of conduction band electrons, the thermalization distance of hydrated electrons produced in vertical ionization is typically on the order of $\sim$4 nm[39,47] and grows gradually with increasing excitation energy.[39]

However, it is a very intriguing aspect of the ionization mechanism that the generation of hydrated electrons is reported for excitation energies well below the band-gap extending down to almost the optical absorption edge of ambient water near 5.8 eV.[36,38,130] Under these conditions the formation of solvated electrons bypasses the conduction band and becomes only energetically feasible due to an involvement of solvent nuclear motions which stabilize the nascent photoproducts e^-_{aq}, H_3O^+ and OH towards the fully equilibrated species.[138] Thus, at below-band-gap excitation excess electrons are not produced directly by the optical transition. Currently two electron injection mechanisms are debated as the leading candidates for below-band-gap ionization of water, namely proton-coupled electron transfer (PCET) and the so-called hot hydrogen atom (HHA) mechanism.[34,35,37,43,99]

The PCET comprises a concerted decomposition of an electronically excited water molecule, H_2O^*, which involves both a motion along the proton transfer coordinate as well as the injection of an electron into a suitable "presolvated" solvent trap that is able to stabilize the charge,[35,38] i.e.

$$2\,H_2O + n\,h\nu \longrightarrow H_2O^* + H_2O \longrightarrow e^-_{aq} + H_3O^+ + OH. \tag{1.15}$$

Due to the dissociative character of the excited electronic states of water,[43,139]

this mechanism essentially competes with a homolytic dissociation of H_2O^* according to $H_2O^* \longrightarrow H + OH$ which is the basis for the alternatively suggested scenario.[37] The homolysis of water may yield an OH radical and a translationally hot hydrogen atom, H_{hot}, which may then collide with a neighboring water molecule to produce the hydrated electron and a hydronium cation according to[35,38]

$$H_2O + n\,h\nu \longrightarrow H_2O^* \longrightarrow H_{hot} + OH \xrightarrow{+H_2O} e^-_{aq} + H_3O^+ + OH. \quad (1.16)$$

Both indirect pathways require significant transformations in the liquid to produce the hydrated electron and thereby clearly demonstrate that the solvent network itself plays an important and complex role in the photoexcitation process at energies below the band-gap.[138] The experimentally determined thermalization distance is smaller than in the case of vertical ionization and on the order of 1 nm[39,99] which is expected for a charge-injection process that either requires the presence of nearby trapping states or follows collisions with H_2O molecules in the surrounding solvation shell.[39] Finally it should be noted that the net result of all the presented ionization mechanisms is equivalent, i.e. they all deliver the same final equilibrated species, namely e^-_{aq}, H_3O^+ and OH.

1.3 Aim of this Thesis

The majority of time-resolved studies devoted to the photoionization of polar and protic liquids was carried out on liquid water where over the recent decades a comprehensive microscopic picture of different ionization pathways has emerged.[30,33–35,37–39,43,47,97–99,121] Despite all effort the different mechanisms are still not fully understood and some of the multiple issues which remain unanswered are:

- What is the exact nature of the ionization pathways above and below the valence-to-conduction band-gap?
- What is the specific involvement of nuclear motions within the solvent network leading to the charge-injection at energies below the valence-to-conduction band gap?
- Are the identified mechanisms generic for the multi-photon ionization of all polar and protic solvents?

- What is the correlation between the ionization pathways and the electronic structure of the solvent network?

All these unresolved questions show that new insight into this topic is highly desirable.

The aim of this thesis is to approach the problems addressed above by extending the body of photoionization studies to pure liquid ammonia which is the prototypical basic water-like solvent[55] and so far has not been subject to a femtosecond multi-photon excitation experiment. Additionally a main focus of this work is to access the dependence of the ionization mechanism on the structural and electronic properties of the solvent. To do so, geminate recombination is investigated as a function of temperature and density, covering a wide range of thermodynamic conditions ranging from the dense cryogenic fluid well into the dilute supercritical phase. This thesis comprises of three publications each of which is presented in a separate chapter.

After a brief description of the experimental setup in Chapter 2, in the third chapter the first-ever experimental study of the femtosecond multi-photon ionization of neat liquid-to-supercritical ammonia is presented. Photoexcitation was carried out using a total energy of 9.3 eV and the generation of the solvated electron was identified based on its characteristic absorption band in the NIR spectral region. The ammoniated electron's geminate recombination was studied over a wide range of thermodynamic conditions and found to be mainly determined by the diffusional encounter of the geminate reactants. The obtained data allow to establish in a systematic fashion, how changes of the temperature and the density affect geminate recombination in neat ammonia.

In the fourth chapter the time-resolved data presented in the preceding chapter were analyzed by a full Monte Carlo analysis of the solvated electron's thermalization distance from its parental ionization hole, NH_3^+. The simulations of the solvated electron's survival probability were compared with the experimental observations to establish the correlation between the vertical ionization mechanism and the electronic properties of the solvent network. An identified dependence of the thermalization distance on the thermodynamic conditions was combined with the current understanding of the temperature and density-dependent electronic structure of the liquid phase in order to resolve the role of thermally induced energy level shifts for the valence-to-conduction band gap.

In the fifth chapter, a complementary experimental study of the photoionization of neat ammonia was carried out employing a total excitation energy of 6.2 eV which is roughly 2 eV below the valence-to-conduction band-gap of the solvent. The geminate recombination of the solvated electron is investigated covering a wide range of thermodynamic conditions identical to that of the first study presented in chapter three. As expected, for an ionization mechanism that bypasses the conduction band of the solvent, the thermalization distance of the solvated electron is found to be significantly smaller than that of the above-band-gap excitation with 9.3 eV. The sequence of ionization and recombination events is found to be appropriately described as a proton-coupled electron transfer (PCET) followed by a proton-coupled back-electron transfer (PCBET). Finally, this thesis is concluded with a summary of the key findings and some recommendations for future research.

2

Experimental Details

Experimental Setup. Time-resolved absorption experiments of fluid ammonia with an optical detection of the solvated electron's resonance were carried out using a femtosecond pump-probe spectrometer which was already used in previous investigations[34,45,46] and is described in detail in the doctoral thesis of Stephan Kratz.[140] The experimental setup will therefore be described only briefly. A home-built 1 kHz Ti:sapphire regenerative chirped pulse amplifier was used as a front-end to a femtosecond ultraviolet (UV)-pump and near-infrared (NIR)-probe spectrometer. The 800 nm, 100 fs pulses delivered by the front-end had an energy of 750 µJ and were split by a 50% dielectric beam splitter. One part of the fundamental was frequency doubled in a 1 mm BBO crystal (type I), to obtain 400 nm photoionization pulses with energies as high as 180 µJ while maintaining the pulse duration of the front-end. For experiments employing 266 nm UV-pulses for the excitation of fluid ammonia, the resulting second harmonic was additionally sum-frequency mixed with the residual fundamental in a 0.4 mm BBO crystal (type I). The remaining 50% fraction of the front-end's fundamental output was used to pump an optical parametric amplifier (OPA, TOPAS, Light Conversion) to provide femtosecond near-IR pulses tunable between 1200 nm and 2400 nm. The signal (or idler) pulses of the OPA were divided by a dielectric beam splitter into probe and reference pulses, both of which were focused into the sample using a 45° off-axis aluminum mirror with a focal length of 100 mm. The pump beam was overlapped inside the sample with the probe beam at an angle of 5° using a 400 mm focal length, fused silica lens. After passing through the cell, probe and reference pulse intensities were detected by PbS-photoresistors whose electrical signals were fed into gated integrators. The pump-beam irradiance was adjusted without changing the diameter of the beam by means of a combination of a half-wave retardation plate and a polarizer. The probe beam was attenuated by neutral density filters.

The geminate dynamics of solvated electrons in fluid ammonia were studied

over a wide range of temperature and density. The thermodynamic state points were organized into a measurement series along the 423 K-isotherm and another one along the 300 bar-isobar. Samples of NH_3 (99.98%, AirLiquide) or ND_3 (99 atom% D, Sigma-Aldrich) were prepared in a stainless steel high-pressure and high-temperature optical cell[141–143] with 2.5 mm thick sapphire windows and an optical path length of 1.0 mm. The entire high pressure system was purged with liquid CO_2 and subsequently evacuated to a pressure below 10^{-3} mbar to remove all traces of impurities such as water.

CHOICE OF THE DETECTION FREQUENCY. When conducting time-resolved multiphoton ionization experiments with an optical detection of the solvated electron, it is important to carefully separate the change in absorption due to the initial localization and thermalization dynamics from the overlapping loss of solvated electrons. If the complete transient absorption spectrum of the solvated electron is recorded, its comparison with the stationary resonance of the solvated electron allows to analytically separate a blue-shift due to thermalization from the geminate recombination dynamics.[135] However, this approach requires an experimental setup that allows to monitor a spectrally several hundred wavenumbers broad region in the NIR, covering the dynamic blue-shift as well as the stationary resonance of the ammoniated electron.

For practical reasons commonly a single detection-wavelength approach is chosen to monitor the photo-generated solvated electron.[34,39] Under such conditions thermalization and geminate recombination cannot be fully disentangled, but as both processes take place on two distinct timescales (e.g. less than a few picoseconds compared to several hundred picoseconds in ambient water),[21,39] it is usually sufficient to establish the time at which the spectro-temporal evolution in the mid-to-near-IR due to thermalization and localization is essentially completed. To do so, the detection wavelength can be chosen in the maximum or on the high frequency shoulder of the solvated electron's stationary absorption. Under these conditions any thermal cooling or any nuclear dynamics within the solvent surrounding of the hydrated electron can only give rise to a temporally delayed growth of the detected absorption. Thus, any decay of the signal is solely due to an actual loss of solvated electrons.[34]

To ascertain that for all investigated thermodynamic conditions the am-

moniated electron was optically detected on the high-frequency edge or the maximum of its stationary absorption spectrum, detailed information was required on the temperature and density-dependent position of its resonance. As already described in section 1.1.2, such data was available from experiments conducted by Schindewolf and co-workers[64,126–128] covering almost the entire range of thermodynamic conditions investigated in this thesis.

[1] Mozumder, A. *Fundamentals of Radiation Chemistry;* Academic Press: San Diego, 1999.

[2] Hart, E. J.; Anbar, M. *The Hydrated Electron;* John Wiley & Sons Inc.: New York, 1970.

[3] Siefermann, K. R.; Abel, B. *Angew. Chem. Int. Edt.* **2011**, *50*, 5264.

[4] Likhtenshtein, G. I. *Solar Energy Conversion: Chemical Aspects;* Wiley-VCH: Weinheim, 2012.

[5] Simons, J. *Acc. Chem. Res.* **2006**, *39*, 772.

[6] Nguyen, J.; Ma, Y.; Luo, T.; Bristow, R. G.; Jaffray, D. A.; Lu, Q.-B. *PNAS* **2011**, *108*, 11778.

[7] Committee on Review and Evaluation of Alternative Technologies for Demilitarization of Assembled Chemical Weapons. *Review and Evaluation of Alternative Technologies for Demilitarization of Assembled Chemical Weapons;* The National Academies Press: Washington, DC, 1999.

[8] Getoff, N. *J. Chem. Sci.* **1993**, *105*, 373.

[9] Marcus, R. A. *J. Chem. Phys.* **1965**, *43*, 3477.

[10] Chen, X.; Bradforth, S. E. *Annu. Rev. Phys. Chem.* **2008**, *59*, 203.

[11] Brückner, R. *Reaktionsmechanismen: Organische Reaktionen, Stereochemie, Moderne Synthesemethoden;* Spektrum Akademischer Verlag: Heidelberg, 2009.

[12] Thomas, S. J. M.; Edwards, P. P.; Kuznetsov, V. L. *ChemPhysChem* **2008**, *9*, 59.

[13] Zurek, E.; Edwards, P. P.; Hoffmann, R. *Angew. Chem. Int. Edt.* **2009**, *48*, 8198.

[14] Hart, E. J.; Boag, J. W. *J. Am. Chem. Soc.* **1962**, *84*, 4090.

[15] Boag, J. W.; Hart, E. J. *Nature* **1963**, *197*, 45.

[16] Matheson, M. S.; Mulac, W. A.; Rabani, J. *J. Phys. Chem.* **1963**, *67*, 2613.

[17] Boyle, J. W.; Ghormley, J. A.; Hochanadel, C. J.; Riley, J. F. *J. Phys. Chem.* **1969**, *73*, 2886.

[18] Walker, D. C. *Q. Rev. Chem. Soc.* **1967**, *21*, 79.

[19] Anbar, M. *Q. Rev. Chem. Soc.* **1968**, *22*, 578.

[20] Buxton, G. V.; Greenstock, C. L.; Helman, W. P.; Ross, A. B. *J. Phys. Chem. Ref. Data* **1988**, *17*, 513.

[21] Hertwig, A.; Hippler, H.; Unterreiner, A.; Vöhringer, P. *Ber. Bunsenges. Phys. Chem.* **1998**, *102*, 805.

[22] Yokoyama, K.; Silva, C.; Son, D. H.; Walhout, P. K.; Barbara, P. F. *J. Phys. Chem. A* **1998**, *102*, 6957.

[23] Bragg, A. E.; Verlet, J. R. R.; Kammrath, A.; Cheshnovsky, O.; Neumark, D. M. *Science* **2004**, *306*, 669.

[24] Larsen, R. E.; Glover, W. J.; Schwartz, B. J. *Science* **2010**, *329*, 65.

[25] Abel, B.; Buck, U.; Sobolewski, A. L.; Domcke, W. *Phys. Chem. Chem. Phys.* **2012**, *14*, 22.

[26] Young, R. M.; Neumark, D. M. *Chem. Rev.* **2012**, *112*, 5553.

[27] Turi, L.; Rossky, P. J. *Chem. Rev.* **2012**, *112*, 5641.

[28] Marsalek, O.; Uhlig, F.; VandeVondele, J.; Jungwirth, P. *Acc. Chem. Res.* **2012**, *45*, 23.

[29] Lu, H.; Long, F. H.; Bowman, R. M.; Eisenthal, K. B. *J. Phys. Chem.* **1989**, *93*, 27.

[30] Lu, H.; Long, F. H.; Eisenthal, K. B. *J. Opt. Soc. Am. B* **1990**, *7*, 1511.

[31] Sander, M. U.; Luther, K.; Troe, J. *Ber. Bunsenges. Phys. Chem.* **1993**, *97*, 953.

[32] Sander, M. U.; Luther, K.; Troe, J. *J. Phys. Chem.* **1993**, *97*, 11489.

[33] Sander, M. U.; Gudiksen, M. S.; Luther, K.; Troe, J. *Chem. Phys.* **2000**, *258*, 257.

[34] Kratz, S.; Torres-Alacan, J.; Urbanek, J.; Lindner, J.; Vöhringer, P. *Phys. Chem. Chem. Phys.* **2010**, *12*, 12169.

[35] Crowell, R. A.; Bartels, D. M. *J. Phys. Chem.* **1996**, *100*, 17940.

[36] Bernas, A.; Ferradini, C.; Jay-Gerin, J.-P. *J. Photochem. Photobiol. A* **1998**, *117*, 171.

[37] Thomsen, C. L.; Madsen, D.; Keiding, S. R.; Thogersen, J.; Christiansen, O. *J. Chem. Phys.* **1999**, *110*, 3453.

[38] Bartels, D. M.; Crowell, R. A. *J. Phys. Chem. A* **2000**, *104*, 3349.

[39] Elles, C. G.; Jailaubekov, A. E.; Crowell, R. A.; Bradforth, S. E. *J. Chem. Phys.* **2006**, *125*, 044515.

[40] Laasonen, K.; Sprik, M.; Parrinello, M.; Car, R. *J. Chem. Phys.* **1993**, *99*, 9080.

[41] Bernas, A.; Ferradini, C.; Jay-Gerin, J.-P. *Chem. Phys.* **1997**, *222*, 151.

[42] Winter, B.; Faubel, M. *Chem. Rev.* **2006**, *106*, 1176.

[43] Elles, C. G.; Shkrob, I. A.; Crowell, R. A.; Bradforth, S. E. *J. Chem. Phys.* **2007**, *126*, 164503.

[44] Simon, J. D. *Acc. Chem. Res.* **1988**, *21*, 128.

[45] Lindner, J.; Unterreiner, A.-N.; Vöhringer, P. *ChemPhysChem* **2006**, *7*, 363.

[46] Lindner, J.; Unterreiner, A.-N.; Vöhringer, P. *J. Chem. Phys.* **2008**, *129*, 064514.

[47] Kambhampati, P.; Son, D. H.; Kee, T. W.; Barbara, P. F. *J. Phys. Chem. A* **2002**, *106*, 2374.

[48] Cavanagh, M. C.; Larsen, R. E.; Schwartz, B. J. *J. Phys. Chem. A* **2007**, *111*, 5144.

[49] Pimblott, S. M. *J. Phys. Chem.* **1991**, *95*, 6946.

[50] Boero, M.; Terakura, K.; Ikeshoji, T.; Liew, C. C.; Parrinello, M. *J. Chem. Phys.* **2001**, *115*, 2219.

[51] do Couto, P. C.; Estacio, S. G.; Cabral, B. J. C. *J. Chem. Phys.* **2005**, *123*, 054510.

[52] Millot, C.; Cabral, B. J. C. *Chem. Phys. Lett.* **2008**, *460*, 466.

[53] do Couto, P. C.; Chipman, D. M. *J. Chem. Phys.* **2010**, *132*, 244307.

[54] Olschewski, M.; Knop, S.; Lindner, J.; Vöhringer, P. *Angew. Chem. Int. Edt.* **2013**, *52*, 9634.

[55] Lagowski, J. J. *Pure Appl. Chem.* **1971**, *25*, 429.

[56] Dorfman, L.; Jou, F. In *Electrons in Fluids*; Jortner, J., Kestner, N., Eds.; Springer Berlin Heidelberg, 1973; pages 447–459.

[57] Edwards, P. P. *Science* **2011**, *333*, 49.

[58] Holleman, A. F.; Wiberg, N. *Lehrbuch der Anorganischen Chemie;* Walter de Gruyter: Berlin, 2007.

[59] Weyl, W. *Ann. Phys.* **1863**, *197*, 601.

[60] Kraus, C. A. *J. Am. Chem. Soc.* **1914**, *36*, 864.

[61] Gibson, G. E.; Argo, W. L. *Phys. Rev.* **1916**, *7*, 33.

[62] Birch, A. J. *J. Chem. Soc.* **1944**, page 430.

[63] Kirschke, E. J.; Jolly, W. L. *Inorg. Chem.* **1967**, *6*, 855.

[64] Schindewolf, U.; Vogelsgesang, R.; Böddeker, K. W. *Angew. Chem.* **1967**, *79*, 1064.

[65] Schindewolf, U. *Angew. Chem.* **1968**, *80*, 165.

[66] Keene, J. P. *Nature* **1963**, *197*, 47.

[67] Wardman, P. *Rep. Prog. Phys.* **1978**, *41*, 259.

[68] Téoule, R. *Int. J. Radiat. Biol.* **1987**, *51*, 573.

[69] Elliot, A. J.; Buxton, G. V. *J. Chem. Soc., Faraday Trans.* **1992**, *88*, 2465.

[70] Cline, J.; Takahashi, K.; Marin, T. W.; Jonah, C. D.; Bartels, D. M. *J. Phys. Chem. A* **2002**, *106*, 12260.

[71] Hatano, Y. *Radiat. Phys. Chem.* **2009**, *78*, 1021.

[72] Yang, J.; Kondoh, T.; Kan, K.; Yoshida, Y. *Nucl. Instr. and Meth. A* **2011**, *629*, 6.

[73] Winter, B.; Weber, R.; Widdra, W.; Dittmar, M.; Faubel, M.; Hertel, I. V. *J. Phys. Chem. A* **2004**, *108*, 2625.

[74] Muroya, Y.; Sanguanmith, S.; Meesungnoen, J.; Lin, M.; Yan, Y.; Katsumura, Y.; Jay-Gerin, J.-P. *Phys. Chem. Chem. Phys.* **2012**, *14*, 14325.

[75] Mozumder, A. *J. Phys. Chem. Lett.* **2011**, *2*, 2994.

[76] Kenney, G. A.; Walker, D. C. *J. Chem. Phys.* **1969**, *50*, 4074.

[77] Freeman, G. R. *Annu. Rev. Phys. Chem.* **1983**, *34*, 463.

[78] Sanguanmith, S.; Meesungnoen, J.; Muroya, Y.; Lin, M.; Katsumura, Y.; Jay-Gerin, J.-P. *Phys. Chem. Chem. Phys.* **2012**, *14*, 16731.

[79] Frongillo, Y.; Goulet, T.; Fraser, M.; Cobut, V.; Patau, J.; Jay-Gerin, J. *Radiat. Phys. Chem.* **1998**, *51*, 245.

[80] Plante, I. *Radiat. Environ. Biophys.* **2011**, *50*, 389.

[81] Pimblott, S. M.; Pilling, M. J.; Green, N. J. *Radiat. Phys. Chem.* **1991**, *37*, 377.

[82] Pimblott, S. M.; LaVerne, J. A. *J. Phys. Chem. A* **1997**, *101*, 5828.

[83] Sanguanmith, S.; Muroya, Y.; Meesungnoen, J.; Lin, M.; Katsumura, Y.; Kohan, L. M.; Guzonas, D.; Stuart, C.; Jay-Gerin, J.-P. *Chem. Phys. Lett.* **2011**, *508*, 224.

[84] Pshenichnikov, M. S.; BaltuÅ¡ka, A.; Wiersma, D. A. *Chem. Phys. Lett.* **2004**, *389*, 171.

[85] Long, F. H.; Lu, H.; Eisenthal, K. B. *J. Chem. Phys.* **1989**, *91*, 4413.

[86] Kimura, Y.; Alfano, J. C.; Walhout, P. K.; Barbara, P. F. *J. Phys. Chem.* **1994**, *98*, 3450.

[87] Sander, M. U.; Brummund, U.; Luther, K.; Troe, J. *J. Phys. Chem.* **1993**, *97*, 8378.

[88] Keszei, E.; Murphrey, T. H.; Rossky, P. J. *J. Phys. Chem.* **1995**, *99*, 22.

[89] Crowell, R. A.; Bartels, D. M. *J. Phys. Chem.* **1996**, *100*, 17713.

[90] Reuther, A.; Laubereau, A.; Nikogosyan, D. N. *J. Phys. Chem.* **1996**, *100*, 16794.

[91] Pepin, C.; Goulet, T.; Houde, D.; Jay-Gerin, J.-P. *J. Phys. Chem. A* **1997**, *101*, 4351.

[92] Siebbeles, L. D. A.; Emmerichs, U.; Hummel, A.; Bakker, H. J. *J. Chem. Phys.* **1997**, *107*, 9339.

[93] Hertwig, A.; Hippler, H.; Unterreiner, A.-N. *Phys. Chem. Chem. Phys.* **1999**, *1*, 5633.

[94] Hertwig, A.; Hippler, H.; Unterreiner, A.-N. *Phys. Chem. Chem. Phys.* **2002**, *4*, 4412.

[95] Lian, R.; Oulianov, D. A.; Shkrob, I. A.; Crowell, R. A. *Chem. Phys. Lett.* **2004**, *398*, 102.

[96] Zhang, T.; Lee, Y. J.; Kee, T. W.; Barbara, P. F. *Chem. Phys. Lett.* **2005**, *403*, 257.

[97] Lian, R.; Crowell, R. A.; Shkrob, I. A. *J. Phys. Chem. A* **2005**, *109*, 1510.

[98] Marsalek, O.; Elles, C. G.; Pieniazek, P. A.; Pluharova, E.; VandeVondele, J.; Bradforth, S. E.; Jungwirth, P. *J. Chem. Phys.* **2011**, *135*, 224510.

[99] Torres-Alacan, J.; Kratz, S.; Vöhringer, P. *Phys. Chem. Chem. Phys.* **2011**, *13*, 20806.

[100] Cady, H. P. *J. Phys. Chem.* **1897**, *1*, 707.

[101] Postl, D.; Schindewolf, U. *Ber. Bunsenges. Phys. Chem.* **1971**, *75*, 662.

[102] Walker, D. C. *Can. J. Chem.* **1967**, *45*, 807.

[103] Schindewolf, U.; Werner, M. *J. Phys. Chem.* **1980**, *84*, 1123.

[104] Werner, M.; Schindewolf, U. *Ber. Bunsenges. Phys. Chem.* **1980**, *84*, 547.

[105] Schindewolf, U.; Schwab, H. *J. Phys. Chem.* **1981**, *85*, 2707.

[106] Gross, W.; Schindewolf, U. *Ber. Bunsenges. Phys. Chem.* **1981**, *85*, 112.

[107] Schindewolf, U. *Ber. Bunsenges. Phys. Chem.* **1982**, *86*, 887.

[108] Telser, T.; Schindewolf, U. *Ber. Bunsenges. Phys. Chem.* **1984**, *88*, 488.

[109] Fisher, J. R.; Barnes, H. L. *J. Phys. Chem.* **1972**, *76*, 90.

[110] Elliot, A. J.; McCracken, D. R.; Buxton, G. V.; Wood, N. D. *J. Chem. Soc., Faraday Trans.* **1990**, *86*, 1539.

[111] Lepoutre, G.; Demortier, A. *Ber. Bunsenges. Phys. Chem.* **1971**, *75*, 647.

[112] Brooks, J. M.; Dewald, R. R. *J. Phys. Chem.* **1971**, *75*, 986.

[113] Anbar, M.; Hart, E. J. *J. Phys. Chem.* **1965**, *69*, 1244.

[114] Arai, S.; Sauer, M. C. *J. Chem. Phys.* **1966**, *44*, 2297.

[115] Dorfman, L. M.; Jou, F. Y.; Wageman, R. *Ber. Bunsenges. Phys. Chem.* **1971**, *75*, 681.

[116] Jou, F.-Y.; Freeman, G. R. *J. Phys. Chem.* **1979**, *83*, 2383.

[117] Quinn, R. K.; Lagowski, J. J. *J. Phys. Chem.* **1969**, *73*, 2326.

[118] Jou, F.-Y.; Freeman, G. R. *J. Phys. Chem.* **1981**, *85*, 629.

[119] Koehler, W. H.; Lagowski, J. J. *J. Phys. Chem.* **1969**, *73*, 2329.

[120] Hare, P. M.; Price, E. A.; Bartels, D. M. *J. Phys. Chem. A* **2008**, *112*, 6800.

[121] Son, D. H.; Kambhampati, P.; Kee, T. W.; Barbara, P. F. *J. Phys. Chem. A* **2001**, *105*, 8269.

[122] Belloni, J.; Cordier, P.; Delaire, J. *Chem. Phys. Lett.* **1974**, *27*, 241.

[123] Belloni, J.; Cordier, P.; Delaire, J. A.; Delcourt, M. O. *J. Phys. Chem.* **1978**, *82*, 537.

[124] Bartels, D. M.; Takahashi, K.; Cline, J. A.; Marin, T. W.; Jonah, C. D. *J. Phys. Chem. A* **2005**, *109*, 1299.

[125] Farhataziz.; Perkey, L. M.; Hentz, R. R. *J. Chem. Phys.* **1974**, *60*, 4383.

[126] Vogelsgesang, R.; Schindewolf, U. *Ber. Bunsenges. Phys. Chem.* **1971**, *75*, 651.

[127] Olinger, R.; Schindewolf, U.; Gaathon, A.; Jortner, J. *Ber. Bunsenges. Phys. Chem.* **1971**, *75*, 690.

[128] Olinger, R.; Hahne, S.; Schindewolf, U. *Ber. Bunsenges. Phys. Chem.* **1972**, *76*, 349.

[129] Steinmeyer, G. *J. Opt. A: Pure Appl. Opt.* **2003**, *5*, R1.

[130] Marin, T. W.; Takahashi, K.; Bartels, D. M. *J. Chem. Phys.* **2006**, *125*, 104314.

[131] Jou, F.-Y.; Freeman, G. R. *Can. J. Chem.* **1979**, *57*, 591.

[132] Nordlund, D.; Ogasawara, H.; Bluhm, H.; Takahashi, O.; Odelius, M.; Nagasono, M.; Pettersson, L. G. M.; Nilsson, A. *Phys. Rev. Lett.* **2007**, *99*, 217406.

[133] Jintana Meesungnoen, Jean-Paul Jay-Gerin, A. F.-M.; Mankhetkorn, S. *Radiat. Res.* **2002**, *158*, 657.

[134] Goulet, T.; Jay-Gerin, J.-P. *J. Chem. Phys.* **1992**, *96*, 5076.

[135] Madsen, D.; Thomsen, C. L.; Thogersen, J.; Keiding, S. R. *J. Chem. Phys.* **2000**, *113*, 1126.

[136] Williams, F.; Varma, S. P.; Hillenius, S. *J. Chem. Phys.* **1976**, *64*, 1549.

[137] Krohn, C. E.; Thompson, J. C. *Phys. Rev. B* **1979**, *20*, 4365.

[138] Coe, J. V.; Earhart, A. D.; Cohen, M. H.; Hoffman, G. J.; Sarkas, H. W.; Bowen, K. H. *J. Chem. Phys.* **1997**, *107*, 6023.

[139] Engel, V.; Schinke, R.; Staemmler, V. *J. Chem. Phys.* **1988**, *88*, 129.

[140] Kratz, S. *Online-Publikationen an deutschen Hochschulen, Bonn, Univ., Dissertation* **2013**, *urn:nbn:de:hbz:5n-32759*.

[141] Schäfer, T.; Lindner, J.; Vöhringer, P.; Schwarzer, D. *J. Chem. Phys.* **2009**, *130*, 224502.

[142] Schäfer, T.; Schwarzer, D.; Lindner, J.; Vöhringer, P. *J. Chem. Phys.* **2008**, *128*, 064502.

[143] Schwarzer, D.; Lindner, J.; Vöhringer, P. *J. Phys. Chem. A* **2006**, *110*, 2858.

Part II

Results and Discussion

3

Femtosecond Two-Photon Ionization and Solvated Electron Geminate Recombination in Liquid-to-Supercritical Ammonia

Janus Urbanek, Annika Dahmen, Joel Torres-Alacan, Peter Königshoven, Jörg Lindner, and Peter Vöhringer*

Abteilung für Molekulare Physikalische Chemie, Institut für Physikalische und Theoretische Chemie, Rheinische Friedrich-Wilhelms-Universität, Wegelerstr. 12, 53115 Bonn, Germany

Urbanek, J.; Dahmen, A.; Torres-Alacan, J.; Königshoven, P.; Lindner, J.; Vöhringer, P. *J. Phys. Chem. B* **2012**, *116*, 2223–2233.

* To whom correspondence should be addressed. Email: p.voehringer@uni-bonn.de

3.1 Abstract

The first-ever femtosecond pump-probe study is reported on solvated electrons that were generated by multi-photon ionization of neat fluid ammonia. The initial ultrafast ionization was carried out with 266 nm laser pulses and was found to require two photons. The solvated electron was detected with a femtosecond probe pulse that was resonant with its characteristic near-infrared absorption band around 1.7 μm. Furthermore, the geminate recombination dynamics of the solvated electron were studied over wide ranges of temperature (227 K $\leq T \leq$ 489 K) and density (0.17 g cm^{-3} $\leq \rho \leq$ 0.71 g cm^{-3}), thereby covering the liquid and the supercritical phase of the solvent. The electron recombines in a first step with ammonium cations originating from the initial two-photon ionization thereby forming transient ion-pairs ($e^-_{am} \cdot NH^+_4$), which subsequently react in a second step with amidogen radicals to reform neutral ammonia. The escape probability, i.e., the fraction of solvated electrons that can avoid the geminate annihilation, was found to be in quantitative agreement with the classical Onsager theory for the initial recombination of ions. When taking the sequential nature of the ion-pair-mediated recombination mechanism explicitly into account, the Onsager model provides a mean thermalization distance of 6.6 nm for the solvated electron, which strongly suggests that the ionization mechanism involves the conduction band of the fluid.

3.2 Introduction

In the recent decades, solvated electrons have raised considerable experimental and theoretical research activities, primarily devoted to understanding their spectroscopic properties, their reactivity, and their interactions with a molecular environment on ultrafast time scales. More specifically, coupled electron-solvent dynamics involve phenomena such as charge localization and delocalization, solvation and thermalization, or reactive and nonreactive electron-solvent scattering including charge transfer, all of which are important aspects in radiation chemistry.[1] The majority of the research devoted to timeresolving such dynamical processes focused on the solvated electron in liquid water[2] where it can be readily prepared via pulse radiolysis or laser-induced multi-photon ionization.

Historically, the solvated electron was first discovered in liquid ammonia (see e.g., Ref. 3 and references therein) where it can be prepared chemically by directly dissolving neat alkali metals into the solvent. However, the ultrafast electron-solvent dynamics in liquid ammonia are much less understood compared to those of the hydrated electron. This is because the preparation of metal-ammonia samples with long-term stabilities and linear optical properties that are suitable for dynamic spectroscopies is not at all trivial. Consequently, experimental studies employing time-resolved optical probing of the ammoniated electron in the bulk liquid are rather scarce.

Central to the existence of solvated electrons are questions related to the very nature of the binding motif of the excess charge to the molecular liquid environment.[4] Is the solvated electron best described as a polaron-like entity occupying a cavity structure within the liquid or is it more appropriately represented as a negatively charged and solvated cluster of molecules over which the total spin density is diffusely distributed?

To address this issue in a systematic fashion, experiments were first performed in supersonic expansions of NH_3. Haberland and co-workers were able to prepare and detect singly negatively charged ammonia clusters using mass spectrometry and to determine their cluster size distribution.[5] Shortly thereafter, photoelectron spectroscopy (PES) was conducted on size selected negatively charged $(NH_3)_n^-$ clusters to determine the vertical detachment energy (*VDE*) as a function of the cluster size. By extrapolation, it was possible to determine the electron binding energy for infinitely large clusters, which in turn should correspond approximately to the photoelectric threshold energy (*PET*) for the bulk liquid ($\sim$1.25 eV), i.e., the minimum energy required to remove a fully thermalized solvated electron from the bulk liquid into the vacuum.[6,7] Photoionization experiments with a tunable laser were carried out by Schulz, Hertel, and coworkers on neutral ammonia clusters that were doped with a single atom of sodium.[8,9] The ion yield spectra were used to extract the ionization potential of the $Na(NH_3)_n$ species, which extrapolated for $n \rightarrow \infty$ roughly to the PET of liquid ammonia extracted from the PES experiments on $(NH_3)_n^-$.

Time-resolved spectroscopies on such gas-phase ammonia clusters were initiated by Schulz and Hertel, who developed femtosecond pump-probe spectroscopy with photoelectron-photoion coincidence detection thereby giving access to the dynamics in the excited states of neutral $(NH_3)_n$ species[10]

and their sodium doped counterparts,[11] $Na(NH_3)_n$. For the metal-ammonia clusters, rates for energy redistribution from the sodium chromophore to the internal vibrations of the solvent molecules were retrieved as a function of the cluster size. While these dynamics occurred on a nanosecond time scale for a simple $Na-NH_3$ heterodimer, they accelerated drastically into the subpicosecond time scale upon adding additional ammonia molecules to the cluster. Finally, Zewail and co-workers carried out pump-probe PES on singly anionic $(NH_3)_n^-$ clusters and observed a 500 fs structural relaxation that was driven by the ultrafast optical excitation and the subsequent internal conversion back to the electronic ground state.[12] The body of these gas phase experiments has led to the general concensus that the size-selected clusters (either their undoped anionic forms or their Na-doped neutral forms) can be viewed as embryonic models of the ammoniated electron in the bulk liquid.[6,7]

As alluded to above, time-resolved spectroscopy on the ammoniated electron in the liquid phase is extremely difficult for technical reasons. Nevertheless, Huppert et al. as well as Belloni et al. reported independently on picosecond pump-probe measurements on metal-ammonia solutions more than 35 years ago.[13,14] Because of an insufficient time-resolution, it was impossible to accurately extract the coupled electron-solvent dynamics following a resonant optical excitation of the ammoniated electron. These remained the only studies until very recently, when our own group[15,16] was finally able to fully time-resolve the spectro-temporal evolution in the near-infrared spectral region of the ammoniated electron from metal-ammonia solutions by optically exciting it with femtosecond pulses at 1300 nm. The data clearly revealed the quasi-prompt nature of an initial nonadiabatic transition that is followed by a subsequent thermal-structural relaxation of the coupled electron-solvent system within less than 200 fs.

Early theoretical work on the ammoniated system was initiated by Jortner who used a simple polaron model to understand the spectral position of the solvated electron resonance and its temperature dependence.[17] More refined path integral molecular simulations were then carried out by Barnett et al. as well as by Klein and co-workers to complement the experimental cluster studies[18–20] and to understand from an atomistic point of view structural and dynamical aspects of electron localization and solvation in ammonia.[21–26] Finally, using density functional theory, the adequacy of representing the ammoniated electron as a solvent stabilized multimer radical anion has been

discussed in the context of nuclear magnetic resonance data.[27]

In this work, we present the first-ever experimental study of ammoniated electrons generated by femtosecond multi-photon ionization of bulk fluid ammonia. While multi-photon ionization has been used extensively to generate hydrated electrons and to investigate their ensuing chemical reactions,[28–41] no such photochemical data are available for ammoniated electrons. We will focus here on the ionization mechanism as well as on the dynamics of geminate recombination. A special emphasis is put on the so-called escape probability. This quantity is equal to the fraction of electrons initially created by the ionization pulse that is able to avoid a reactive encounter with the geminate counter fragments. The escape probability will finally be discussed in the framework of Onsager's classical theory for the initial recombination of ions.[42]

3.3 Experimental Section

The experimental setup was a slightly modified version of that used in a previous experiment[39] and will therefore be described only briefly. Femtosecond transient absorption measurements were carried out using a home-built 1 kHz Ti:sapphire regenerative chirped pulse amplifier as a front-end to an ultraviolet (UV)-pump and near-infrared (IR)-probe spectrometer. The front-end delivered 800 nm pulses with a duration of 150 fs and an energy of 750 μJ that were split by a 50% dielectric beam splitter. One part of the fundamental was frequency doubled in a 1 mm BBO crystal (type I), and the resulting second harmonic was then sum-frequency mixed with the residual fundamental in a 0.4 mm type I-BBO crystal to obtain 266 nm UV-pulses that were used for photoionization of fluid ammonia. The other 50% fraction of the front-end's fundamental output was used to pump an optical parametric amplifier (OPA, TOPAS, Light Conversion) to provide femtosecond near-IR pulses tunable between 1200 nm and 2400 nm. The signal (or idler) pulses of the OPA were divided by a dielectric beam splitter into probe and reference pulses, both of which were focused into the sample using a 45° off-axis aluminum mirror with a focal length of 100 mm. The pump beam was focused with a fused silica lens (400 mm focal length) and was spatially overlapped inside the sample with the probe pulses at an angle of 5°. The pump beam radius directly at the sample was 460 μm, whereas that of the probe beam was 240 μm. The

pump pulse irradiance in front of the sample cell was roughly 30 GW cm^{-2}. After passing through the cell, probe and reference pulse intensities were detected by PbS-photoresistors whose electrical signals were fed into gated integrators. The pump could be adjusted by a combination of a half-wave retardation plate and a polarizer without changing the diameter of the beam and the probe beam was attenuated by neutral density filters.

We investigated the geminate recombination kinetics over a wide temperature and density range, as illustrated in the phase diagram of ammonia (see Figure 3.1). The experiments were organized into a measurement series carried out along the 300 bar-isobar (see solid circles, Figure 3.1) and another one along the supercritical 423 K-isotherm (open circles). The pressure and temperature dependent density was calculated using the PROPATH program package.[43] The temperature and density dependent dielectric constant of ammonia was taken from ref 44. Samples of pure NH_3 (99.98%, Linde) were prepared in a stainless steel high-temperature and high-pressure optical cell described in detail previously.[45–47] The entire high pressure system was purged with liquid CO_2 and subsequently evacuated to remove all traces of impurities such as water. The windows were cleaned with acetone prior to assembly of the cell. Its optical path length was 1.0 mm and 2.5 mm thick sapphire substrates were employed as windows. We upgraded the cell by an external cooling jacket to extend our measurements to cryogenic temperatures. No permanent photodamage or changes in the kinetics were observed upon continuously photolyzing the sample for several hours. Furthermore, the kinetics remained invariant to changes of the pump beam irradiance between 15 GW cm^{-2} and 40 GW cm^{-2}. The recombination dynamics were recorded in a time window of altogether 800 ps in which 350 data points were acquired. At each data point, an average over 400 pump/probe cycles was calculated.

3.4 Results and Discussion

3.4.1 Solvated Electron Formation and Decay

Irradiation of fluid ammonia with 266 nm light pulses generates a transient species that is characterized by a very broad absorption spectrum in the near-infrared (NIR). As shown in Figure 3.2, this near-IR resonance is very similar in spectral shape and position to the linear absorption spectrum of solvated

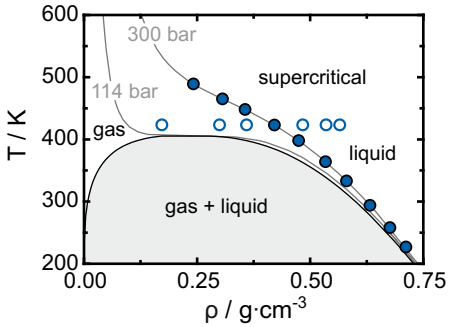

Figure 3.1: Phase diagram of ammonia. The gray-shaded area corresponds to the liquid-vapor coexistence region as defined by the liquid-vapor binodal (black solid curve). The gray curves display two representative isobars. CP is the critical point at 112.8 bar, 405.4 K, and 0.235 g cm^{-3}. The symbols represent the thermodynamic conditions at which kinetic experiments were carried out.

electrons that are generated chemically by dissolving an alkali metal such as sodium in liquid ammonia.[15,16] There can be no doubt that the species generated photolytically from the neat solvent at 266 nm carrying the strong and broad near-IR spectroscopic transition is identical to the chemically generated ammoniated electron from metal-ammonia solutions.

It is well-known that photoionization of neat liquids prepares excess electrons in a nonequilibrium configuration. The ensuing relaxation processes leading to a fully localized and thermalized solvated electron by structural rearrangements and thermal cooling of the solvent shell give rise to a dynamic blue shift of the solvated electron's optical resonance.[15,16,32,34] Therefore, the spectro-temporal evolution in the mid-to-near-IR at early times will inevitably contain contributions arising from these solvation and cooling dynamics. Such contributions can, however, be disentangled from the recombination kinetics by optically probing the system exclusively on the highfrequency edge or on the maximum of the stationary absorption spectrum of the solvated electron, i.e., by tuning the probe pulses to detection wavelengths that are shorter than or equal to the wavelength of maximal stationary absorbance of the solvated electron at the current temperature and density of the experiment.[39] In that case, thermal cooling and/or solvent reorganization can only result in a temporal rise of the absorbance, while a temporal decay is unequivocally related to a time-dependent loss of solvated electrons, i.e., to the decay of the solvated

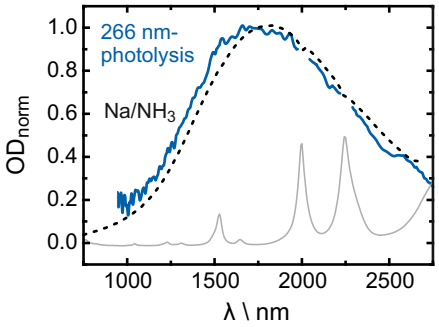

Figure 3.2: Comparison of the absorption spectrum of liquid ammonia upon 266 nm photolysis (solid curve, $T = 295\,\mathrm{K}$, $p = 300\,\mathrm{bar}$, $\rho = 0.631\,\mathrm{g\,cm^{-3}}$, recorded 400 ns after excitation) with an absorption spectrum of a metal-ammonia solution (dashed curve, $T = 295\,\mathrm{K}$, $p = 9.07\,\mathrm{bar}$, $\rho = 0.608\,\mathrm{g\,cm^{-3}}$, see Ref. 16). The gray curve represents a scaled absorption spectrum of the pure solvent, which is dominated in this spectral region by strong NH-stretching vibrational overtones and combination bands. The spectrum obtained by photolysis peaks at roughly 1760 nm, while that of the metal ammonia solution is maximal at 1820 nm. The small relative shift between the ammoniated electron absorption bands is due to the different pressure and density.

electron population by virtue of their recombination with reactive fragments in the fluid.

Therefore, prior to carrying out femtosecond experiments on the recombination dynamics, detailed information is required on the spectral position of the ammoniated electron's absorption band as a function of temperature and density. Fortunately, throughout almost the entire temperature and density range studied here, such data are available from experiments conducted by Schindewolf and co-workers many years ago.[48–50] Interestingly, at high temperatures and pressures, the stationary absorption of ammoniated electrons is reported to be barely sensitive to the thermodynamic conditions. At $T \geq 294\,\mathrm{K}$, our probe wavelength was set to 1760 nm, whereas for lower temperatures the probe pulses had to be tuned to 1450 nm.

A representative pump-probe signal obtained by photoexcitation of neat ammonia with 266 nm pulses and probing in the near-IR at 1450 nm is shown in Figure 3.3 (top). Under all conditions, the pump-induced optical density, $\Delta OD(t)$, consisted of an instrument-limited rise of a transient absorption that was followed by a slower decay. The observation of a temporally unresolved rise is consistent with a time constant of 150 fs for the relaxation dynamics that follow an optical (s-to-p type) excitation of fully thermalized solvated elec-

trons in metal ammonia solutions.[15,16] The slower decay is indicative of the recombination loss of solvated electrons with increasing time delay. A careful inspection of the signal indicates that these features were superimposed on an artifactual signal contribution, which we could unambiguously assign to a pump-induced absorption in the window of the sample cell. Therefore, for each pump-probe experiment on fluid ammonia, a second complementary experiment had to be carried out on the emptied cell. The undistorted response of the ammoniated electron, $\Delta\Delta OD(t)$, was then retrieved by simply subtracting the two data sets as demonstrated in Figure 3.3 (bottom). This approach is identical to that applied previously in our study of the geminate recombination of solvated electrons in liquid-to-supercritical water.[39] A peak amplitude of this window component of $\sim$10% relative to the electron contribution was seen regardless of the probe wavelength used for the experiment. Note that the window contribution was also much smaller than in our previous studies on the hydrated electron.[39] Finally, the quality of the subtraction procedure can be assessed from the rising edge of the pure electron signal (cf. Figure 3.3, bottom).

It is also important to emphasize at this point that the focus here is solely on the peak signal amplitude, which is directly linked to the ionization mechanism, and on the decay of the signal, which is exclusively related to the loss of solvated electrons due to recombination reactions. The highest pump-induced optical density ever observed in our experiments was 0.16. Using an extinction coefficient of the solvated electron in ammonia[51] $4.9 \times 10^4\,\mathrm{M^{-1}\,cm^{-1}}$, an average concentration of $3.5 \times 10^{-5}\,\mathrm{M}$ can be estimated. Furthermore, the decay seen in Figure 3.3 occurs on a time scale below 1 ns. On such short time scales and at such low concentrations, the apparent recombination dynamics are undoubtedly geminate in nature. This is further supported by the long-time plateau of the pump-induced optical density. In other words, the electron reacts with fragments that originate from the same ionization site. A fraction of solvated electrons is, however, able to escape from this initial annihilation and to diffuse away into the bulk. This fraction represents a solvated electron population that appears quasi-stationary on the subnanosecond time scale of the experiment and becomes apparent as an asymptotic pump-induced absorption for long pump-probe delays. Nongeminate recombination of solvated electrons in liquid ammonia is temporally very well separated from the

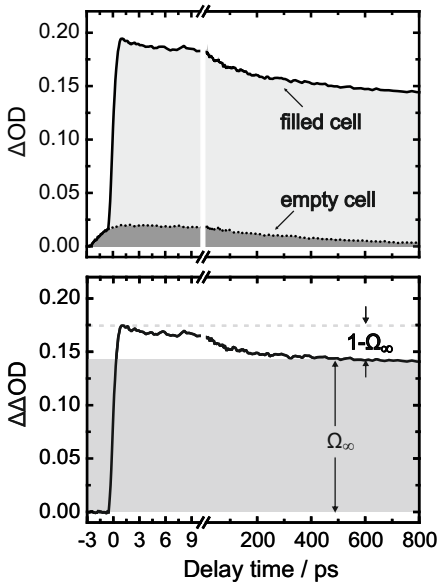

Figure 3.3: Top: Pump-probe signal of liquid ammonia (solid curve, $p = 300\,\text{bar}$, $\rho = 0.68\,\text{g cm}^{-3}$) and of the empty cell (dashed curve). The excitation wavelength was 266 nm, the probe wavelength was 1450 nm, and the temperature was 258 K in both cases. Bottom: Induced optical density difference, $\Delta\Delta OD$, obtained from the two measurements. The escape probability, Ω_∞(258 K, 0.68 g cm^{-3}) can be deduced from the maximal and long-time values of $\Delta\Delta OD$.

geminate recombination and occurs in a homogeneous second-order reaction on time scales well in excess of 1 ns extending even into the microsecond regime.[52–55]

Geminate recombination is commonly characterized by the time-dependent survival probability, $\Omega(t)$, that corresponds to the fraction of solvated electrons still being present at a time, t, subsequent to the ionization event at $t = 0$. Assuming that the recombination and thermal equilibration dynamics are sufficiently separated in time, $\Omega(t)$ is immediately obtained from the ratio of the time-dependent induced absorption, $\Delta\Delta OD(t)$, to the peak induced absorption at early delays, $\Delta\Delta OD_{max}$. The asymptotic limit of this ratio for long pump-probe delays is accordingly referred to as geminate escape (or survival) probability, Ω_∞, as shown in Figure 3.3.

3.4.2 PHOTOIONIZATION MECHANISM

To understand the photophysical processes responsible for the appearance and subsequent disappearance of solvated electrons following the UV irradiation of ammonia, it is of paramount importance to establish the number of photons involved in the primary matter-field interaction. The concentration of photolytically generated electrons is expected to increase with the n-th power of the pump irradiance where n photons simultaneously interact with the medium in the rate-limiting ionization step.[31] To establish this number, n, for the 266 nm photoionization of ammonia, the peak value of the induced optical density, $\Delta\Delta OD_{max}$, was determined for various pump pulse irradiances, I, at the sample. The peak induced optical density is a direct measure of the initially prepared solvated electron concentration prior to recombination and is unaffected by the solvation and thermalization dynamics.

Figure 3.4 displays a double-logarithmic representation of $\Delta\Delta OD_{max}$ as a function of I, where the irradiance is normalized to a value of 40 GW cm^{-2} corresponding to the maximum pump intensities achieved in our experiments. The data closely follow a straight line having a slope of 1.89 $\pm$ 0.10, indicating that the photoejection process requires two photons, i.e., the matter-field interaction is a two-photon ionization. Two simultaneous photons with a wavelength of 266 nm have a total ionization energy of 9.3 eV. The slight deviation from the ideal slope of 2 can be attributed to inaccuracies of the correction for the window artifact, which becomes increasingly difficult with diminishing irradiance.

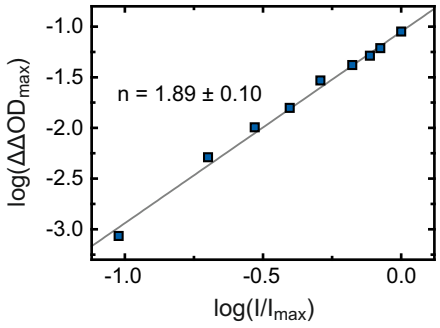

Figure 3.4: Dependence of the induced absorption of the ammoniated electron on the normalized pump-pulse intensity in a double-logarithmic plot. The data were recorded at a temperature of 294 K and a density of 0.63 g cm^{-3}. The straight line corresponds to a linear fit with a slope of 1.89.

The electronic structure of polar liquids like water and ammonia can be understood conceptually in terms of a lone-pair amorphous semiconductor[56,57] in which short-range orientational order permits the merging of intermolecularly interacting nonbonding orbitals into a completely filled valence band. The latter is separated by a large energy gap from the conduction band, i.e., a continuum of quasi-free states, in which excess electrons are delocalized over many molecules in the liquid network.[56,57] A detailed discussion of the energetics relevant to the formation of solvated electrons is given by Bowen and co-workers[58] as well as Elles et al.[59] for the specific case of water.

In bulk liquid H_2O, the *VDE* corresponding to the most probable transition energy from the valence band to the ionization continuum is reported[60] to be 11.1 eV, while the photoelectric threshold, *PET*, corresponding to the minimal energy at which there is a sufficient spatial wave function overlap allowing for the detection of photoelectrons is 9.9 eV.[36] Vertical photoionization and vibrationally assisted autoionization of water[30] at such energies generate initially electrons within the conduction band, which delocalize on a time scale of less than 500 as.[61] Asymmetric or broken hydrogen-bond geometries present trapping sites for the electron, thereby serving as precursors for the fully solvated hydrated electron. Consistent with the delocalized nature of conduction band electrons, the average distance migrated before the electron becomes fully localized and thermalized is denoted ejection length (or equivalently, thermalization distance). At such excitation energies, it is typically of the order of 4 nm in water.[31,62,63]

However, energies as low as 6.5 eV have been reported in the literature as threshold for the production of hydrated electrons in the bulk liquid, i.e., well below the *PET*.[64,65] Apparently, the photo-induced generation of solvated electrons can also involve solvent nuclear motions thereby bypassing the conduction band. Currently, a proton-coupled electron transfer and the ballistic hot H-atom mechanism are discussed.[30,37,39,41,65] Both mechanisms result in much smaller ejection lengths of around 1 nm.[36,41]

For ammonia, the energetics are significantly different.[66] All of the ammonia electronically excited states are of Rydberg character due to the promotion of an electron from the highest occupied lone-pair orbital connected with a geometry change from pyramidal (C_{3v}) to planar (D_{3h}). As a result, the absorption bands of ammonia in the gas phase are dominated by pronounced progressions in the ν_2 umbrella mode of NH_3.[67,68] The lowest excited state $(\tilde{A}^1A_2'')$

has its origin at 5.74 eV, and is, like many of the other excited states, predissociative leading predominantly to ground state NH_2 $(\tilde{X}^2B_1)$ and hydrogen atoms.[69] The *VDE* of an isolated molecule in the gas phase is 10.85 eV;[70] however, the adiabatic ejection of a photoelectron into the vacuum is possible via autoionization down to 10.07 eV.[71,72]

Experimental data pertaining to the energetics of the condensed phases of ammonia are scarce. In a theoretical study comprising sequential molecular dynamics simulations and density functional theory, Almeida et al. estimated the *VDE* of the liquid to be (9.7 ± 0.7) eV.[73] The energetic lowering of about 1 eV on entering the liquid was attributed to polarization effects and hydrogen bonding. A more reliable value for the *VDE* of 9.4 eV has been deduced from a recent photoelectron spectrum by Lindblad et al. on large ammonia clusters, $(NH_3)_n$, with a mean size of $n \approx 1600$ molecules/cluster.[74] Their spectrum also provides an upper limit for the *PET* of roughly 8 eV. If one takes into account a polarization-induced stabilization of the excess electron in the conduction band of ammonia of about 0.2 eV relative to the vacuum (i.e., similar to water, see Ref. 75), one arrives at a *VDE* of about 9.2 eV and at an upper limit for the onset of direct ionization of approximately 7.8 eV in the condensed phase. Of course, this estimate assumes that the existing cluster data are already converged to the true bulk phase values.[7,73]

Here, we report on ammoniated electrons that were generated photolytically using 266 nm laser pulses. The pump intensity dependence of the solvated electron's induced absorption indicated that the total photoionization energy in our experiments is 9.3 eV corresponding to two photons at 266 nm. This energy is very similar to the above estimate for the most probable transition energy for a vertical ionization of the fluid and certainly exceeds the above estimate of the *PET* of ammonia. Consequently, one can conclude that the underlying mechanism for photoejection is either direct vertical ionization or autoionization, both of which involve the intermediate formation of conduction band electrons having a delocalized character. There is no need for invoking mechanisms that bypass the conduction band as in the case of water for ionization energies below the band gap.

The hole remaining at the ionization core is an ammonia cation, NH_3^+, which has been reported to rapidly transfer a proton in the gas phase to a neutral ammonia molecule thereby forming an ammonium cation, NH_4^+, and the

amidogen radical, NH_2.[76] The net result of the photoexcitation process is thus

$$2NH_3 + 2\,h\nu \longrightarrow e^-_{am} + NH_2 + NH_4^+ \tag{3.1}$$

in correspondence to Ref. 54 and in analogy to water, where the photoionization at 9.3 eV generates hydroxyl radicals and hydronium cations as side products. Whereas the two primary molecular fragments will be produced in close proximity to the ionization site in the fluid, the electron will become localized at a remote location due to its intrinsic high mobility as a conduction band electron. Quasi-free electron states in polar media have been investigated in dense vapors, where excess electrons do not become solvated but prevail as highly mobile, delocalized species. On the basis of these results, the mobility of excess electrons in ammonia is significantly larger than in water at the same temperature.[77] Recalling the ejection lengths in water for ionization energies above the *VDE*,[36] thermalization distances in excess of 4 nm can be expected for solvated electrons generated in ammonia by two-photon-ionization at 266 nm.

3.4.3 Temperature and Density-Dependent Geminate Recombination

A representative selection of the pump-probe traces obtained at different thermodynamic conditions is presented in Figure 3.5. To facilitate a comparison, the induced absorption was normalized to its peak value and is hereafter referred to as $\Delta\Delta OD_{\mathrm{norm}}(t)$. As before, all traces exhibit the instrument-limited rise at early times indicating that the primary thermalization dynamics of the solvated electron retain their subpicosecond character throughout the entire thermodynamic range covered in this work, i.e., from the dense cryogenic liquid all the way up to the dilute supercritical fluid. Furthermore, it can be seen that the subsequent decay of $\Delta\Delta OD_{\mathrm{norm}}(t)$ to its asymptotic offset is complete within several 100 ps; however, it appears as if the decay is accelerated upon increasing the temperature or decreasing the density. This finding is consistent with our recent report on the geminate recombination dynamics of the solvated electron in liquid-to-supercritical water.[39]

From each individual kinetic trace, the geminate escape probability was calculated as an arithmetical mean of $\Delta\Delta OD_{\mathrm{norm}}(t)$ over the delay interval

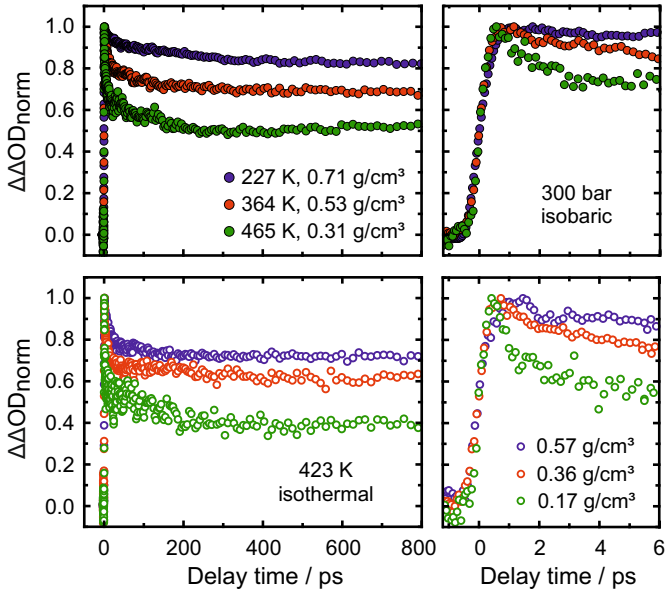

Figure 3.5: Temperature and density-dependent kinetic traces of the ammoniated electron recorded along the 300 bar isobar (top panels) and along the 423 K isotherm (bottom panels). The probe wavelength was 1450 nm for 227 K and 1760 nm for 364 K, 423 K and 465 K, respectively.

between 400 ps and 800 ps. At a temperature of 227 K and a solvent density of 0.71 g cm^{-3}, the escape probability, Ω_∞, assumes a value of 89%, i.e., only 11% of the initially produced electrons are able to recombine in a geminate fashion. Upon isobarically heating the sample, the escape probability decreases markedly to 76% at 294 K and assumes a value of only 45% at a supercritical temperature of 489 K. Note that this temperature rise by about a factor of 2 is accompanied by a reduction of the solvent density of roughly a factor of 3. To disentangle in a systematic fashion, the density dependence of the escape probability from the temperature dependence, a complementary series of pump-probe experiments was conducted along the supercritical 423 K isotherm (see Figure 3.5, bottom row) thereby allowing for a variation of the density by more than a factor of 3. Again, the value of Ω_∞ decreases from 73% at a density of 0.57 g cm^{-3} to about 40% at an almost vapor-like density of 0.17 g cm^{-3}. The complete temperature and density-dependence of the escape probability is summarized in Figure 3.6.

At the highest densities ($\rho \geq 0.7$ g cm^{-3}), a very large fraction of ammoniated electrons of up to 90% is able to escape from geminate recombination.

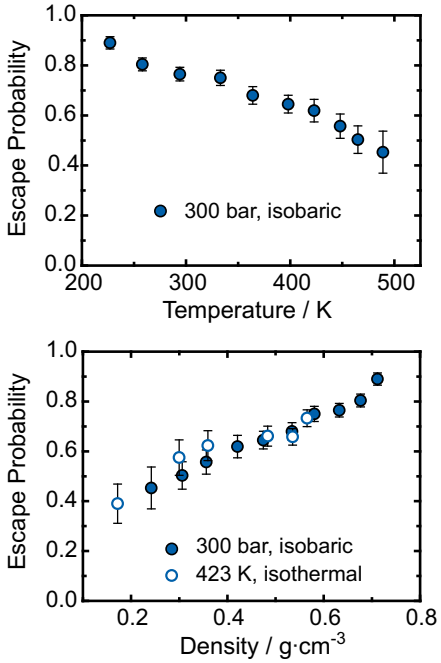

Figure 3.6: Temperature (top panel) and density (bottom) dependence of the escape probability for solvated electrons generated by 266 nm two-photon ionization of neat ammonia.

For comparison, in liquid water, the highest escape yields of hydrated electrons ever observed at an ionization energy of 9.3 eV were only about 70%.[35] Although at a higher temperature (600 K), survival probabilities even as low as 15% have been detected in water at similar densities around 0.7 g cm^{-3}.[39] The dynamics of geminate recombination of solvated electrons in fluid ammonia subsequent to photoionization has not been studied so far. However, a number of nanosecond pulse radiolysis experiments[53–55,78–83] have been reported according to which the decay of the ammoniated electron can be traced back exclusively to the reaction with the amidogen radical,

$$e^-_{am} + NH_2 \longrightarrow NH_2^- . \tag{3.2}$$

Reaction 3.2 was found to be diffusion-controlled.[52,84] In other words, the reaction of the solvated electron with NH_2 radicals under formation of the amide anion features no significant energy barrier, and consequently, every encounter between the two particles is reactive. In this case, the temperature and density dependence of the reaction rate is governed by the diffusion

coefficients of the recombining particles. Nevertheless, an anomalously large primary electron yield was reported,[79,80] which was attributed to the poor efficiency of the alternative recombination pathway

$$e^-_{am} + NH^+_4 \longrightarrow NH_3 + H. \tag{3.3}$$

This interpretation was further corroborated by a stopped-flow measurement of the kinetics of the reaction 3.3 using solvated electrons from a metal ammonia solution on the one hand and ammonium cations from a solution of NH_4Br in liquid ammonia on the other.[85] At 223 K, the measured second-order rate constant for reaction 3.3 is $1.2 \times 10^6\,M^{-1}\,s^{-1}$, which is several orders of magnitude smaller than the calculated diffusion limit of $5.0 \times 10^{11}\,M^{-1}\,s^{-1}$.[52,85] A lower limit for the reaction barrier can be estimated from thermochemical data published by Schindewolf[86] according to whom the reaction enthalpy for reaction 3.3 is +30 kJ/mol, while the reaction entropy is -12 J/mol K. Thus, the charge neutralization is not only endothermic but in the temperature range studied here, also endergonic by at least 33 kJ/mol! Therefore, the charge neutralization reaction can safely be neglected.[84]

Our finding of surprisingly large escape probabilities as compared to water is in qualitative agreement with these early radiolysis studies. However, the pronounced dependence of Ω_∞ on temperature and density seemingly contradicts the conclusions from Ref. 80 according to which the radiolytical yield is more or less insensitive to temperature changes along the liquid branch of the liquid-vapor binodal between 198 K and 296 K (i.e., for the liquid held under saturation pressure). The apparent contradiction between photolysis and radiolysis is most likely due to the different ionization conditions. Pulse radiolysis with badly defined ionization energies above hundreds of keV is well-known to yield significantly broader spatial electron distributions[1] as well as molecular radicals and ionic fragments from secondary spur reactions[87] that cannot occur in multi-photon ionization at a well-defined energy. Therefore, it might not be so surprising that the recombination kinetics of these two distinct approaches differ with respect to their dependence on the thermodynamic state variables.

Although the ammonium cation does not directly annihilate the ammoniated electron, it enhances the diffusional drift of the electron toward the dipolar radical. This is because shortly after ionization, the two geminate frag-

ments, NH_2 and NH_4^+, are still in close spatial proximity, while the electron is located farther away due to the involvement of the solvent's conduction band during ionization. Whereas the reactivity of the electron is essentially defined through its interaction with the dipole, its diffusional drift is governed by the interaction with the cation simply because at any given separation, the Coulomb attraction between e^-_{am} and NH_4^+ outweighs the charge-dipole attraction between e^-_{am} and NH_2. Furthermore, the latter interaction is likely to be obscured by the presence of the overwhelming ammonia solvent dipoles. Consequently, the geminate recombination processes should be described more adequately by the following sequence of events:[54]

$$e^-_{am} + NH_4^+ \rightleftharpoons (e^-_{am} \cdot NH_4^+) \tag{3.4}$$

$$(e^-_{am} \cdot NH_4^+) + NH_2 \longrightarrow NH_2^- + NH_4^+. \tag{3.5}$$

The existence of ion-pairs, $(e^-_{am} \cdot NH_4^+)$, has been deduced from early studies of the absorption spectrum of solvated electrons in metal-ammonia solutions and its dependence on the sample composition.[88] Jou and Freeman[89] have compared such concentration-dependent spectra with those obtained from pulse radiolysis and concluded that the formation of the ion-pair does not alter the electronic resonance significantly. Therefore, the direct recombination of the ammoniated electron with the amidogen radical according to reaction 3.2 and the consecutive recombination following reactions 3.4 and 3.5 are indistinguishable by optical absorption spectroscopy.

3.4.4 Comparison with Onsager's Escape Probability.

In the absence of external forces, the probability for two ions of opposite charge overcoming their mutual Coulomb attraction, $V(r_0)$, by thermal excitations at the temperature, T, is given by the reciprocal of the Boltzmann factor[42]

$$\Omega_\infty(r_0) = exp(V(r_0)/k_BT) = exp(-r_c/r_0) \tag{3.6}$$

wherer r_0 denotes the initial separation, and k_B is Boltzmann's constant. The Coulomb energy,$V(r_0)$, is equal to the thermal energy, k_BT, at the Onsager radius, $r_c = e^2/(4\pi\epsilon\epsilon_0 k_BT)$, when the solvent continuum has a dielectric permittivity of ϵ relative to that of the vacuum, ϵ_0. Notice that the escape probability depends not only on the temperature explicitly but also in an im-

plicit fashion through the temperature dependence of the solvent's dielectric constant. Furthermore, even at constant temperature, ϵ is also a function of the density of the solvent. Taken together, $\epsilon = \epsilon(T, \rho)$ and Onsager's geminate escape probability in eq 3.6 should be written more appropriately as $\Omega_\infty = \Omega_\infty(r_0, T, \rho)$. Qualitatively, the theory predicts a decreasing recombination efficiency associated with an increasing free ion yield as the temperature is raised. Conversely, as the dielectric constant is lowered, the solvent screening of the attractive interionic forces is diminished, and the recombination becomes increasingly effective, which in turn leads to smaller free ion yields.

Equation 3.6 is based on the 2-fold assumption that the charge annihilation occurs instantly when the relative ion separation becomes zero. In the past, the Onsager model has been refined by several groups, most notably by Tachiya and co-workers,[90–92] to account for the fact that the recombination event corresponds to a charge transfer reaction. This requires the introduction of a finite reaction rate and of a finite reaction radius, R, with/at which the charge can actually be transferred back. To make use of eq 3.6 and to calculate an experimental observable, the escape probability has to be averaged over the distribution, $f(r_0)$, of initial separations of ion-pairs constituting the ensemble, i.e., $\langle \Omega_\infty \rangle = 4\pi \int r_0^2 f(r_0) \Omega_\infty(r_0) dr_0$.

In an effort to analyze pulse radiolysis data on different liquids, various functional forms have been proposed for $f(r_0)$ including exponentials, Gaussians, truncated Gaussians, or power laws. For photolytically generated hydrated electrons, it was shown that the detailed functional form is not so crucial because of the superior definition of the ionization energy in multi-photon ionization experiments as compared to pulse radiolysis. Indeed, numerical simulations using the delta-functional form, $f(r_0) = \delta(r_0 - \langle r_0 \rangle)$, where $\langle r_0 \rangle$ is the average ejection length (or thermalization distance), are able to reproduce the experimentally observed hydrated electron recombination dynamics very well.[41] Therefore, we will omit in the following an averaging over the detailed spatial distribution of fragments around the solvated electron and use the delta-function instead for describing the geminate survival probability. This leaves the ejection length, $\langle r_0 \rangle$, as the only adjustable parameter for fitting the dependence of the experimental values of Ω_∞ on the thermodynamic state variables, T and ρ.

Following eq 3.6 strictly, the survival probability determined from the experimental pump-probe transients as described above is plotted in Figure 3.7

as a function of the density-dependent dielectric constant[44] multiplied by the temperature. To facilitate a comparison with other solvents, it is advantageous to reduce the quantity, $\epsilon(T,\rho)T$, to the critical data, i.e., by dividing it by the product of $(\epsilon T)_{\text{crit}} = \epsilon(T_{\text{crit}}, \rho_{\text{crit}})T_{\text{crit}}$ at the critical point, where for the special case of ammonia $T_{\text{crit}} = 405.4\,\text{K}$, $\rho_{\text{crit}} = 0.235\,\text{g cm}^{-3}$, and $\epsilon(T_{\text{crit}}, \rho_{\text{crit}}) = 4.7$. The bottom panel of Figure 3.7 corresponds to a semilogarithmic plot of the escape probability as a function of the inverse of the totally reduced product, $\epsilon T/(\epsilon T)_{\text{crit}}$.

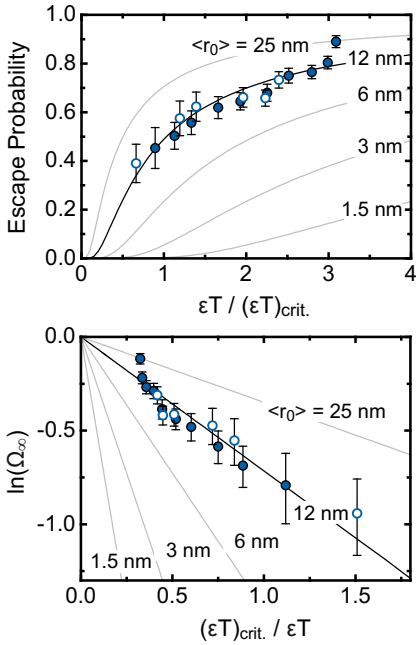

Figure 3.7: Experimental escape probabilities of the solvated electron in liquid-to-supercritical ammonia (filled circles, isobaric at 300 bar; open circles, isothermal at 423 K) as a function of the totally reduced product of the relative solvent permittivity and the temperature. For comparison, the prediction of the Onsager model according to eq 3.6 is also shown (solid curves) for various average ejection lengths. The Onsager radius varies between 2.8 nm (at 227 K and $\epsilon T/(\epsilon T)_{\text{crit}} = 3.1$) and 13.2 nm (at 423 K and $\epsilon T/(\epsilon T)_{\text{crit}} = 0.67$).

From both panels, it can be seen that within the accuracy of the experiment, the Onsager model is able to quantitatively reproduce the data. Furthermore, the data are optimally fitted when a mean thermalization distance of ∼12.2 nm is assumed. An average ejection length of around 12 nm is indeed very large. Notice that a thermalization distance around 1 nm was found for

photolytically generated hydrated electrons in water at the same ionization energy of 9.3 eV used here.[93] The discrepancy can be rationalized by the different energetics in the two systems as described above. At 9.3 eV, the conduction band is accessible only in ammonia thereby creating highly mobile electrons that become trapped at locations far away from the initial ionization site. Therefore, the order-of-magnitude larger value of $\langle r_0 \rangle$ as compared to water is indeed in very strong support of our above hypothesis of an ionization mechanism requiring the solvent conduction band.

A slight residual curvature of the experimental data points in the linearized representation (Figure 3.7, bottom panel) might indicate that the ejection length weakly increases as the temperature is isobarically raised or the density is isothermally reduced. In fact, there is no physical rationale justifying the assumption of a thermalization distance that does not vary with the thermodynamic conditions. It could very well be that upon altering the inter-particle distances, the interactions between the nonbonding orbitals leading to the formation of a conduction band change, and as a result, the average migration distances of an intermediate conduction band electron also vary. As the data were recorded in the vicinity of the critical point, further complications may arise due to local density enhancement effects.[94] Qualitatively, one would expect the orbital overlap to deteriorate as the density is isothermally decreased and the dielectric constant is lowered. This would actually lead to a decreasing ejection length with decreasing ϵT, and as a result, the data should exhibit a negative curvature in the $\ln(\Omega_\infty)$ versus $1/\epsilon T$ plot. Such a behavior can, however, not be confirmed.

3.4.5 Onsager's Escape Probability for Ion-Pair-Dipole Recombination

Although the Onsager prediction matches our experimental data nicely, an application of the underlying model to the recombination of ammoniated electrons neglects the chemical nature of the annihilation mechanism. As discussed above, the actual loss of e^-_{am} occurs through their reaction with the dipolar radical, NH_2, rather than with their ammonium counter-ion. Therefore, we are dealing primarily with a reaction involving dipoles and not exclusively with an ion-ion recombination for which the theory was originally developed.[42,90]

The Onsager model would describe the escape probability correctly, if every

encounter between the electron and the cation led to recombination. However, quite the opposite is the case. Most of the time, the ion-ion encounters are unreactive and only ion-pairs, ($e^-_{am} \cdot NH^+_4$), are transiently formed. The solvated electron and the ammonium cation diffuse as a pair without neutralizing and disappearing as ammonia molecules and hydrogen atoms. The actual recombination occurs only at the instant, when the ion-pair finally meets with the dipole. Thus, one would severely overestimate the ejection length from fitting the experimentally observable escape probability with eq 3.6. This is easily seen by introducing the geminate electron- ion recombination probability, W^{ion}_{∞}, or the probability for ion-pair formation

$$W^{\text{ion}}_{\infty}(r_0) = 1 - \Omega^{\text{ion}}_{\infty}(r_0) \tag{3.7}$$

where r_0 is the initial separation at the instant of solvated electron generation. If every ion-ion encounter would directly lead to solvated electron annihilation, the ion-pair dissociation probability, $\Omega^{\text{ion}}_{\infty}$, would be equal to the measured escape probability, Ω_{∞}. This is, however, not the case because the ion-pair itself needs to encounter the amidogen radical before the solvated electron is lost. Since the ion-pair itself represents a strongly bound dipole, its reaction with the NH_2 dipole can be regarded as a dipole-dipole recombination, which can be treated in the framework of the neutral pair approximation[95] where any electrostatic interaction between the reaction partners is neglected. In this case, the probability for geminate recombination is simply given by the ratio of the reaction distance to the initial dipole-dipole distance

$$W^{\text{dip}}_{\infty}(r_1) = R/r_1. \tag{3.8}$$

In our case, the reaction distance, R, takes into account the finite separation between the dipoles at which their reaction occurs, while the dipole-dipole distance, r_1, is equal to the separation between the ion-pair, ($e^-_{am} \cdot NH^+_4$), and the NH_2 dipole at the instant when the ion-pair is formed. As the annihilation occurs diffusion-controlled, the ultimate recombination probability is then given by the probability for the ion-pair formation multiplied by the dipole-dipole reaction probability, i.e.,

$$W^{\text{total}}_{\infty}(r_0, r_1) = W^{\text{ion}}_{\infty}(r_0) W^{\text{dip}}_{\infty}(r_1) \tag{3.9}$$

and the ultimate escape probability seen experimentally then becomes

$$W_{\infty}^{\text{total}}(r_0, r_1) = 1 - W_{\infty}^{\text{ion}}(r_0) W_{\infty}^{\text{dip}}(r_1). \tag{3.10}$$

In principle, as with eq 3.6, an averaging over the distribution of initial ion-ion distances would have to be carried out. Furthermore, because of the diffusive nature of the relative approach between the ion-pair and the NH_2 radical, a distribution of dipole-dipole distances will be established in solution over which an additional averaging is in principle also required. For simplicity, this effect of the diffusional spreading of the radial dipole pair distribution will be neglected as will be the influence of the distribution of ejection lengths.

The transient existence of the ion-pair introduces two additional parameters to the model, namely, the dipole-dipole reaction radius, R, and the initial dipole-dipole distance, r_1. The former quantity has been determined by Kieffer et al. from pulse radiolysis experiments to 0.58 nm at a temperature of 223 K.[52] No temperature dependence of this quantity has been reported so far, and we therefore assume it to be constant throughout the thermodynamic range studied here. The initial dipole-dipole separation, r_1, can be approximated as the average distance, $r_{\text{NH}_4^+}$, traveled by the ammonium cation relative to the radical during the time period between the initial photoionization and the ion-pair formation (see Figure 3.8). Similarly, an average distance, r_{e^-}, migrated by the solvated electron during that time window can also be defined. The ejection length is then simply given by the sum of the two electrostatic drift distances, $r_0 = r_{\text{NH}_4^+} + r_{\text{e}^-}$. Since the distance ratio, $r_{\text{e}^-}/r_{\text{NH}_4^+}$, can be expressed by the ratio of the particles' diffusion constants, $D_{\text{e}^-}/D_{\text{NH}_4^+}$, the initial dipole-dipole separation is obtained in the form

$$r_1 = r_0 \cdot \frac{D_{\text{NH}_4^+}}{D_{\text{NH}_4^+} + D_{\text{e}^-}} \tag{3.11}$$

Once again, we reiterate that the diffusional nature of the particle motions will lead to a spatial spreading of the density distributions with time, which can be dealt with optimally by numerically solving the relevant Smoluchowski diffusion equations[35,41,93,96,97] or by means of Monte Carlo simulations.[41,98,99] At this stage, it suffices to use eq 3.11 for estimating the relative distances between the peaks of the density distributions of the recombining particles.

The diffusion coefficient of the solvated electron is 1.5 $\text{Å}^2\,\text{ps}^{-1}$ at 223 K,

while at the same temperature, those of the ammonium cation and the amidogen radical are only 0.23 $Å^2$ ps^{-1} and 0.5 $Å^2$ ps^{-1}, respectively.[54] Therefore, the collisional dynamics of the recombining particles in the liquid solvent are dominated by the mobility of the solvated electron. Since no information is available regarding the temperature and density dependencies of the diffusion coefficients, we assume that they scale identically with the T and ρ-dependent diffusivity of the neat solvent. In that case, the ratio of r_1 to r_0 remains constant (see eq 3.11), and the only fitting parameter in the model is again the thermalization distance (cf. Figure 3.8).

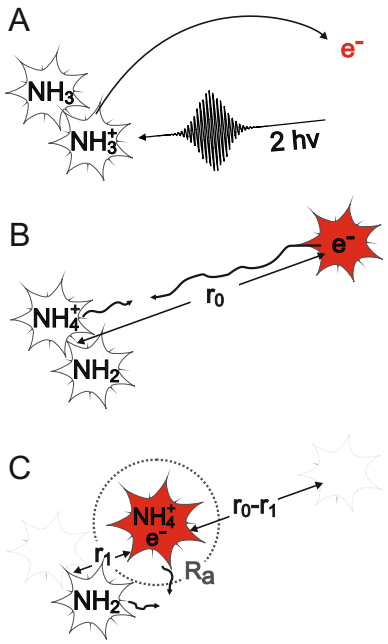

Figure 3.8: Sketch of the recombination dynamics relevant to the ammoniated electron. (A) The 2-photon ionization generates solvated electrons at the thermalization distance, r_0, from the ionization site. (B) The ammonium cation and the solvated electron drift toward each other in their mutual Coulomb field to form the ion-pair. (C) The ion-pair is created at the average distance, r_1, from the initial ionization site, which can be estimated from the diffusion coefficients of the two independently diffusing particles.

Figure 3.9 shows a comparison of the experimental survival probabilities with the Onsager model that is extended to describe the ion-pair-mediated

electron dipole recombination. The most important difference to the unmodified model (cf. Figure 3.7) is that indeed for the same thermodynamic conditions, significantly smaller thermalization distances are required to obtain the same escape yield. Whereas the unmodified Onsager model (eq 3.6) suggested an ejection length of ∼12 nm, a satisfactory fit is now obtained with $\langle r_0 \rangle = r_0 = 6.6\,\text{nm}$. This value is still perfectly consistent with an ionization mechanism that creates the electrons transiently in the conduction band of the solvent. For the hydrated electron generated photolytically above the band gap,[31,62,100] a thermalization distance of 4 nm was determined thereby confirming a previous report that quasi-free electrons are slightly more mobile in ammonia as compared to water.[77]

Finally, Figure 3.9 reveals that the escape probability does not vanish when the product, $\epsilon(T,\rho)T$, approaches zero. According to eq 3.10, the escape probability assumes a value of $\Omega_\infty^{\text{total}} = 1 - R/r_1$ in the limit $\epsilon(T,\rho)T \to 0$. In other words, regardless of the solvent screening, the solvated electron can only be quantitatively annihilated in a configuration where the ion-pair is generated within the reaction radius for its recombination with the dipole. The finite intercept leads to a considerably bent model prediction in the linearized representation (Figure 3.9, bottom panel). Therefore, the curved behavior of the experimental data that we already noticed in Figure 3.7 can at least partially be attributed to the sequential nature of the recombination mechanism. Unfortunately, the accuracy of our data is currently not good enough to decide whether or not the ejection length depends on the temperature and the density. Here, it seems as if the assumption of a constant thermalization distance from the compressed liquid to the dilute supercritical fluid is sufficiently accurate. We are currently engaged in numerical Monte Carlo simulations to provide a more sophisticated molecular level description of the effect of ion-pair formation on the geminate recombination dynamics of the ammoniated electron. These simulations will also serve as a basis for a detailed analysis of the apparent recombination kinetics, a subject whose discussion is postponed to a forthcoming publication.

3.5 Conclusions

In summary, we have investigated for the first time the initial recombination of photolytically generated solvated electrons in liquid and supercritical

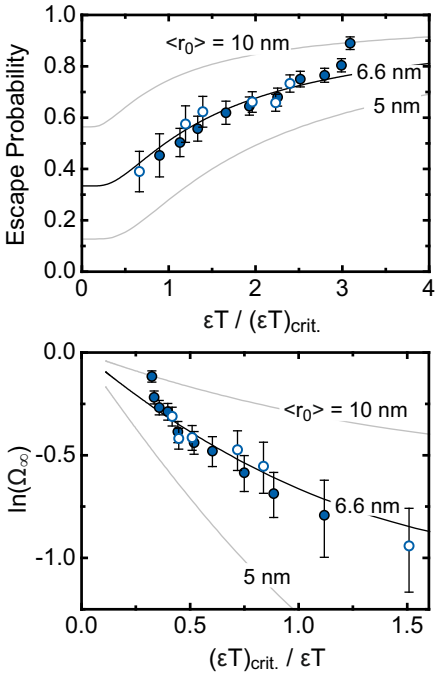

Figure 3.9: Comparison of the extended Onsager model with experimental escape probabilities of the solvated electron in liquid-to-supercritical ammonia (filled circles, isobaric at 300 bar; open circles, isothermal at 423 K).

ammonia. The mechanism creating the ammoniated electron relies on an initial two-photon ionization with a transient formation of electrons in the conduction band of the solvent. The conduction band electrons feature a high mobility thereby resulting in a thermalization distance that is much larger than that of solvated electrons generated at comparable ionization energies from water where the conduction band is energetically not accessible. Because of the large ejection length, the geminate escape probability is surprisingly high. The dependence of the escape yields on the thermodynamic state variables, temperature, density, and dielectric constant has been explored in a systematic fashion and was found to be in remarkable agreement with the theoretical predictions from the classical Onsager model for the initial recombination of ions. Within the accuracy of the experimental data there is no need to invoke a temperature and density dependent thermalization distance. The Onsager model was further refined to account for the transient appearance of the ammonium-electron ion-pairs, which diffusively migrate in the liquid solution in a correlated manner. While the reactant motions are governed by

the electrostatic drift of the electron toward the ammonium cation and the ion-pair formation, the reactivity of the solvated electron is dictated by the reactivity of the ion-pair toward the amidogen radical. We therefore speak of an ion-pair-mediated electron-dipole recombination. Future experiments of the multi-photon ionization of liquid-to-supercritical amines and aminoalcohols are currently underway in our laboratories to further unravel specifically the role of hydrogen-bonding for the recombination dynamics of solvated electrons in condensed phases. To explore the thermalization dynamics prior to electron recombination, additional experiments with tunable probe pulses will be carried out. In addition, we are planning to conduct experiments on the geminate recombination of electrons with NH_2 in the absence of the cation following a photodetachment of the electron by charge transfer to solvent excitation of amide anions in the ultraviolet. Finally, multiple pulse experiments including photolysis-pump-probe spectroscopy are targeted at comparing the relaxation dynamics of photolytically generated solvated electrons with those from our previous studies on solvated electrons from metal-ammonia solutions. Such a comparison might prove very helpful in exploring the solvated electron's mode of binding to the medium and its time-dependent changes during the localization dynamics, i.e., as the highly mobile conduction band electron becomes trapped and fully thermalized at a local solvent site.

Acknowledgements

Financial support by the Deutsche Forschungsgemeinschaft through the Collaborative Research Center, SFB 813 "Chemistry at Spin Centers", and through project VO 593/6-1 is gratefully acknowledged. We are furthermore indebted to Professor Dirk Schwarzer for continued support and inspiring discussion.

[1] Mozumder, A. *Fundamentals of Radiation Chemistry;* Academic Press: San Diego, 1999.

[2] Hart, E. J.; Anbar, M. *The Hydrated Electron;* John Wiley & Sons Inc.: New York, 1970.

[3] Zurek, E.; Edwards, P. P.; Hoffmann, R. *Angew. Chem. Int. Edt.* **2009**, *48*, 8198.

[4] Larsen, R. E.; Glover, W. J.; Schwartz, B. J. *Science* **2010**, *329*, 65.

[5] Haberland, H.; Ludewigt, C.; Schindler, H.-G.; Worsnop, D. R. *Surf. Sci.* **1985**, *156*, 157.

[6] Lee, G. H.; Arnold, S. T.; Eaton, J. G.; Sarkas, H. W.; Bowen, K. H.; Haberland, H. *Z. Phys. D* **1991**, *20*, 9.

[7] Sarkas, H. W.; Arnold, S. T.; Eaton, J. G.; Lee, G. H.; Bowen, K. H. *J. Chem. Phys.* **2002**, *116*, 5731.

[8] Hertel, I. V.; Huglin, C.; Nitsch, C.; Schulz, C. P. *Phys. Rev. Lett.* **1991**, *67*, 1767.

[9] Schulz, C. P.; Gerber, A.; Nitsch, C.; Hertel, I. V. *Z. Phys. D* **1991**, *20*, 65.

[10] Stert, V.; Radloff, W.; Schulz, C. P.; Hertel, I. V. *Eur. Phys. J. D* **1999**, *5*, 97.

[11] Schulz, C. P.; Scholz, A.; Hertel, I. V. *Isr. J. Chem.* **2004**, *44*, 19.

[12] Lee, I.-R.; Lee, W.; Zewail, A. H. *ChemPhysChem* **2008**, *9*, 83.

[13] Huppert, D.; Rentzepis, P. M.; Struve, W. S. *J. Phys. Chem.* **1975**, *79*, 2850.

[14] Belloni, J.; Clerc, M.; Goujon, P.; Saito, E. *J. Phys. Chem.* **1975**, *79*, 2848.

[15] Lindner, J.; Unterreiner, A.-N.; Vöhringer, P. *ChemPhysChem* **2006**, *7*, 363.

[16] Lindner, J.; Unterreiner, A.-N.; Vöhringer, P. *J. Chem. Phys.* **2008**, *129*, 064514.

[17] Jortner, J. *J. Chem. Phys.* **1959**, *30*, 839.

[18] Barnett, R. N.; Landman, U.; Cleveland, C. L.; Kestner, N. R.; Jortner, J. *Chem. Phys. Lett.* **1988**, *148*, 249.

[19] Barnett, R. N.; Landman, U.; Cleveland, C. L.; Kestner, N. R.; Jortner, J. *J. Chem. Phys.* **1988**, *88*, 6670.

[20] Marchi, M.; Sprik, M.; Klein, M. L. *J. Chem. Phys.* **1988**, *89*, 4918.

[21] Sprik, M.; Klein, M. L. *J. Chem. Phys.* **1988**, *89*, 1592.

[22] Sprik, M.; Impey, R. W.; Klein, M. L. *J. Chem. Phys.* **1985**, *83*, 5802.

[23] Barnett, R. N.; Landman, U.; Nitzan, A. *Phys. Rev. Lett.* **1989**, *62*, 106.

[24] Sprik, M.; Klein, M. L. *J. Chem. Phys.* **1989**, *91*, 5665.

[25] Sprik, M.; Klein, M. L. *J. Chem. Phys.* **1989**, *90*, 7614.

[26] Marchi, M.; Sprik, M.; Klein, M. L. *Faraday Discuss. Chem. Soc.* **1988**, *85*, 373.

[27] Shkrob, I. A. *J. Phys. Chem. A* **2006**, *110*, 3967.

[28] Migus, A.; Gauduel, Y.; Martin, J. L.; Antonetti, A. *Phys. Rev. Lett.* **1987**, *58*, 1559.

[29] Long, F. H.; Lu, H.; Eisenthal, K. B. *Phys. Rev. Lett.* **1990**, *64*, 1469.

[30] Sander, M. U.; Luther, K.; Troe, J. *J. Phys. Chem.* **1993**, *97*, 11489.

[31] Crowell, R. A.; Bartels, D. M. *J. Phys. Chem.* **1996**, *100*, 17940.

[32] Hertwig, A.; Hippler, H.; Unterreiner, A.; Vöhringer, P. *Ber. Bunsenges. Phys. Chem.* **1998**, *102*, 805.

[33] Assel, M.; Laenen, R.; Laubereau, A. *J. Phys. Chem. A* **1998**, *102*, 2256.

[34] Hertwig, A.; Hippler, H.; Unterreiner, A.-N. *Phys. Chem. Chem. Phys.* **1999**, *1*, 5633.

[35] Madsen, D.; Thomsen, C. L.; Thogersen, J.; Keiding, S. R. *J. Chem. Phys.* **2000**, *113*, 1126.

[36] Elles, C. G.; Jailaubekov, A. E.; Crowell, R. A.; Bradforth, S. E. *J. Chem. Phys.* **2006**, *125*, 044515.

[37] Elles, C. G.; Shkrob, I. A.; Crowell, R. A.; Bradforth, S. E. *J. Chem. Phys.* **2007**, *126*, 164503.

[38] Petersen, C.; Thogersen, J.; Jensen, S. K.; Keiding, S. R. *J. Phys. Chem. A* **2007**, *111*, 11410.

[39] Kratz, S.; Torres-Alacan, J.; Urbanek, J.; Lindner, J.; Vöhringer, P. *Phys. Chem. Chem. Phys.* **2010**, *12*, 12169.

[40] Iglev, H.; Fischer, M. K.; Rossmadl, H. *J. Chem. Phys.* **2011**, *134*, 214507.

[41] Torres-Alacan, J.; Kratz, S.; Vöhringer, P. *Phys. Chem. Chem. Phys.* **2011**, *13*, 20806.

[42] Onsager, L. *Phys. Rev.* **1938**, *54*, 554.

[43] PROPATH Group. *PROPATH: A Program Package for Thermophysical Properties, version 13.1* **2008**.

[44] Buback, M.; Harder, W. D. *Ber. Bunsenges. Phys. Chem.* **1977**, *81*, 609.

[45] Schäfer, T.; Lindner, J.; Vöhringer, P.; Schwarzer, D. *J. Chem. Phys.* **2009**, *130*, 224502.

[46] Schäfer, T.; Schwarzer, D.; Lindner, J.; Vöhringer, P. *J. Chem. Phys.* **2008**, *128*, 064502.

[47] Schwarzer, D.; Lindner, J.; Vöhringer, P. *J. Phys. Chem. A* **2006**, *110*, 2858.

[48] Vogelsgesang, R.; Schindewolf, U. *Ber. Bunsenges. Phys. Chem.* **1971**, *75*, 651.

[49] Olinger, R.; Schindewolf, U.; Gaathon, A.; Jortner, J. *Ber. Bunsenges. Phys. Chem.* **1971**, *75*, 690.

[50] Olinger, R.; Hahne, S.; Schindewolf, U. *Ber. Bunsenges. Phys. Chem.* **1972**, *76*, 349.

[51] Koehler, W. H.; Lagowski, J. J. *J. Phys. Chem.* **1969**, *73*, 2329.

[52] Kieffer, F.; Klein, J.; Lapersonne-Meyer, C.; Magat, M.; Belloni, J.; Billiau, F.; Cordier, P.; Delaire, J.; Delcourt, M. O. *Faraday Discuss. Chem. Soc.* **1977**, *63*, 55.

[53] Belloni, J.; Cordier, P.; Delaire, J. *Chem. Phys. Lett.* **1974**, *27*, 241.

[54] Belloni, J.; Cordier, P.; Delaire, J. A.; Delcourt, M. O. *J. Phys. Chem.* **1978**, *82*, 537.

[55] Farhataziz.; Perkey, L. M.; Hentz, R. R. *J. Chem. Phys.* **1974**, *60*, 4383.

[56] Williams, F.; Varma, S. P.; Hillenius, S. *J. Chem. Phys.* **1976**, *64*, 1549.

[57] Krohn, C. E.; Thompson, J. C. *Phys. Rev. B* **1979**, *20*, 4365.

[58] Coe, J. V.; Earhart, A. D.; Cohen, M. H.; Hoffman, G. J.; Sarkas, H. W.; Bowen, K. H. *J. Chem. Phys.* **1997**, *107*, 6023.

[59] Elles, C. G.; Rivera, C. A.; Zhang, Y.; Pieniazek, P. A.; Bradforth, S. E. *J. Chem. Phys.* **2009**, *130*, 084501.

[60] Winter, B.; Weber, R.; Widdra, W.; Dittmar, M.; Faubel, M.; Hertel, I. V. *J. Phys. Chem. A* **2004**, *108*, 2625.

[61] Nordlund, D.; Ogasawara, H.; Bluhm, H.; Takahashi, O.; Odelius, M.; Nagasono, M.; Pettersson, L. G. M.; Nilsson, A. *Phys. Rev. Lett.* **2007**, *99*, 217406.

[62] Son, D. H.; Kambhampati, P.; Kee, T. W.; Barbara, P. F. *J. Phys. Chem. A* **2001**, *105*, 8269.

[63] Son, D. H.; Kambhampati, P.; Kee, T. W.; Barbara, P. F. *Chem. Phys. Lett.* **2001**, *342*, 571.

[64] Boyle, J. W.; Ghormley, J. A.; Hochanadel, C. J.; Riley, J. F. *J. Phys. Chem.* **1969**, *73*, 2886.

[65] Bartels, D. M.; Crowell, R. A. *J. Phys. Chem. A* **2000**, *104*, 3349.

[66] Ashfold, M.; Langford, S.; Morgan, R.; Orr-Ewing, A.; Western, C.; Scheper, C.; de Lange, C. *Eur. Phys. J. D* **1998**, *4*, 189.

[67] Walsh, A. D.; Warsop, P. A. *Trans. Faraday Soc.* **1961**, *57*, 345.

[68] Douglas, A. E. *Discuss. Faraday Soc.* **1963**, *35*, 158.

[69] Ashfold, M.; Bennett, C.; Dixon, R. *Chem. Phys.* **1985**, *93*, 293.

[70] Banna, M. S.; Shirley, D. A. *J. Chem. Phys.* **1975**, *63*, 4759.

[71] Rabalais, J. W.; Karlsson, L.; Werme, L. O.; Bergmark, T.; Siegbahn, K. *J. Chem. Phys.* **1973**, *58*, 3370.

[72] Locht, R.; Leyh, B.; Denzer, W.; Hagenow, G.; Baumgärtel, H. *Chem. Phys.* **1991**, *155*, 407.

[73] Almeida, T. S.; Coutinho, K.; Costa Cabral, B. J.; Canuto, S. *J. Chem. Phys.* **2008**, *128*, 014506.

[74] Lindblad, A.; Bergersen, H.; Pokapanich, W.; Tchaplyguine, M.; Ohrwall, G.; Bjorneholm, O. *Phys. Chem. Chem. Phys.* **2009**, *11*, 1758.

[75] Krohn, C. E.; Antoniewicz, P.; Thompson, J. *Surf. Sci.* **1980**, *101*, 241.

[76] Huntress, W. T.; Mosesman, M. M.; Elleman, D. D. *J. Chem. Phys.* **1971**, *54*, 843.

[77] Krebs, P. *J. Phys. Chem.* **1984**, *88*, 3702.

[78] Belloni, J.; Billiau, F.; Cordier, P.; Delaire, J. A.; Delcourt, M. O. *J. Phys. Chem.* **1978**, *82*, 532.

[79] Farhataziz.; Perkey, L. M.; Hentz, R. R. *J. Chem. Phys.* **1974**, *60*, 717.

[80] Farhataziz.; Perkey, L. M. *J. Phys. Chem.* **1975**, *79*, 1651.

[81] Fletcher, J. W.; Seddon, W. A. *Faraday Discuss.* **1977**, *63*, 18.

[82] Seddon, W. A.; Fletcher, J. W.; Sopchyshyn, F. C.; Jevcak, J. *Can. J. Chem.* **1974**, *52*, 3269.

[83] Dye, J. L.; Debacker, M. G.; Dorfman, L. M. *J. Chem. Phys.* **1970**, *52*, 6251.

[84] Belloni, J.; Billiau, F.; Delaire, J.; Delcourt, M.; Marignier, J. *Radiat. Phys. Chem.* **1983**, *21*, 177.

[85] Brooks, J. M.; Dewald, R. R. *J. Phys. Chem.* **1971**, *75*, 986.

[86] Schindewolf, U. *Ber. Bunsenges. Phys. Chem.* **1982**, *86*, 887.

[87] Buxton, G. V. *Radiation Chemistry: Present Status and Future Trends;* Elsevier: Amsterdam, The Netherlands, 2001.

[88] Rubinstein, G.; Tuttle, T. R.; Golden, S. *J. Phys. Chem.* **1973**, *77*, 2872.

[89] Jou, F.-Y.; Freeman, G. R. *J. Phys. Chem.* **1981**, *85*, 629.

[90] Sano, H.; Tachiya, M. *J. Chem. Phys.* **1979**, *71*, 1276.

[91] Tachiya, M. *J. Chem. Phys.* **1988**, *89*, 6929.

[92] Wojcik, M.; Tachiya, M. *J. Chem. Phys.* **2009**, *130*, 104107.

[93] Thomsen, C. L.; Madsen, D.; Keiding, S. R.; Thogersen, J.; Christiansen, O. *J. Chem. Phys.* **1999**, *110*, 3453.

[94] Egorov, S.; Yethiraj, A.; Skinner, J. *Chem. Phys. Lett.* **2000**, *317*, 558.

[95] Collins, F. C.; Kimball, G. E. *J. Colloid Sci.* **1949**, *4*, 425.

[96] Pimblott, S. M. *J. Phys. Chem.* **1991**, *95*, 6946.

[97] Green, N. J. B.; Pilling, M. J.; Pimblott, S. M.; Clifford, P. *J. Phys. Chem.* **1990**, *94*, 251.

[98] Cobut, V.; Frongillo, Y.; Patau, J. P.; Goulet, T. andFraser, M. J.; Jay-Gerin, J. P. *Radiat. Phys. Chem.* **1998**, *51*, 229.

[99] Frongillo, Y.; Goulet, T.; Fraser, M.; Cobut, V.; Patau, J.; Jay-Gerin, J. *Radiat. Phys. Chem.* **1998**, *51*, 245.

[100] Sander, M. U.; Luther, K.; Troe, J. *Ber. Bunsenges. Phys. Chem.* **1993**, *97*, 953.

4

Vertical Photoionization of Liquid-to-Supercritical Ammonia: Thermal Effects on the Valence-to-Conduction Band-Gap

Janus Urbanek, and Peter Vöhringer*

Abteilung für Molekulare Physikalische Chemie, Institut für Physikalische und Theoretische Chemie, Rheinische Friedrich-Wilhelms-Universität, Wegelerstr. 12, 53115 Bonn, Germany

* To whom correspondence should be addressed. Email: p.voehringer@uni-bonn.de

4.1 ABSTRACT

We recently reported first femtosecond pump-probe experiments on the geminate recombination dynamics of solvated electrons in fluid ammonia (Urbanek et al., *J. Phys. Chem. B* **2012**, *116*, 2223-2233). The electrons were generated through a vertical two-photon ionization at a total energy of 9.3 eV. Here, we present a full Monte Carlo analysis of the time-resolved data to determine the solvated electron's thermalization distance from the ionization hole, NH_3^+. The simulations are compared with the experiment over wide thermodynamic conditions to obtain insight into the dependence of the vertical ionization mechanism on the electronic properties of the solvent network. The simulations reveal that the average thermalization distance, $\langle r_0 \rangle$, decreases strongly with both increasing temperature, T, and decreasing density, ρ, from 3.2 nm in the cryogenic fluid down to roughly 0.5 nm in the dilute supercritical phase with almost gas-like densities. We combine our results with the current understanding of the T, ρ-dependence of the electronic structure of the liquid phase and discuss in detail the role of thermally induced energy level shifts for the valence-to-conduction band-gap. The observed changes of the thermalization distance can be well attributed to a gradual decrease of the excess energy initially imparted on the ejected electron as gas-like conditions are progressively approached.

4.2 INTRODUCTION

Solvated electrons produced by femtosecond multi-photon excitation of the neat solvent carry important information about the primary photoionization process, thereby offering a window into structural, dynamical, and electronic properties of the liquid phase.[1] Usually, the recombination of the solvated electron with the molecular byproducts of the matter-field interaction is monitored in such experiments.[2–6] The early time (subnanosecond) dynamics of electron annihilation is governed by the nonhomogeneous spatial distribution of the recombining species produced upon ultrafast laser excitation and results almost exclusively from reactive encounters between geminate particles originating from one and the same ionization site within the fluid (i.e., geminate recombination). The electron recombination dynamics is typically quantified by the time-dependent survival probability, i.e., by the fraction of solvated

electrons that is able to escape from the recombination reactions. It turns out that this probability is a highly sensitive function of the relative spatial distribution of all reactants arising from the primary matter-field interaction.

Of special interest is the distance from the ionization site where the photoejected electron becomes localized and where a fully thermalized solvation structure around the excess negative charge is established. This so-called thermalization distance (or alternatively, ejection length) is a particularly intriguing quantity because it offers insight into the nature of the electronic state of the liquid from which the electron is initially ejected. Conduction band electrons are typically highly mobile and are able to travel much larger distances prior to thermalization as compared to electrons resulting from excitation below the optical band-gap.[7]

It is possible to obtain the thermalization distance by comparing experimental data that accurately trace the recombination dynamics in the time domain with predictions from analytical models or computer simulations, which take into account the reactive events between the recombination partners including their relative microscopic motions in the fluid system.[8,9] Interestingly, in the context of such simulations, the migration of the solvated electron in polar fluids can be mimicked sufficiently well by the Brownian motion of a classical ion despite the solute's undisputed quantum nature.[10,11] A very general method for modeling geminate recombination is based on Monte Carlo simulations of the individual trajectories of motion for all reactive particles in a statistically large number of ionization events.[8] The advantage of this approach is its broad adaptability to specific properties of the reaction system that is produced by photoionization like multiple competing reaction pathways or specific electrostatic interactions between the recombining particles.[12]

The majority of time-resolved studies devoted to the photoionization of liquids were conducted on water where the hydrated electron e^-_{aq} is produced alongside a hydroxyl radical, OH, and a hydronium cation, H_3O^+.[13] Owing to the large body of experimental and theoretical data, a comprehensive microscopic mechanism for the photoionization of liquid water has emerged in recent years, in which different ionization pathways prevail depending upon the total ionization energy provided by the incident radiation. Each pathway is associated with a characteristic thermalization distance, which in turn is reflected in different geminate recombination dynamics.[2,14–16]

For excitation energies at which the conduction band of the liquid can

be accessed, a quasi-free electron is directly injected into the bulk upon a vertical ionization. In this case, all nuclear coordinates remain frozen at the instant of electron ejection such that a positively charged molecular hole in the equilibrium geometry of the neutral solvent molecule is coproduced with the solvated electron. In a polar and protic solvent medium, the nascent photolysis products do not represent the final equilibrated chemical species. The relaxation processes of the electron and those of the corresponding cationic hole are largely decoupled because of their relatively large separation in comparison to the intermolecular distances in the liquid. They involve chemical transformations as well as a substantial reorganization of the solvent network.[16] Strikingly, the generation of solvated electrons is reported for significantly lower excitation energies extending almost down to the UV absorption edge of the solvent.[17,18] In this energy regime, the formation of solvated electrons becomes energetically feasible only because of a concerted stabilization of the nascent photolysis products by the solvent network, which ultimately yields the fully equilibrated species, e.g., e^-_{aq}, OH, and H_3O^+ for the ionization of water. Various indirect photoionization mechanisms have been proposed for such low ionization energies including autoionization, proton-coupled electron transfer, or the hot hydrogen-atom mechanism, all of which are subject of ongoing discussions.[16,19,20] All indirect ionization mechanisms have in common that nuclear rearrangements are strongly coupled to the actual electron ejection. Some of these molecular motions must involve molecules within the liquid network that are located far off the initial site of optical excitation. To establish the importance of the molecular environment in direct and indirect ionization, the geminate recombination of the solvated electron can be studied over a wide range of thermodynamic conditions ranging from the densely packed liquid well into the dilute supercritical fluid with gas-like densities. Such experiments were recently performed in our laboratory on the femtosecond-to-picosecond time scale following 266 nm two-photon ionization of water[4,12] and of ammonia.[21]

In this paper, we further elucidate the role of structural and electronic properties of the solvent in the vertical ionization of polar and protic fluids. Compared to the numerous investigations of the low energy photoionization of water, this issue is hitherto rather unexplored.[22,23] The data from our previous study[21] of the geminate recombination of solvated electrons following femtosecond two-photon ionization of liquid-to-supercritical ammonia at

9.3 eV forms the experimental basis for the computational studies reported here. In the language of solid state physics, the electronic structure of fluid ammonia at sufficiently high excitation energies resembles that of an amorphous semiconductor with a large band-gap.[24] With reference to the isolated gas phase molecule, the orbital interaction between a large number of neighboring molecules in the liquid results in a splitting of occupied and virtual molecular orbitals into continuous bands of energy levels. Above the band-gap, excitation of liquid NH_3 with 9.3 eV promotes an electron from the completely filled valence band directly into a quasi-free state in the conduction band.[21] Thus, vertical ionization of ammonia initially produces a cationic hole, NH_3^+, and a nonthermal ballistic excess electron, $e^-_{CB,hot}$, in the conduction band of the bulk, as in the case of the 266 nm two-photon absorption

$$NH_3 + 2\,h\nu \longrightarrow e^-_{CB,hot} + NH_3^+. \tag{4.1}$$

Elastic and inelastic scattering of the quasi-free electron give rise to a loss of its momentum. Subsequent solvation leads to the formation of the well-localized ammoniated electron, e^-_{am}, in some distance from the parental cationic hole,

$$e^-_{CB,hot} \longrightarrow \longrightarrow e^-_{am}. \tag{4.2}$$

The NH_3^+ cation is known to be highly unstable and decomposes by transferring a proton to a neighboring solvent molecule,[25] i.e.,

$$NH_3^+ + NH_3 \longrightarrow NH_2 + NH_4^+. \tag{4.3}$$

Therefore, the two-photon ionization of fluid ammonia produces an ammonium cation, NH_4^+, and an aminyl radical, NH_2, as byproducts of the solvated electron and is thus fully analogous to the 2-photon ionization of fluid water, i.e.,

$$2NH_3 + 2\,h\nu \longrightarrow e^-_{am} + NH_4^+ + NH_2. \tag{4.4}$$

Here, the geminate recombination dynamics of the ammoniated electron with the two molecular fragments, NH_4^+ and NH_2, will be treated by detailed Monte Carlo simulations. The computer results will be compared in depth with our experimental data in an effort to determine the electron's average thermalization distance, $\langle r_0 \rangle$, as a function of T and ρ. We will then discuss our findings in terms of thermally induced shifts of the electronic energy

levels of the fluid or alternatively, in terms of the dependence of the optical band-gap on the thermodynamic state variables, T and ρ.

4.3 Simulation of the Recombination Process

According to eq 4.4, the irradiation of fluid ammonia with 266 nm femtosecond light pulses produces a system composed of the thermalized reactants, e^-_{am}, NH_2, and NH_4^+.[21] The subsequent decay of the solvated electron can be attributed to two different recombination channels, both of which involve an annihilation with the radical species.[26,27] The first corresponds to the direct electron-radical recombination

$$e^-_{am} + NH_2 \longrightarrow NH_2^- \tag{4.5}$$

while the other channel represents an ion-pair mediated recombination sequence

$$e^-_{am} + NH_4^+ \longrightarrow (e^-_{am} \cdot NH_4^+) \tag{4.6}$$

$$(e^-_{am} \cdot NH_4^+) + NH_2 \longrightarrow NH_2^- + NH_4^+. \tag{4.7}$$

It is important to emphasize that in fluid ammonia the direct neutralization between the charged reactants, e^-_{am} and NH_4^+, according to $e^-_{am} + NH_4^+ \longrightarrow NH_3 + H$ is conceivable. This reaction is, however, known to be endergonic in the temperature range studied here, and therefore it must be dismissed as an effective decay channel for the solvated electron.[21,28] In the following, the focus will be on the time scale below 1 ns, where the recombination process is predominantly geminate in nature. This is further rationalized by the low concentration of solvated electrons of roughly 10^{-5} mol dm^{-3} that was generated by the 266 nm pump pulse in our previous experimental study.[21] Consequently, the individual microscopic ionization events can be dealt with in terms of spatially isolated sites in the solvent. In this case, the probability for the solvated electron to recombine during the time t after its generation at $t = 0$ ps (i.e., the complement, $1 - \Omega(t)$, of the survival probability) is proportional to the two-body encounter probability for the pair consisting of e^-_{am} and NH_2 in the presence of a parental NH_4^+ cation. This includes direct electron-radical encounters as in reaction 4.5 as well as ion-pair mediated encounters of the electron and the radical according to reaction 4.7. As outlined below, the temporal evolution of $\Omega(t)$ is highly sensitive to the initial spatial distribution

of the three geminate particles e^-_{am}, NH_2 and NH_4^+ originally produced by the photolysis pulse.

The initial distribution of the solvated electron's thermalization distances can be determined from the experimental ensemble averaged decay of the pump-induced optical density of the solvated electron, $\Delta OD(t)$ by comparison with predictions of $\Omega(t)$ from Monte Carlo calculations of the microscopic trajectories of motion under explicit consideration of reactive encounters of the three particles. In propagating the dynamic trajectories of the system, the solvent is treated as a structureless dielectric continuum. The basic ideas behind this approach were worked out for the recombination dynamics of hydrated electrons by Goulet et al.[8]

For our purposes, the time-dependent survival probability of the ammoniated electron, $\Omega(t)$ was simulated by preparing in silico a computationally large number (ensemble, $N = 10^5$) of noninteracting reaction systems, each composed of three particles representing the thermalized species e^-_{am}, NH_2 and NH_4^+. Their initial spatial distribution is chosen to reflect the vertical ionization process according to eq 4.1 to 4.3, i.e., the ejection of the electron into the bulk is completely decoupled from the chemical decomposition of the resulting NH_3^+ cationic hole. The latter transformation was accounted for by assuming an immediate proton-transfer onto a nearest-neighbor NH_3 molecule. A migration of the proton over longer distances can be neglected because the Grotthus-mechanism for proton diffusion in fluid ammonia was found to be insignificant.[29,30] Each trajectory was initialized by placing the NH_2 fragment at the origin of the simulation box and by positioning the NH_4^+ cation at a distance of 0.34 nm from the aminyl radical under a randomly chosen pair of polar angles. Such initial conditions mimic the proton transfer from the cationic core to an arbitrary molecule of the first solvation shell and are consistent with the local structure of fluid ammonia as observed in neutron scattering[31] or recent molecular dynamics simulation.[32,33] The solvated electron itself was then placed randomly around the NH_2 radical at a separation, r_0, corresponding to its thermalization distance (or alternatively, ejection length). To obtain a realistic representation of the broad distribution of trapping sites for the quasi-free electron in the solvent, r_0 was sampled from the radial distribution function

$$f(r_0) = \frac{r_0^2}{2b^3} exp(-\frac{r_0}{b}), \tag{4.8}$$

where $\langle r_0 \rangle = 3b$ denotes the mean thermalization distance.[8] Such a distribution was already successfully applied in previous simulations of the geminate recombination of solvated electrons in liquid-to-supercritical water.[12] Note that eq 4.8 depends on the thermodynamic conditions through a temperature and density dependence of the mean thermalization distance.

Following its initialization, each trajectory was then propagated by computing the motion of the three particles in space and time. To this end, a sufficiently small incremental time step, Δt, was chosen that results in a spatial displacement, $\Delta\vec{r}$, for each of the three particles. The total displacement contains a random diffusive component, $\Delta\vec{r}_{\text{diff}}$, and a directed electrostatically induced drift, $\Delta\vec{r}_{\text{drift}}$, such that $\Delta\vec{r} = \Delta\vec{r}_{\text{diff}} + \Delta\vec{r}_{\text{drift}}$.[8] Consistent with a three-dimensional random walk, diffusive jumps were distributed in all spatial directions with equal probability and their length, $\Delta\vec{r}_{\text{diff}}$, was sampled between 0 and $4R$ from the radial distribution function

$$f(r_0) = \frac{4\Delta\vec{r}_{\text{diff}}^2}{R^3 \cdot \sqrt{\pi}} exp(\frac{\Delta\vec{r}_{\text{diff}}^2}{R^2}). \tag{4.9}$$

Here, $R = \sqrt{4D\Delta t}$ and D is the diffusion coefficient of the moving particle.[8] The electrostatic interactions within the reactive three-body system are undoubtedly dominated by the mutual long-range Coulomb attraction between the charged species, e^-_{am} and NH_4^+, with the charge dipole interactions involving the aminyl radical being much weaker. Moreover, the dipole moment of NH_2 is likely to be completely obscured in the condensed phase by thermal averaging and the abundant dipole moments of the surrounding solvent molecules. Based on this assessment, the radical's motion was treated purely diffusional, i.e., $\Delta\vec{r}_{\text{drift}} = 0$. The charged reactants were dealt with as point charges and their electrostatic drift component to the motion was computed from

$$\Delta\vec{r}_{\text{drift}} = u\vec{E}\Delta t \tag{4.10}$$

where $\vec{E}$ is the Coulomb electric field. The ion mobility, u,is obtained from the diffusion coefficient, D, of the moving particle according to $u = eD/k_BT$, with e being the elementary charge and k_B being the Boltzmann constant.[8] A calculation of $\vec{E}$ requires the knowledge of the temperature and density dependent relative permittivity, $\epsilon_r(T, \rho)$, of the solvent, which is available from an experimental study by Buback and Harder.[34] The relevant values are

compiled in Table 4.1 for the various thermodynamic conditions pertaining to our experimental data. It should be noted that the Debye relaxation time in liquid ammonia is roughly 600 fs at 294 K.[35] Therefore, the solvent electronic response is significantly faster than the simulated recombination process, which rationalizes our use of the static permittivity in the simulations to account for the screening of the electrostatic interactions by the solvent.

Table 4.1: Average thermalization Distance of the solvated electron (prepared by 266 nm two-photon ionization of liquid and supercritical ammonia) for various thermodynamic conditions. The values of $\langle r_0 \rangle$ were determined by a comparison of experimental geminate recombination kinetics with Monte Carlo computer simulations.

T/K	p/bar	ρ/g cm^{-3}	$\langle r_{\mathrm{NN}} \rangle$/nm	ϵ_r	Δt/fs	$\langle r_0 \rangle$/nm
227	300	0.712	0.34	26.1	100	3.20 ± 0.25
258	300	0.676	0.35	22.2	50	2.70 ± 0.30
294	300	0.632	0.35	18.2	25	2.70 ± 0.25
333	300	0.580	0.37	14.5	25	2.50 ± 0.20
364	300	0.534	0.38	11.9	20	2.10 ± 0.20
398	300	0.475	0.39	9.3	10	1.75 ± 0.25
423	300	0.421	0.41	7.5	10	1.70 ± 0.20
448	300	0.356	0.43	5.7	5	1.40 ± 0.35
465	300	0.306	0.45	4.7	5	1.10 ± 0.35
489	300	0.242	0.49	3.5	3	0.65 ± 0.25
423	1300	0.565	0.37	10.8	15	2.15 ± 0.25
423	950	0.535	0.38	10.1	15	1.80 ± 0.15
423	550	0.484	0.39	8.9	10	1.75 ± 0.20
423	200	0.359	0.43	6.3	5	1.60 ± 0.25
423	165	0.300	0.45	5.4	5	1.40 ± 0.25
423	140	0.172	0.55	3	2	0.50 ± 0.30

To carry out trajectory calculations for different thermodynamic conditions, the temperature and density dependence of the diffusion coefficients, $D(T, \rho)$, for each of the three species, e^-_{am}, NH_4^+, or NH_2, is required. Since no experimental data are currently available over the broad T, ρ-range of our experiment, these quantities were extrapolated here using the solvent's self-diffusion coefficient, $D_{\mathrm{self}}(T, \rho)$, i.e.,

$$D(T, \rho) = (T_{\mathrm{ref}}, \rho_{\mathrm{ref}}) \frac{D_{\mathrm{self}}(T, \rho)}{D_{\mathrm{self}}(T_{\mathrm{ref}}, \rho_{\mathrm{ref}})}. \tag{4.11}$$

In the context of recombination kinetics of radiolytically and photolytically generated electrons, such a scaling procedure has been shown to provide sufficiently reliable diffusivities under conditions where experimental values are lacking.[12,36] Once again, we stress that in contrast to water, the proton

diffuses in ammonia as a Brownian NH_4^+ cation[29] rather than as a structural protonic defect in which case the scaling procedure would no longer be adequate.[12,36] At the reference state, $T_{ref} = 240\,K$ and $\rho_{ref} = 0.682\,g\,cm^{-3}$, the individual diffusion coefficients of the species e_{am}^-, NH_4^+, and NH_2 are $1.5 \times 10^{-8}\,m^2\,s^{-1}$, $2.3 \times 10^{-9}\,m^2\,s^{-1}$, and $5.0 \times 10^{-9}\,m^2\,s^{-1}$, respectively.[26] The self-diffusion coefficient, $D_{self}(T, \rho)$, of ammonia was derived by interpolation from experimental data reported by Lüdemann and co-workers[37] using the Chapman-Enskog expression for a rough hard-sphere fluid.

After every single time step, Δt, (with incremental translocations, $\Delta\vec{r}$, of e_{am}^-, NH_4^+, and NH_2), the trajectories were tested for recombination events by comparing their inter-particle separations against predefined reaction distances, R. The direct recombination of the solvated electron with the aminyl radical according to eq 4.5 is known to be diffusion limited,[27,38] and its reaction distance was specified by Belloni et al. to be 0.41 nm.[26] Thus, the loss of a solvated electron was recorded and the corresponding trajectory eliminated from the ensemble, once the distance between the electron and the NH_2 became less than or equal to this critical separation. The indirect decay sequence involving the electrostatically favored formation of the ion-pair $(e_{am}^- \cdot NH_4^+)$ was implemented by assuming a charge association according to eq 4.6 whenever the distance between the electron and the ammonium cation was less than or equal to $R = 0.54\,nm$ as derived in Ref. 26. Once formed, the ion-pair was implemented as stable against dissociation for the remaining duration of the trajectory as indicated by ion-pairing theory. Following the approach of Catterall et al.[39] and taking the closest approach parameter equal to the reaction distance R, i.e., $a = 0.54\,nm$, the encounter lifetime of $(e_{am}^- \cdot NH_4^+)$ in liquid ammonia can be estimated to be on the nanosecond time scale under all thermodynamic conditions relevant to our study. Ion-pairing does not significantly alter the solvated electron's resonance[40] and hence, its decay is spectroscopically observed only upon a consecutive encounter of the ion-pair with NH_2. The motion of the ion-pair subsequent to an electron-ammonium encounter was assumed to be limited by the least mobile constituent, i.e., the ion-pair diffusion coefficient was taken to be identical to that of NH_4^+. As the cation itself does not represent a reactive species in eq 4.7, only the position of the solvated electron was traced after ion-pair formation. Its annihilation was realized whenever the separation to the aminyl radical adopted a distance of $R = 0.41\,nm$ or less, i.e., identical to the value for the direct electron-dipole

recombination. The quantities R were assumed to be temperature and density independent.

Finally, for the Monte Carlo simulation to provide reliable trajectories at a reasonable computational cost, an adequate temporal step size, Δt, has to be chosen. Neither the electrostatic drift nor the diffusional component to the total displacements are allowed to exceed the above-mentioned reaction radii. Otherwise, recombination events or ion-pair formation events may accidentally be missed along the trajectory due to temporal under-sampling. The temporal step sizes used in this work are compiled in Table 4.1 for the various thermodynamic conditions. Convergence of the results was ascertained by iteratively shortening Δt until the simulated survival probability remained unchanged.

Prior to modeling the experimental data, it is instructive to study the general influence of the thermodynamic state variables, temperature, and density, on the dynamics of electron loss and consequently, on the decay of the time-dependent survival probability. Moreover, it is also important to assess the sensitivity of the escape probability to systematic variations in T and ρ in relation to systematic variations of the only adjustable simulation parameter; the thermalization distance. To this end, computer simulations of $\Omega(t)$ were carried out in which one of these parameters was systematically varied while the other two were kept constant and were chosen such that they represented physically reasonable values (cf. Figure 4.1).

Intuitively, one might expect that isochoric heating of the liquid allows a larger fraction of solvated electrons to avoid the geminate recombination because the increasing thermal energy enables the geminate pairs to more easily overcome their mutual electrostatic attractions. This is the essence of Onsager's theory for the initial recombination of ions, and the competition between directed electrostatic drift on the one hand and undirected thermal Brownian motion on the other should influence the recombination of the charged particles as given by reaction 4.6. Because the NH_4^+ cation is initially located in immediate proximity to the NH_2 radical, the same competition can be expected to affect the electron-dipole recombination (4.5) at least to some extent. However and in stark contrast to these expectations, the simulations reveal that an increase of the temperature from 333 K to 513 K has no significant impact on $\Omega(t)$ as shown in Figure 4.1, a. This surprising observation must be attributed to the simultaneous decrease of the dielectric constant of

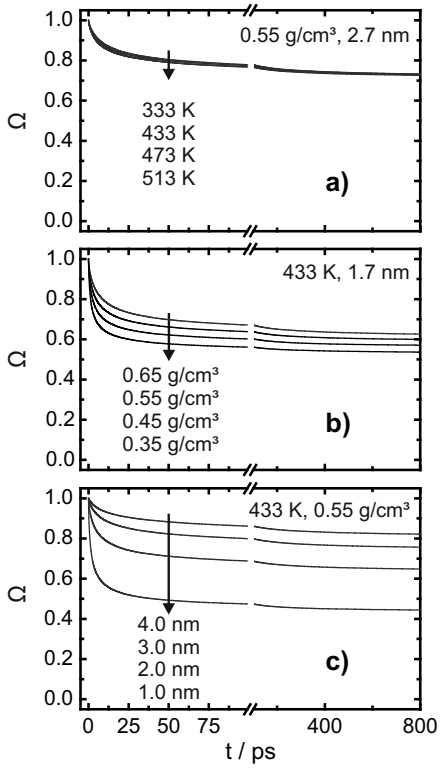

Figure 4.1: Influence of a variation of the temperature (a), of the density (b), and of the average thermalization distance (c) on the survival probability, $\Omega(t)$, of the solvated electron in fluid ammonia. The transient decays were calculated using Monte Carlo simulations by systematically changing one of the three parameters while keeping the other two fixed.

the solvent that occurs upon heating (in this case, ϵ_r decreases from 13.4 to 8.6).[34] As a result, the diminished screening of the electrostatic interactions by the solvent compensates almost completely the thermally induced escape from the interfragment Coulomb field as the temperature is raised.

On the other hand, the escape probability displays a rather significant dependence on the solvent density. Along the supercritical 433 K isotherm, a dilution of the system from $\rho = 0.65\,\mathrm{g\,cm^{-3}}$ to $\rho = 0.35\,\mathrm{g\,cm^{-3}}$ leads to a reduction of the relative permittivity[34] from 12.7 to 5.8 while at the same time, the diffusion coefficients grow by more than a factor of 3.[37] Both of these effects should enhance the efficiency of electron recombination. Furthermore, because of the increased mobility of the reactants, the recombination dynamics can be expected to accelerate upon decreasing the density. As seen in

panel b of Figure 4.1, these expectations are fully confirmed by the numerical simulations.

Finally, the average thermalization distance should also critically affect the recombination dynamics because it specifies the initial geometric conditions for the three-body encounter problem. Intuitively, the larger the interfragment separations are at time $t = 0$, the higher is the ultimate electron yield and the less efficient are the recombination processes. Furthermore, we can expect the recombination dynamics to accelerate with a decreasing thermalization length because the average distance the fragments have to migrate to annihilate the electron becomes shorter. As can be seen Figure 4.1c, both of these effects are clearly reproduced by the Monte Carlo simulations.

The diffusion coefficients and the mean thermalization distance are the critical and highly entangled parameters that determine the ultimate survival probability. As our goal is to obtain the T and ρ-dependent thermalization distance (by fitting the experimental kinetic traces with the Monte Carlo simulations of $\Omega(t)$), the major sources of error are the inaccuracies of the diffusion coefficients of the recombining particles. These quantities have been estimated from the scaling procedure as outlined above (eq 4.11). For the hydrated electron the very same scaling procedure[12] yields diffusivities whose error is smaller than a factor of 2 as compared to the most recent experimental estimates.[41] An increase of $D(T, \rho)$ for all species by a factor of 2 must be compensated by a simultaneous decrease of $\langle r_0 \rangle$ by a factor of 0.8 to conserve the agreement between experiment and simulation.

4.4 Results and Discussion

4.4.1 Experiment versus Simulation

Multiphoton ionization of liquid and supercritical NH_3 with 266 nm femtosecond pulses was investigated over a wide range of temperatures (227 K $\leq T \leq$ 489 K) and densities (0.17 g cm^{-3} $\leq \rho \leq$ 0.71 g cm^{-3}). Time-resolved traces of the solvated electron's pump-induced absorption, $\Delta OD(t)$, normalized to its maximum value are displayed in Figure 4.2 for a selection of thermodynamic conditions. Following optical excitation with a total energy of 9.3 eV, the electron is ejected into the solvent, where it becomes initially localized in a nonequilibrium configuration. Thermal cooling and solvation result in a spectral shift of the electronic resonance to higher frequencies with increasing

delay.[42,43] An inspection of the experimental signals reveals that the initial rise is fully instrument limited, i.e., the solvated electron is completely thermalized within the temporal resolution of our setup, which is mainly determined by the temporal walk-off between pump and probe pulses. When choosing the detection wavelength to be at the maximum or on the high frequency edge of the stationary absorption spectrum, the primary localization and thermalization dynamics can only result in a temporally delayed appearance of the signal. Consequently, the decay of $\Delta OD(t)$ observed on the picosecond time scale is indeed exclusively related to a loss of e^-_{am} due to geminate recombination with NH_2.

Figure 4.2 shows a comparison between the experimental results and the Monte Carlo simulations of the solvated electron's survival probability. As outlined above, the only adjustable parameter entering the simulations is the average thermalization distance, $\langle r_0 \rangle$, of the photoejected electron. Using the radial distribution function specified in eq 4.8 the experimental data was successfully reproduced over the whole range of investigated thermodynamic conditions. This is in line with our previous study on hydrated electrons produced by photoionization of water below the band-gap, where the same functional form of $f(r_0)$ sufficed to reproduce the recombination kinetics over a wide range of temperature and density.[12] To obtain such a good agreement, it was however necessary to allow the thermalization distance $\langle r_0 \rangle$ to vary with T and ρ (cf. Figure 4.3). At 227 K and a density of 0.712 g cm^{-3}, the photoionization produces solvated electrons at a mean ejection length of 3.20 nm $\pm$ 0.25 nm. Upon heating the sample at a constant pressure of 300 bar to a final temperature of 489 K (corresponding to a final density of 0.242 g cm^{-3}), the thermalization distance gradually decreases to a value of only 0.65 nm $\pm$ 0.25 nm. The magnitude of this change becomes even more apparent from a microscopic point of view. Crudely estimating the average inter-particle distances from the expression, $\langle r_{\mathrm{NN}} \rangle = (\rho N_A/M)^{-1/3}$, where N_A is Avogadro's constant and M is the molar mass, the solvated electron is initially separated from its parental hole by roughly 10 solvent molecules in the high density cryogenic liquid, whereas, in the supercritical phase, localization occurs already in the first or second solvation shell, i.e., in immediate proximity to the primary ionization center.

The temperature dependence of $\langle r_0 \rangle$ depicted in the upper panel of Figure 4.3 was determined under isobaric conditions. However, raising the tempera-

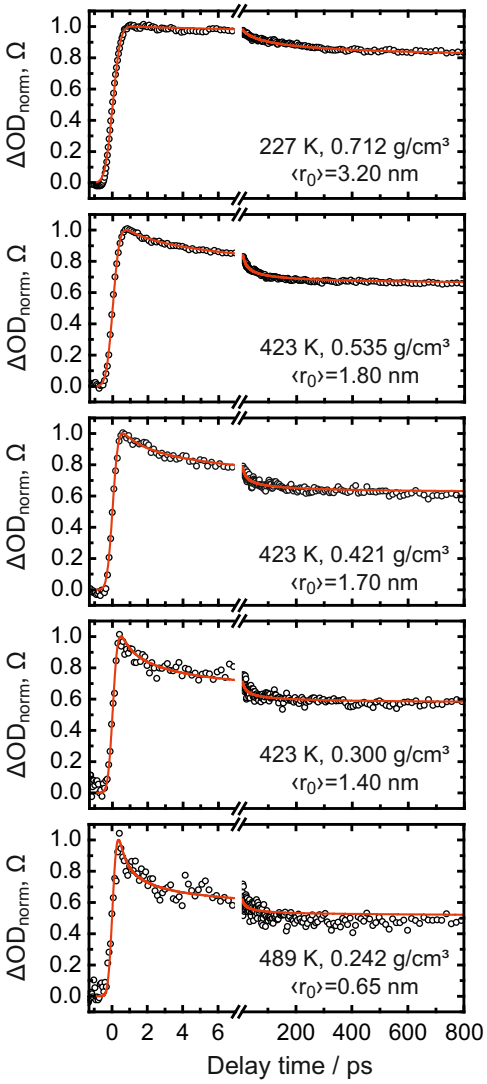

Figure 4.2: Comparison between the experimental pump-induced optical density, ΔOD of the solvated electron created by 266 nm two-photon ionization of liquid and supercritical ammonia (open circles) and corresponding Monte Carlo simulations (solid line) of the survival probability, $\Omega(t)$. The simulation results were convoluted with a Gaussian instrument response function to allow for a quantitative comparison with the experiment.

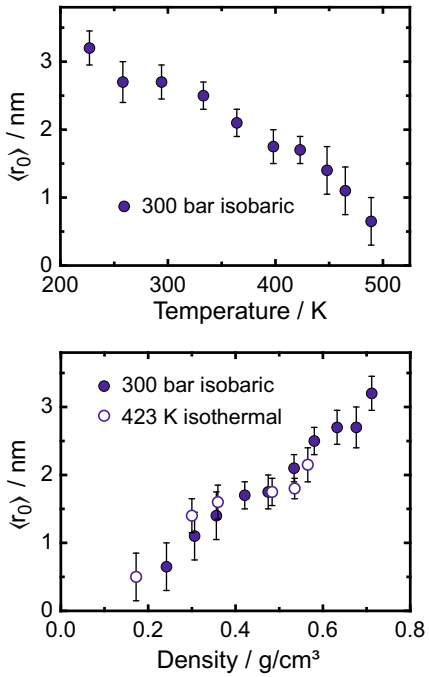

Figure 4.3: Mean thermalization distance $\langle r_0 \rangle$ of the solvated electron generated by 9.3 eV femtosecond photoionization of fluid NH_3 as a function of temperature (top panel) and density (bottom panel). The values were obtained from analyzing the geminate recombination of the solvated electron along the 300 bar isobar (filled circles) and the 423 K isotherm (open circles) using Monte Carlo simulations.

ture at a constant pressure involves also a lowering of the density. To separate the density effect on $\langle r_0 \rangle$ from the unperturbed (i.e., density-independent) temperature effect, additional experiments have been performed under isothermal conditions in the supercritical phase, which allowed a change of the density by more than a factor of 3. From the bottom panel of Figure 4.3, it can be seen that the density dependence obtained under isothermal conditions qualitatively agrees with that obtained from the isobaric series of experiments.

A linear regression of the data displayed in Figure 4.3 (top) provides an isobaric slope of the temperature-dependent thermalization distance of $(\partial\langle r_0 \rangle/\partial T)_p = 8.7 \times 10^{-3}$ nm K^{-1}. Likewise, an isothermal slope of the density-dependent ejection length of $(\partial\langle r_0 \rangle/\partial \rho)_T = 2.2$ nm g^{-1} cm^3 is obtained from the data in Table 4.1 when neglecting the experiment carried out at the lowest density. The unknown isochoric temperature-dependence of $\langle r_0 \rangle$ can now be calculated from

$$(\partial\langle r_0 \rangle/\partial T)_\rho = (\partial\langle r_0 \rangle/\partial T)_p - (\partial\langle r_0 \rangle/\partial \rho)_T (\partial \rho/\partial T)_p \tag{4.12}$$

where the last term containing the temperature-dependence of the density at constant pressure (here $p = 300$ bar) is readily obtained from Table 4.1. Using a value for $(\partial \rho/\partial T)_p$ of -1.76×10^{-3} g cm^{-3} K^{-1}, we obtain an estimate of -4.8×10^{-3} nm K^{-1} for $(\partial\langle r_0 \rangle/\partial T)_\rho$. Thus, only about one-half of the thermally induced decrease of the ejection length displayed in Figure 4.2 (top) is a true temperature effect. It must be further emphasized that this contribution becomes even smaller ($\sim$30%) if we include the experiment at the lowest density. Thus, we conclude that thermally induced modifications of the electron ejection length are mostly the result of an average solvent structure that varies with the imposed thermodynamic conditions.

It should be stressed at this point that for simulating the data from the highly dilute supercritical phase, very short thermalization distances were required. In this regime, $\langle r_0 \rangle$ becomes similar to the reaction distances, R, of the two recombination channels. Neglecting the molecular nature of the solvent – as is intrinsically done in the Monte Carlo simulation – becomes rather questionable. Indeed, it can be seen (cf. Figure 4.2, bottom panel) that under such conditions the agreement between experiment and model calculations slightly deteriorates, which we take as an indication for a breakdown of the continuum description of the solvent as gas-like densities are gradually

approached and as the solvated electron becomes localized ever more closely to the primary site of ionization.

In a previous paper,[21] we analyzed the asymptotic escape probability, Ω_∞, (i.e., the apparent fraction of solvated electrons that escapes geminate recombination for delay times in excess of 0.8 ns), in terms of the classical Onsager theory for the initial recombination of ions. The theory was extended to account for the transient formation of ion-pairs and more importantly, a temperature and density-independent thermalization distance was assumed. Quantitative agreement between the experimental data and the classical model was obtained with a constant value of $\langle r_0 \rangle$ of 6.6 nm independent of T and ρ. The rather large thermalization distance (compared to complementary values found for the hydrated electron that was generated at the same ionization energy) was taken as direct evidence for the electron being born initially as a highly mobile conduction band electron.[21] The question arises here as to why the classical Onsager theory yields a thermalization distance that is at least a factor of 2 larger than in the Monte Carlo simulation. The discrepancy between the Onsager model and the numerical analysis may originate from the former treatment neglecting the direct recombination of the electron with the aminyl radical, which may or may not efficiently compete with the ion-pair mediated recombination channel. In addition, it is not at all clear whether or not the assumption within the Onsager theory of a temperature and the density independent ejection length is strictly correct.

The Monte Carlo simulations allow us to address this issue simply by decomposing the total time-dependent escape probability into separate contributions from the two competing recombination pathways, i.e., electron-dipole recombination on the one hand and ion-pair mediated recombination on the other. Figure 4.4 illustrates the fraction of solvated electrons, ϕ, annihilated through the intermediate formation of an ion-pair relative to the total number of recombination events. At the highest densities investigated, both reaction channels contribute evenly to the electron decay indicating that the electrostatic interaction between e^-_{am} and NH_4^+ is effectively screened by the solvent. This is because under such conditions, the primary ionization generates the electron at a very large distance from the ionization site while leaving behind the two molecular fragments, NH_4^+ and NH_2, in relatively close spatial proximity. Thus, in the limit of low T and high ρ with a complete screening of the cationic charge, both recombination channels are equally likely. How-

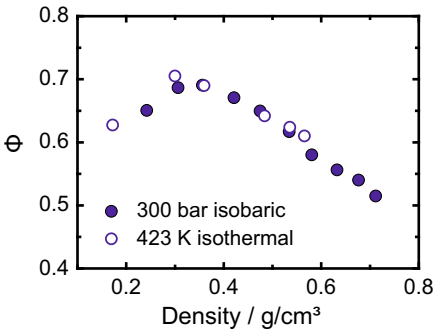

Figure 4.4: Fraction of solvated electrons, ϕ that decays through the ion-pair mediated recombination channel with respect to the total number of annihilations. Consequently, $(1-\phi)$ corresponds to the contribution of the direct recombination pathway between the solvated electron and the radical.

ever, as the density is lowered or alternatively, the temperature is raised, the solvent screening effect weakens. Consequently, the electron-ion Coulomb attraction gradually gains in importance and the fraction of ion-pair mediated recombination events increases. Surprisingly, the quantity, ϕ, displays a pronounced maximum at a density of $\sim$0.33 g cm^{-3} below which geometrical effects related to the three-body recombination take over. For sufficiently small densities, the thermalization distance becomes so small that the cation effectively drags the more mobile e^-_{am} into the reaction radius of the radical even before the charges can form the intermediate ion-pair. Thus, it indeed turns out that neglecting the direct recombination channel, as we had done previously in Ref. 21 to test Onsager's theory, results in an overestimation of the electrostatic attraction, which in turn yields artificially high thermalization distances.

4.4.2 Thermally Induced Shifts of the Band-Gap

As summarized in Figure 4.3, clear dependencies of $\langle r_0 \rangle$ on the thermodynamic state variables, T and ρ, are revealed by systematically studying the solvated electron's geminate recombination dynamics over a wide range of conditions ranging from the dense cryogenic fluid all the way into the supercritical phase with almost gas-like densities. Recall that the excitation conditions remained unaltered throughout the course of the investigation; that is, regardless of T and ρ, the ionization of fluid NH_3 was carried out with 266 nm pulses corresponding to a constant two-photon ionization energy

of 9.3 eV (cf. also Ref. 21). It was argued above that the apparent thermally induced variations of the ejection length are to a large extent brought about by modifications of the average solvent structure as the thermodynamic conditions are changed. The microscopic structure of the fluid is imprinted into its electronic structure, which in turn impacts on the vertical ionization mechanism. Whereas in the highly dilute gas phase, the electronic structure of the system is reminiscent of the manifold of electronic states of the individual unperturbed ammonia molecules, the electronic states in the dense liquid extend over more than a single NH_3 monomer and should be viewed more appropriately as collective excitations of larger structural motifs within the fluid. The degree of delocalization of the electronic excitations in the system depends quite generally on the nature of the intermolecular interactions as well as their magnitude in relation to the thermal energy. Thus, the electronic structure of the fluid is subject to line broadening dynamics and can be inhomogeneous or homogeneous depending upon the observation time scale. The distribution of thermalization distances as defined by eq 4.8 relies on the assumption of a finite structural inhomogeneity of the fluid on the time scale of the ionization pulse. In this spirit, the distance, $r_{0,\mathrm{max}} = 2\langle r_0 \rangle/3$, specifying the most probable thermalization distance as well as the mean thermalization distance, $\langle r_0 \rangle$, can be taken as an indicator of the delocalized character of the initial state prepared upon two-photon excitation. Similarly, the width of the distribution (given by $r_{0,\mathrm{max}}[W_{-1}(-x) - W_0(-x)]$, where $x = 1/\sqrt{2}e$ and W_i denotes the ith branch of the Lambert W-function) can be read as a measure of the structural inhomogeneity of the fluid.

Before addressing the detailed effect of temperature and density on the valence-to-conduction band-gap relevant for vertical ionization of liquid ammonia, it is highly instructive to first reconsider the correlation between the total excitation energy used for generating the solvated electron and the apparent thermalization distance, $\langle r_0 \rangle$. This relationship was established by Elles et al.[16] for the photoionization of liquid water and for the special case of ambient conditions (i.e., $T = 298\,\mathrm{K}$, $p = 1\,\mathrm{atm}$, $\rho = 1\,\mathrm{g\,cm^{-3}}$). By increasing the total ionization energy from 8.3 eV to 12.4 eV, the electron ejection length was observed to monotonously increase from $\sim$0.9 nm all the way up $\sim$4 nm. A particularly sharp increase of the ejection length was noted to coincide with the onset of vertical ionization of water (the minimum energy required for a direct inter-band transition from the valence to the conduction band of water

is known from photoelectron spectroscopy to be located at 9.9 eV).[16] Such a trend is readily explained by physical intuition: With rising excitation energy provided by the primary matter-field interaction, the quasi-free electron is prepared higher up in the conduction band and hence, dressed with an increasing amount of excess kinetic energy. The growing excess energy initially imparted on the electron then translates directly into an increase of $\langle r_0 \rangle$. A very fast electron is more likely to localize farther from the primary ionization site than a resting zero-kinetic energy electron. From this perspective, variations of $\langle r_0 \rangle$ such as those shown in Figure 4.3 for a fixed ionization energy can be regarded as shifts of the valence-to-conduction band-gap due to thermally induced changes of the average solvent structure.

To follow up on such an interpretation, let us briefly examine the energetics relevant to the photoionization of ammonia (cf. Figure 4.5). Its vertical photoionization promotes a valence electron directly into the conduction band thereby producing a quasi-free electron, e^-_{CB}, and an ammonia cation, NH_3^+, with the nuclear coordinates frozen at the neutral geometry. The barrier associated with the direct interband transition, $NH_3 \longrightarrow e^-_{CB,hot} + NH_3^+$, is usually referred to as the optical band-gap, E_{opt}.[44] Because the motions of the primary fragments are decoupled, the electron will be dressed with an excess energy, E_{ex}, that is given by $E_{ex} = nh\nu - E_{opt}$, where in our case the multi-photon ionization energy, $nh\nu$, equals 9.3 eV. The value of E_{opt} can be assessed from recent photoelectron spectroscopy experiments on large ammonia clusters, $(NH_3)_N$ with $N \approx 1600$, by Lindblad et al.[45] These data are reproduced in Figure 4.5a from which we can infer an energy of 9.4 eV for the most probable transition from the valence band into the vacuum while producing at the same time a zero-kinetic energy electron. This transition energy is also referred to as vertical detachment energy (*VDE*) of the neutral ammonia cluster. The onset of photoemission is observed at a slightly lower energy of roughly 8 eV and represents the so-called photoelectric threshold (*PET*), which can be understood as the minimum energy required to remove an electron from the cluster and to bring it without any kinetic energy into the vacuum. It should be noted briefly that the (*VDE*) and (*PET*) are currently unavailable for the bulk liquid. For anionic clusters it is known that the (*VDE*) is proportional to $N^{1/3}$ with N being the number of molecules in the cluster.[46] Assuming that this correlation holds also true for the neutral clusters and using (*VDEs*) of 10.9 eV and 9.4 eV for the monomer[47] and for

the cluster[45] with $N \approx 1600$ respectively, one can extrapolate to a value of 9.3 eV for the bulk liquid. Similarly, the bulk *PET* is extrapolated to be around 7.9 eV. In the case of photoemission into the bulk, both the (*VDE*) and the *PET* need to be corrected for the energy, V_0, by which a quasi-free electron is stabilized through the solvent network relative to the vacuum level. This stabilization energy is a negative quantity, which is why the optical band-gap is below the vertical detachment energy as illustrated in Figure 4.5. The valence-to-conduction band-gap for a vertical transition in fluid NH_3 can then be estimated according to $E_{\text{opt}} = VDE + V_0$. Based on measurements of the photoemission from metal electrodes into neat liquid NH_3, two different experimental values for V_0 have been proposed for liquid ammonia, namely −0.95 eV and −1.29 eV.[48,49] Taking the average of both values, i.e., $V_0 = -1.1$ eV, the optical band-gap assumes a value of $E_{\text{opt}} = 8.2$ eV as indicated in Figure 4.5b. From the *PET* of the cluster data, we can then estimate the bottom of the conduction band to be located around 6.8 eV. Hence, for our case of a total ionization energy of 9.3 eV, the most probable excess kinetic energy that is available to a conduction band electron in liquid ammonia is $E_{\text{ex}} \approx 1.1$ eV. Note that this is the most probable value, and that ionization can also occur from energetically more favorable sites such as those associated with the *PET*. We reiterate that this estimate requires the cluster data to be representative of the bulk.

Returning to the data in Figure 4.3, the thermalization distance suggests that the excess kinetic energy of the electron decreases with increasing temperature and decreasing density. Since the total ionization energy remains fixed at 9.3 eV, this requires the bottom of the conduction band to experience an upward energetic shift as the liquid is heated, its density is reduced, and, in the extreme case, the highly dilute gas phase is gradually approached (cf. Figure 4.5). Therefore, the optical band-gap needs to be written more appropriately as $E_{\text{opt}}(T, \rho) = VDE(T, \rho) + V_0(T, \rho)$. The asymptotic energetics of the gas phase ($\rho \to 0$) can be derived from an equivalent photoelectron spectrum of monomeric ammonia molecules (cf. Figure 4.5d, data taken again from Ref. 45). The vertical detachment energy of the monomer is 10.9 eV[47] and is thus, about 1.6 eV higher than the *VDE* of the bulk liquid. It is obvious that ($V_0 \to 0$) for ($\rho \to 0$) because the monomer photoemission cannot be stabilized by the vacuum. Precise and detailed information pertaining to the evolution of both the $VDE(T, \rho)$ and $V_0(T, \rho)$ with the thermodynamic state variables is

not available to date. However, an interpretation of the T and ρ–dependent ejection length as a mirror image of the electron's excess kinetic energy seems highly plausible in light of the existing photoelectron spectra of ammonia monomers andclusters.

Additional support for our notion of thermally induced level shifts comes from theoretical calculations of the optical transitions of bulk liquids. Although not directly comparable to ammonia, the optical spectrum of water was studied some time ago by Bursulaya et al.[50] using a truncated adiabatic basis set description. In the region around 8 eV, the water spectrum is believed to be governed by the $\tilde{X}^1A_1 \rightarrow \tilde{A}^1B_1$ resonance of the monomer, which is attributed to the promotion of an electron from the nonbonding $1b_1$ highest occupied molecular orbital to the unoccupied antibonding $4a_1$ orbital (an O3s-Rydberg orbital). It turns out that in contrast to the conduction band (cf. Ref. 51), the $\tilde{X} \rightarrow \tilde{A}$ transition finds itself blue-shifted in the condensed phase with respect to the gas phase by about 1 eV. Theoretical calculations

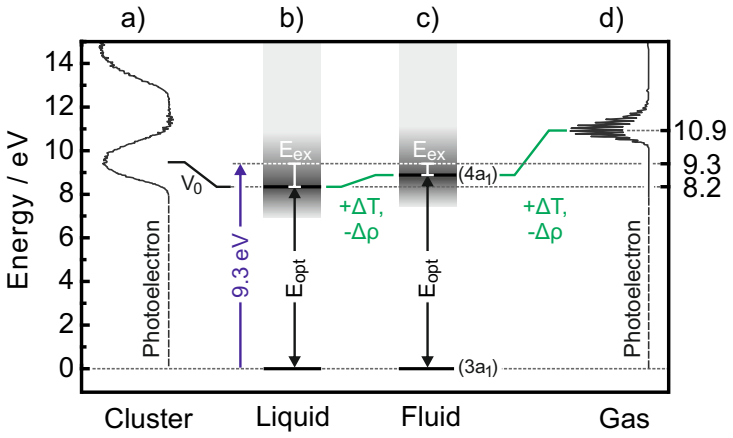

Figure 4.5: Photoelectron spectra (a and d, both reproduced from Ref. 45) and schematic energy level diagrams pertaining to the vertical photoionization (b and c) of liquid-to-supercritical ammonia. Assuming that the cluster data are fully converged toward the bulk values, the energetics for vertical photoemission into the liquid phase (b) can be estimated by taking into account a solvent-stabilization of the quasi-free electron by the solvent (see text). The conduction band of the liquid and fluid phases is indicated by the gray-shaded areas. Changing the thermodynamic conditions by increasing the temperature or decreasing the density gives rise to a gradual blueshift of the band-gap energy as indicated in panel c. Conceptually this shift is attributed to a gradual return of the bottom of the conduction to the isolated molecule limit (d), as more gas-like conditions are approached.

attribute this surprising finding to a Rydbergization effect, in which high lying Rydberg excited states overlap with the core electronic states of nearby molecules. The resultant Pauli repulsion is much stronger in the dense liquid as compared to the gas phase, and, consequently, the $\tilde{X} \rightarrow \tilde{A}$ transition is energetically lifted on increasing the particle packing. By calculating the optical spectrum of water for a variety of supercritical conditions Bursulaya et al.[50] was able to predict for this $\tilde{X} \rightarrow \tilde{A}$ transition a gradual approach of the gas phase energy gap as the thermodynamic conditions are continuously changed from liquid-like to gas-like. This behavior of the optical spectrum of liquid-to-supercritical water was later on confirmed through experimental measurement of the temperature and density dependent ultraviolet absorption edge of water by Marin et al.[18] as well as through theoretical calculations based on the perturbed matrix method combined with molecular dynamics simulations by d'Adramo et al.[52] In this context, a gradual approach of the optical band-gap on transiting from liquid-like to gas-like conditions as proposed in Figure 4.5 for ammonia is not at all unreasonable. Finally, we come back to previous experiments on the excitation energy dependence of the mechanism for two-photon ionization by Elles et al.[16] of ambient water and compare them to our data on fluid ammonia. For water, the thermalization distance was found to increase by as much as 1.5 nm per eV of excess energy around the presumed optical band-gap of 9.9 eV (at 298 K and 1 atm). Assuming that $\langle r_0 \rangle$ of the ammoniated electron scales equally with the excess energy as that of the hydrated electron, the apparent range of thermalization distances seen in our experiments (cf. Figure 4.3 and Table 4.1) would correspond to an increase of the excess energy of about 1.8 eV. Having estimated the optical band-gap of liquid ammonia at roughly 8.2 eV, the conduction band would then be located at about 10.0 eV at the lowest density and the highest temperature employed here. That the bottom of the conduction band is located roughly 1.4 eV below this value (see above) explains why solvated electrons can still be observed under such conditions. Furthermore, an extrapolation of these data to $\rho \rightarrow 0$, i.e., vanishing $\langle r_0 \rangle$ implies that the conduction band would be located at $\sim$10.3 eV. This is indeed not too far off the vertical detachment energy of the ammonia monomer as determined through photoelectron spectroscopy and implies that the thermally induced level-shifts in water and in ammonia are similar in magnitude.

The electronic structure of ammonia does bear some similarities to that of

water. The lowest energy transition, $\tilde{X}^1A_1^{'} \rightarrow \tilde{A}^1A_1^{''}$, involves the promotion of an electron from the nonbonding highest occupied $1a_2^{''}$ lone pair molecular orbital to the unoccupied antibonding $3sa_1^{'}$ (an N3s-Rydberg orbital). In the gas phase, the $\tilde{X} \rightarrow \tilde{A}$ transition shows a vibrational progression due to the planarization of the molecular frame in the excited state and each line is significantly broadened due to predissociation.[53–55] At room temperature, the gas phase spectrum is maximal around 6.4 eV.[56] Just like in water, the $\tilde{X} \rightarrow \tilde{A}$ transition shifts upward in energy upon entering the condensed phase where it is found to peak around 7.0 eV and to lack any vibrational substructure.[57] This blue-shift is slightly less than what was found for water but may equally be attributed to the destabilization of the diffuse Rydberg excited state due to repulsive exchange interaction with nearest neighbor molecules. It could, however, be that the small difference of the energetic shifts reflects the strength of the interactions between the molecules in the liquid (including hydrogen-bonding).[58] It is a great pity that information complementary to the water data from Ref. 18 regarding the temperature and density dependence of the ultraviolet absorption edge of ammonia is entirely missing.

Finally, our findings suggest that the T, ρ-dependence of the electronic energy states in the liquid phase is likely to be equally important for the modeling of the final stages of electron scattering (i.e., once subexcitation energies are reached) in temperature dependent radiolysis experiments of polar and protic fluids.[59–61] A full quantum mechanical study of the electron transmission in terms of wave packet dynamics as a function of temperature and density therefore appears highly desirable.[62]

4.5 Conclusions

We have presented a full analysis of the geminate dynamics of solvated electrons produced by 266 nm two-photon excitation of liquid and supercritical ammonia based on Monte Carlo simulations of the recombination process. The model explicitly accounted for the two known reaction pathways of the solvated electron, namely, a direct and an indirect ion-pair mediated annihilation with the aminyl radical NH_2. At the excitation energy pertaining to our data of 9.3 eV, the ionization mechanism is vertical in nature, i.e., initially quasi-free electrons are produced in the conduction band of the solvent network, which subsequently localize in the solvent. Our results reveal a grad-

ual, but drastic decrease of the solvated electron's thermalization distance on moving from the cryogenic high density liquid to the dilute supercritical fluid. We have correlated this dependence with an increasing threshold for direct, vertical photoemission into the polar protic solvent, which gives rise to a decrease of the excess energy initially imparted on the photoejected electron. Qualitatively speaking, increasing the temperature or decreasing the density at a constant excitation energy has that same effect as raising the total photoionization energy at constant thermodynamic conditions. In the future, we will further test this notion of thermally induced shifts of the optical band-gap by extending our studies to the excitation energy dependence of the multi-photon ionization of liquid-to-supercritical ammonia.

ACKNOWLEDGEMENTS

The authors are grateful to Dr. A. Lindblad for providing the photoelectron spectra of ammonia. Financial support by the Deutsche Forschungsgemeinschaft through the Collaborative Research Center, SFB 813 "Chemistry at Spin Centers" is gratefully acknowledged.

[1] Chen, X.; Bradforth, S. E. *Annu. Rev. Phys. Chem.* **2008**, *59*, 203.

[2] Crowell, R. A.; Bartels, D. M. *J. Phys. Chem.* **1996**, *100*, 17940.

[3] Sander, M. U.; Gudiksen, M. S.; Luther, K.; Troe, J. *Chem. Phys.* **2000**, *258*, 257.

[4] Kratz, S.; Torres-Alacan, J.; Urbanek, J.; Lindner, J.; Vöhringer, P. *Phys. Chem. Chem. Phys.* **2010**, *12*, 12169.

[5] Hertwig, A.; Hippler, H.; Unterreiner, A.; Vöhringer, P. *Ber. Bunsenges. Phys. Chem.* **1998**, *102*, 805.

[6] Lu, H.; Long, F. H.; Eisenthal, K. B. *J. Opt. Soc. Am. B* **1990**, *7*, 1511.

[7] Kambhampati, P.; Son, D. H.; Kee, T. W.; Barbara, P. F. *J. Phys. Chem. A* **2002**, *106*, 2374.

[8] Goulet, T.; Jay-Gerin, J.-P. *J. Chem. Phys.* **1992**, *96*, 5076.

[9] Pimblott, S. M. *J. Phys. Chem.* **1991**, *95*, 6946.

[10] Turi, L.; Rossky, P. J. *Chem. Rev.* **2012**, *112*, 5641.

[11] Sprik, M.; Klein, M. L. *J. Chem. Phys.* **1989**, *91*, 5665.

[12] Torres-Alacan, J.; Kratz, S.; Vöhringer, P. *Phys. Chem. Chem. Phys.* **2011**, *13*, 20806.

[13] Hart, E. J.; Anbar, M. *The Hydrated Electron;* John Wiley & Sons Inc.: New York, 1970.

[14] Sander, M. U.; Luther, K.; Troe, J. *Ber. Bunsenges. Phys. Chem.* **1993**, *97*, 953.

[15] Sander, M. U.; Luther, K.; Troe, J. *J. Phys. Chem.* **1993**, *97*, 11489.

[16] Elles, C. G.; Jailaubekov, A. E.; Crowell, R. A.; Bradforth, S. E. *J. Chem. Phys.* **2006**, *125*, 044515.

[17] Bernas, A.; Ferradini, C.; Jay-Gerin, J.-P. *J. Photochem. Photobiol. A* **1998**, *117*, 171.

[18] Marin, T. W.; Takahashi, K.; Bartels, D. M. *J. Chem. Phys.* **2006**, *125*, 104314.

[19] Bartels, D. M.; Crowell, R. A. *J. Phys. Chem. A* **2000**, *104*, 3349.

[20] Elles, C. G.; Shkrob, I. A.; Crowell, R. A.; Bradforth, S. E. *J. Chem. Phys.* **2007**, *126*, 164503.

[21] Urbanek, J.; Dahmen, A.; Torres-Alacan, J.; Königshoven, P.; Lindner, J.; Vöhringer, P. *J. Phys. Chem. B* **2012**, *116*, 2223.

[22] Nordlund, D.; Ogasawara, H.; Bluhm, H.; Takahashi, O.; Odelius, M.; Nagasono, M.; Pettersson, L. G. M.; Nilsson, A. *Phys. Rev. Lett.* **2007**, *99*, 217406.

[23] Lian, R.; Oulianov, D. A.; Shkrob, I. A.; Crowell, R. A. *Chem. Phys. Lett.* **2004**, *398*, 102.

[24] Krohn, C. E.; Thompson, J. C. *Phys. Rev. B* **1979**, *20*, 4365.

[25] Huntress, W. T.; Mosesman, M. M.; Elleman, D. D. *J. Chem. Phys.* **1971**, *54*, 843.

[26] Belloni, J.; Cordier, P.; Delaire, J. A.; Delcourt, M. O. *J. Phys. Chem.* **1978**, *82*, 537.

[27] Kieffer, F.; Klein, J.; Lapersonne-Meyer, C.; Magat, M.; Belloni, J.; Billiau, F.; Cordier, P.; Delaire, J.; Delcourt, M. O. *Faraday Discuss. Chem. Soc.* **1977**, *63*, 55.

[28] Schindewolf, U. *Ber. Bunsenges. Phys. Chem.* **1982**, *86*, 887.

[29] Liu, Y.; Tuckerman, M. E. *J. Phys. Chem. B* **2001**, *105*, 6598.

[30] This assumption is consistent with most recent ab intio molecular dynamics simulations of the cationic hole formed in bulk liquid water upon ionization. These simulations demonstrate that the cationic hole localizes within 30 fs and then transfers practically immediately a proton to a neighboring water molecule. The dynamic trajectories show that the radical and the hydronium cation are formed as direct nearest neighbors

and that they separated only by a short hydrogen bond, see: Marsalek, O.; Elles, C. G.; Pieniazek, P. A.; Pluharova, E.; VandeVondele, J.; Bradforth, S. E.; Jungwirth, P. *J. Chem. Phys.* **2011**, *135*, 224510.

[31] Ricci, M. A.; Nardone, M.; Ricci, F. P.; Andreani, C.; Soper, A. K. *J. Chem. Phys.* **1995**, *102*, 7650.

[32] Feng, H.; Liu, X.; Gao, W.; Chen, X.; Wang, J.; Chen, L.; Ludemann, H.-D. *Phys. Chem. Chem. Phys.* **2010**, *12*, 15007.

[33] Tassaing, T.; Soetens, J.-C.; Vyalov, I.; Kiselev, M.; Idrissi, A. *J. Chem. Phys.* **2010**, *133*, 214505.

[34] Buback, M.; Harder, W. D. *Ber. Bunsenges. Phys. Chem.* **1977**, *81*, 603.

[35] Kindt, J. T.; Schmuttenmaer, C. A. *J. Chem. Phys.* **1997**, *106*, 4389.

[36] LaVerne, J. A.; Pimblott, S. M. *J. Phys. Chem.* **1993**, *97*, 3291.

[37] Buchhauser, J.; Gross, T.; Karger, N.; Ludemann, H.-D. *J. Chem. Phys.* **1999**, *110*, 3037.

[38] Belloni, J.; Billiau, F.; Delaire, J.; Delcourt, M.; Marignier, J. *Radiat. Phys. Chem.* **1983**, *21*, 177.

[39] Catterall, R.; Edwards, P. P.; Slater, J.; Symons, M. C. *Chem. Phys. Lett.* **1979**, *64*, 275.

[40] Jou, F.-Y.; Freeman, G. R. *J. Phys. Chem.* **1981**, *85*, 629.

[41] Schmidt, K. H.; Han, P.; Bartels, D. M. *J. Phys. Chem.* **1995**, *99*, 10530.

[42] Lindner, J.; Unterreiner, A.-N.; Vöhringer, P. *ChemPhysChem* **2006**, *7*, 363.

[43] Lindner, J.; Unterreiner, A.-N.; Vöhringer, P. *J. Chem. Phys.* **2008**, *129*, 064514.

[44] Coe, J. V.; Earhart, A. D.; Cohen, M. H.; Hoffman, G. J.; Sarkas, H. W.; Bowen, K. H. *J. Chem. Phys.* **1997**, *107*, 6023.

[45] Lindblad, A.; Bergersen, H.; Pokapanich, W.; Tchaplyguine, M.; Ohrwall, G.; Bjorneholm, O. *Phys. Chem. Chem. Phys.* **2009**, *11*, 1758.

[46] Sarkas, H. W.; Arnold, S. T.; Eaton, J. G.; Lee, G. H.; Bowen, K. H. *J. Chem. Phys.* **2002**, *116*, 5731.

[47] Edvardsson, D.; Baltzer, P.; Karlsson, L.; Wannberg, B.; Holland, D. M. P.; Shaw, D. A.; Rennie, E. E. *J. Phys. B: At., Mol. Opt. Phys.* **1999**, *32*, 2583.

[48] Bennett, G. T.; Coffman, R. B.; Thompson, J. C. *J. Chem. Phys.* **1987**, *87*, 7242.

[49] Harima, Y.; Sato, H.; Suga, K. *J. Phys. Chem.* **1989**, *93*, 6418.

[50] Bursulaya, B. D.; Jeon, J.; Yang, C.-N.; Kim, H. J. *J. Phys. Chem. A* **2000**, *104*, 45.

[51] Winter, B.; Weber, R.; Widdra, W.; Dittmar, M.; Faubel, M.; Hertel, I. V. *J. Phys. Chem. A* **2004**, *108*, 2625.

[52] D'Abramo, M.; Nola, A. D.; Aschi, M.; Amadei, A. *J. Chem. Phys.* **2008**, *128*, 021103.

[53] Walsh, A. D.; Warsop, P. A. *Trans. Faraday Soc.* **1961**, *57*, 345.

[54] Vaida, V.; McCarthy, M. I.; Engelking, P. C.; Rosmus, P.; Werner, H.-J.; Botschwina, P. *J. Chem. Phys.* **1987**, *86*, 6669.

[55] Ashfold, M.; Langford, S.; Morgan, R.; Orr-Ewing, A.; Western, C.; Scheper, C.; de Lange, C. *Eur. Phys. J. D* **1998**, *4*, 189.

[56] Cheng, B.-M.; Lu, H.-C.; Chen, H.-K.; Bahou, M.; Lee, Y.-P.; Mebel, A. M.; Lee, L. C.; Liang, M.-C.; Yung, Y. L. *Astrophys. J.* **2006**, *647*, 1535.

[57] Mason, N. J.; Dawes, A.; Holtom, P. D.; Mukerji, R. J.; Davis, M. P.; Sivaraman, B.; Kaiser, R. I.; Hoffmann, S. V.; Shaw, D. A. *Faraday Discuss.* **2006**, *133*, 311.

[58] Dawes, A.; Mukerji, R. J.; Davis, M. P.; Holtom, P. D.; Webb, S. M.; Sivaraman, B.; Hoffmann, S. V.; Shaw, D. A.; Mason, N. J. *J. Chem. Phys.* **2007**, *126*, 244711.

[59] Hervé du Penhoat, M.-A.; Goulet, T.; Frongillo, Y.; Fraser, M.-J.; Bernat, P.; Jay-Gerin, J.-P. *J. Phys. Chem. A* **2000**, *104*, 11757.

[60] Sanguanmith, S.; Muroya, Y.; Meesungnoen, J.; Lin, M.; Katsumura, Y.; Kohan, L. M.; Guzonas, D.; Stuart, C.; Jay-Gerin, J.-P. *Chem. Phys. Lett.* **2011**, *508*, 224.

[61] Muroya, Y.; Sanguanmith, S.; Meesungnoen, J.; Lin, M.; Yan, Y.; Katsumura, Y.; Jay-Gerin, J.-P. *Phys. Chem. Chem. Phys.* **2012**, *14*, 14325.

[62] Barnett, R. N.; Landman, U.; Nitzan, A. *J. Chem. Phys.* **1990**, *93*, 6535.

5

Below-Band-Gap Ionization of Liquid-to-Supercritical Ammonia: Geminate Recombination via Proton-Coupled Back-Electron-Transfer

Janus Urbanek, and Peter Vöhringer*

Abteilung für Molekulare Physikalische Chemie, Institut für Physikalische und Theoretische Chemie, Rheinische Friedrich-Wilhelms-Universität, Wegelerstr. 12, 53115 Bonn, Germany

* To whom correspondence should be addressed. Email: p.voehringer@uni-bonn.de

5.1 Abstract

Femtosecond multi-photon ionization experiments have been conducted on ammonia over a wide range of temperature (225 K $\leq T \leq$ 490 K) and density (0.18 g cm^{-3} $\leq \rho \leq$ 0.71 g cm^{-3}) thereby covering the liquid and supercritical phases. The experiments were carried out with excitation pulses having a wavelength of 400 nm and the ionization was found to involve two photons. Therefore, the total ionization energy in this study corresponds to 6.2 eV, which is roughly 2 eV below the valence-to-conduction band-gap of the fluid. The ionization generates solvated electrons, which have been detected through their characteristic near-infrared resonance, and must be facilitated through a coupling to nuclear degrees of freedom of the liquid. The recombination of the solvated electron with the geminate fragments was found to obey predominantly single-exponential kinetics with time constants between 500 fs and 1 ps. Only a very minor fraction of the photo-generated electrons is able to escape from the geminate recombination. The results indicate that the majority of electrons are injected into suitable trapping sites located between the first and second solvation shell of the initially ionized ammonia molecules. Such configurations can be considered as instantly reactive and facilitate an ultrafast barrierless electron annihilation. This process is found to exhibit a pronounced kinetic isotope effect, which indicates that the electronic decay is accompanied by the transfer of a proton. The sequence of ionization and recombination events can therefore be described appropriately as a proton-coupled electron transfer (PCET) followed by a proton-coupled back-electron transfer (PCBET).

5.2 Introduction

Solvated electrons are primary intermediates in the interaction of condensed matter with high energy radiation.[1] They can be employed as exquisitely sensitive probes for the investigation of the structural, dynamical, and electronic properties of their microscopic environment.[2–6] In the last decades, numerous femtosecond multi-photon ionization (fs-MPI) studies have been carried out on neat water where the hydrated electron e^-_{aq} is produced alongside the molecular fragments OH andH_3O^+.[7–16] Such studies provided a comprehensive picture of the mechanisms leading to the generation, localization,

solvation, and thermalization of the photoelectrons injected into the hydrogen bonded aqueous network.[7,8,11,15,17–19] In particular, the spatial distribution of all the photolysis products is inhomogenous and as a result, the initial (sub-nanosecond) recombination of the solvated electron with the molecular fragments is predominantly geminate in nature.[20–27] The intricate dynamics, i.e. the mechanistic pathways and their microscopic reaction rates, eventually leading to the annihilation of the solvated electron is governed by the finer details of this initial spatial fragment distribution.

The crucial quantity characterizing the distribution of inter-fragment configurations is termed mean "thermalization distance", $\langle r_0 \rangle$, or alternatively, "injection length".[1] It is understood as the distance that the electron is able to travel from the primary site of matter-field interaction before becoming fully localized by and thermalized with the surrounding solvent environment. Contrary to pulse radiolysis, which exposes the condensed material to a high energy ($\sim$MeV) electron beam and where the solvated electron's fate is dictated by its inelastic collisions with solvent molecules and a complex network of secondary spur reactions,[21,22,28–33] the excitation conditions of multi-photon ionization are very well defined. This opens up the possibility to systematically study solvated electron dynamics as a function of the ionization energy thereby offering a unique spectroscopic window into the complicated electronic structure of dynamically disordered condensed matter.[7,8,11,19] In this context, the specific involvement of nuclear motions within the solvent network leading to electron injection at excitation energies well below the optical valence-to-conduction band gap of the liquid remains a fundamental issue that needs to be clarified.[8,10,13,14,17,19,34,35]

For liquid water and due to the dissociative character of the excited electronic states of H_2O,[36,37] the below-band-gap excitation may yield an OH radical and a translationally hot hydrogen atom. The H atom may then collide with a neighboring water molecule to form a hydronium cation and the solvated electron.[8,38,39] An alternative scenario invokes a proton-coupled electron transfer between two nearest neighbor water particles in the liquid network[38,40] thereby generating a H_3O^+ and an electronically excited hydroxide anion. The latter then transforms into a hydroxyl radical by injecting an electron into a suitably pre-configured solvent trap. Whether or not these mechanisms are generic for the multi-photon ionization of all polar protonated solvents is a subject that has not been fully addressed so far.

Along these lines, we recently reported the first ever femtosecond multi-photon ionization study of another member of the isoelectronic series of first-row hydrides, namely ammonia, NH_3.[41,42] We investigated this system over as wide a range of thermodynamic conditions as possible starting from the dense cryogenic liquid phase all the way over to the supercritical phase at elevated temperatures with almost gas phase densities. In doing so it was possible to examine in detail the influence of the particle packing within the liquid onto the electronic structure of the liquid and in particular, on the magnitude of the optical valence-to-conduction band gap.[42–44]

The ionization was carried out with 266 nm light pulses and involved the interaction with two photons. As a result, the total ionization energy was 9.3 eV. Since the band gap of the dense liquid[42,45–47] corresponds to about 8.2 eV, the ionization mechanism in these experiments is vertical in nature, i.e. the optical excitation directly induces the injection of an electron into the bulk according to

$$NH_3 + 2\,h\nu \longrightarrow NH_3^+ + e_{CB}^-. \tag{5.1}$$

Thus, the electron is initially born as a quasi-free electron, e_{CB}^-, in the conduction band of the solvent and it is accompanied by an ammonia cation, NH_3^+, in the nuclear configuration of the neutral NH_3 molecule. The ensuing localization of the electron by the solvent is entirely decoupled from any nuclear rearrangements involving the cationic hole. The positively charged ammonia then transfers a proton onto a nearest-neighbor NH_3 molecule thereby forming an aminyl radical and an ammonium cation.[48] The net result of the two-photon ionization is therefore entirely analogous to that of water

$$2NH_3 + 2\,h\nu \longrightarrow e_{am}^- + NH_4^+ + NH_2. \tag{5.2}$$

The time-dependence of the fs-MPI data on time scales ranging up to about 1 ns track precisely the geminate recombination dynamics of the solvated electron. These were analyzed in terms of Monte-Carlo simulations by taking into account two competing reaction channels that annihilate the solvated electron by a diffusion-limited encounter with the aminyl radical.[41,42,49,50] The first of which is the direct electron-radical recombination

$$e_{am}^- + NH_2 \longrightarrow NH_2^- \tag{5.3}$$

while the second pathway represents an indirect, ion-pair mediated recombination sequence

$$e^-_{am} + NH_4^+ \rightleftharpoons (e^-_{am} \cdot NH_4^+) \tag{5.4}$$

$$(e^-_{am} \cdot NH_4^+) + NH_2 \longrightarrow NH_2^- + NH_4^+. \tag{5.5}$$

The chemical nature of the ion pair is an intriguing issue in itself that has recently been addressed in Ref. 51 in the context of lithium-ammonia solutions. In analogy, the solvated ion-pair can be thought of as an ammoniated ammonium cation that is in spatial proximity to the ammoniated electron, i.e., $[NH_4^+(NH_3)_m \cdot e^-(NH_3)_n]$. Depending upon the distance between the ion partners (i.e., with varying solvation shells m and n), the excess electron wave function can either be localized on the ammonia or the ammonium cluster. In the latter case, we would formally speak of a solvated ammonium radical, $NH_4(NH_3)_{m+n}$, which is formally equivalent to the solvated neutral metal from metal-ammonia solutions.

The computer simulations revealed that an increasing temperature and a decreasing density give rise to a diminishing average thermalization distance from 3.2 nm in the cryogenic liquid down to roughly 0.5 nm in the high temperature supercritical fluid.[42] We primarily attributed this decrease of the injection length to an energetic upshift of the optical valence-to-conduction band gap as the character of the solvent is continuously changed from "liquid-like" to more "gas-like". At a fixed ionization energy, this level shifting leads to a lowering of the excess kinetic energy imparted to the ejected quasi-free electron and thus to a smaller injection length.[42]

To further explore the impact of the solvent's electronic structure on the solvated electron dynamics, we now extend these fs-MPI studies in NH_3 to significantly lower excitation energies by using laser pulses centered at 400 nm (rather than 266 nm as we had used previously). Provided the primary matter-field interaction involves again two photons, the total ionization energy corresponds to 6.2 eV, which is now $\sim$2 eV below the optical band gap.[42,45–47] As mentioned above, at such low energies, the localization of the electron is no longer decoupled from the molecular transformations of the remaining cationic hole.[7] The formation of solvated electrons necessitates a substantial stabilization of the nascent photolysis products by nuclear rearrangements within the solvent network. Such an indirect ionization can be facilitated e.g. by a proton-coupled electron transfer (PECT),[38,40] where the process of

electron injection into localized "pre-solvated" states in the solvent is coupled to a simultaneous proton-transfer onto a nearest-neighbor molecule in the solvent. Accordingly, much shorter thermalization distances can be expected than for direct ionization above the band gap where quasi-free electrons are produced.[52] As the recombining fragments are now created in closest spatial proximity the geminate dynamics may no longer be affected by the diffusional encounter of the recombining particles. Thus, lowering the ionization energy can be expected to change the nature of the apparent recombination dynamics from "bimolecular and diffusion controlled" for excitation above the band gap to "quasi-unimolecular and reaction controlled" for excitation below the band gap.

5.3 Experimental Section

Transient absorption measurements were carried out using a home-built 1 kHz Ti:sapphire regenerative chirped pulse amplifier as a front-end to a femtosecond ultraviolet (UV)-pump and near-infrared (NIR)-probe spectrometer which was already used in previous experiments.[12,53,54] Briefly, the 800 nm, 100 fs pulses delivered by the front-end had an energy of 750 µJ and were split by a 50% dielectric beam splitter. One portion of the fundamental was frequency doubled in a 1 mm thick type I β-BaB_2O_4-crystal to obtain 400 nm photoionization pulses with energies as high as 180 µJ while maintaining the pulse duration of the front-end.

The remaining 50% of the fundamental output were used to pump an optical parametric amplifier (OPA, TOPAS, light conversion) to provide femtosecond NIR-pulses tunable between 1200 nm and 2400 nm. The pulses were divided by a dielectric beam splitter into probe and reference-pulses, both of which were focused into the sample using a 45° off-axis aluminum mirror with a focal length of 100 mm. The pump beam was overlapped inside the sample with the probe beam at an angle of 5° using a 0.4 m focal length, fused silica lens. The pump-beam radius at the sample was 670 µm and that of the probe beam was 240 µm. The probe and reference pulse intensities were detected behind the cell by PbS-photoresistors. The pump-beam irradiance was adjusted without changing the diameter of the beam by means of a combination of a half-wave retardation plate and a polarizer.

We studied the geminate dynamics of solvated electrons in fluid ammonia

over a wide range of temperature and density. The exact thermodynamic state points were chosen to coincide with those of our previous investigation of the 266 nm photoionization,[41,42] i.e. they were organized into a measurement series along the 423 K-isotherm and another one along the 300 bar isobar. To this end, samples of NH_3 (99.98%, AirLiquide) or ND_3 (99 atom% D, Sigma-Aldrich) were prepared in a stainless steel high-pressure and high-temperature optical cell[55,56] with 2.5 mm thick sapphire windows and an optical path length of 1.0 mm. The solvated electron's dynamics were monitored using probe pulses with a center wavelength of 1450 nm. This ascertains for all chosen thermodynamic conditions an optical detection of the solvated electrons on the highfrequency edge of their stationary absorption spectrum thereby precluding a contamination of the pump-probe data by the electronic localization / thermalization dynamics (see below).[9,53,54]

5.4 Results and Discussion

5.4.1 400 nm Mixed Multi-Photon Ionization of Fluid NH_3

It is well established that the multi-photon ionization of neat fluids produces solvated electrons in a non-equilibrium configuration at early times.[9,53,54,57] The initial relaxation leading to the formation of fully equilibrated electrons involves thermal cooling and structural rearrangements of their solvation shells. These dynamics give rise to a dynamic spectral blue-shift of the solvated electron's optical resonance which inevitably affects the temporal evolution in the mid-to-near-IR pump-probe signals at short delays. To obtain recombination kinetics that are unperturbed by these thermalization/solvation dynamics, the system was optically probed on the high frequency edge of the solvated electron's stationary absorption spectrum.[58,59] Under such probing conditions, dynamic solvation and cooling can only result in a temporally delayed rise of the transient absorption, whereas a decay of the signal is exclusively related to a loss of solvated electrons due to recombination.[12,41] Thus, to conduct fs-MPI experiments with an optical detection of the solvated electron, prior knowledge of its absorption spectrum at thermal equilibrium is required. Luckily, information on the temperature and density dependent spectral position of the resonance in liquid-to-supercritical ammonia is available from previous work by Schindewolf and coworkers.[60,61] Note also that we have previously reported an absorption spectrum of solvated electrons following multi-photon

ionization of neat fluid ammonia, which is in very good agreement with the absorption spectrum of the ammoniated electron from metal/NH_3-solutions.

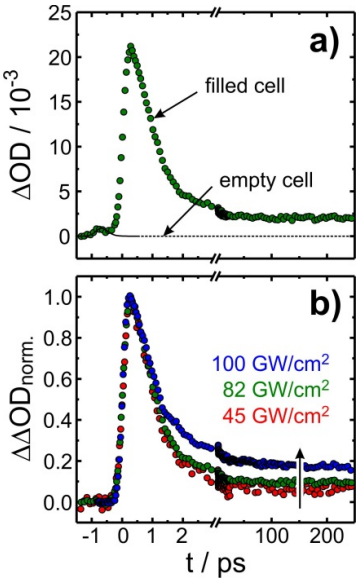

Figure 5.1: a) Pump-probe signal of liquid ammonia (filled circles, $T = 294\,\mathrm{K}$ and $\rho = 0.632\,\mathrm{g\,cm^{-3}}$) and of the empty cell (solid and dashed line, $T = 294\,\mathrm{K}$) recorded with a pump-pulse irradiance of $82\,\mathrm{GW\,cm^{-2}}$. b) Normalized induced optical density difference, $\Delta\Delta OD$, calculated from both measurements for various pump-beam irradiances.

A representative pump-probe signal obtained from photoionization of liquid ammonia with 400 nm femtosecond pulses at room temperature and 300 bar (corresponding to a density of $0.632\,\mathrm{g\,cm^{-3}}$) is shown in Figure 5.1. The pump-induced optical density, $\Delta OD(t)$, is characterized by an instrument response limited rise of the transient absorption and a subsequent, slower decay to an asymptotic limit within a few tens of picoseconds. The observation of a temporally unresolved rise of the signal is consistent with a time constant of 150 fs determined for the relaxation of solvated electrons from sodium-ammonia solutions following an optical s-to-p type electronic excitation.[53,54] It is important to emphasize that throughout this work the initial rise of the transient absorption remained instantaneous in character regardless of the thermodynamic conditions imposed on the sample.

The subsequent decay of the transient absorption is attributed to the recombination of the solvated electrons with the aminyl radicals according to reactions (5.3) through (5.5). Since the decay occurs on a sub-nanosecond

timescale, the recombination dynamics must predominantly be geminate in nature. A closer inspection of the data at the earliest delay times reveals a short lived signal contribution with a very small amplitude compared to the total maximal absorption. This feature can be traced back unambiguously to a pump-induced absorption in the sapphire window of the optical cell.[12] To remove this artifact and to obtain the pure recombination dynamics of the solvated electron, the pure window contribution was independently determined by measuring the response of the empty cell using the identical optical alignment and at the very same set of temperatures that was used for the experiments with the filled cell. As described previously,[12] the pure solvated electron response is then obtained from the difference of these two signals and is denoted $\Delta\Delta OD(t)$. As can be seen from Figure 5.1a, the pure electron response does not decay completely but instead reaches a constant signal for very long time delays. For the two-photon ionization of liquid-to-supercritical ammonia with 266 nm light,[41,42] such an absorption plateau could be attributed to the fraction of solvated electrons that is able to avoid the geminate recombination.

However, in stark contrast to the ionization with two 266 nm photons, the geminate dynamics seen here feature a pronounced dependence on the irradiance, I, of the 400 nm pump-beam. This effect is displayed in Figure 5.1b for the same thermodynamic conditions as before and for three representative pump intensities. To facilitate a comparison, each trace was normalized to its peak amplitude, $\Delta\Delta OD_{\text{max}}$ around $t \approx 0$. It can clearly be seen that with decreasing irradiance the ratio of the asymptotic absorption at around 200 ps to the peak absorption around zero time delay gradually decreases from about 18% at 100 GW cm^{-2} to only $\sim$6% at 45 GW cm^{-2}. Unfortunately, it was not possible to decide whether or not the signals converged to a low-irradiance limit because the signal-to-noise ratio became insufficient for irradiances smaller than 20 GW cm^{-2}.

To understand the underlying photo-physical processes responsible for this peculiar irradiance dependence, we accurately established the number of photons involved in the primary matter field interaction leading to the generation of solvated electrons. It turned out that the solvated electron signal scaled with the pump irradiance according to a power law, $\Delta\Delta OD(t, I) \propto I^n$. The exponent, n, is usually an indicator for the number of photons involved in the interaction of the material with the pump electric field. However, in

the experiments reported here, $n = n(t)$, is a pronounced function of the pump-probe time delay. In particular, the exponent was close to two for the earliest delays while it reached a value of ∼2.5 for delays in excess of 200 ps. As demonstrated in the supporting information, this behavior can be traced back to a mixed multi-photon ionization process that generates solvated electrons at two different ionization energies simultaneously, namely at 6.2 eV (corresponding to the combined energy of two 400 nm photons) and at 9.3 eV (equivalent to the total energy of three 400 nm photons). Thus, the pump-induced optical density has to be regarded as a superposition of two independent solvated electron signals

$$\Delta\Delta OD(t, I) = \Omega_2(t)\sigma_2 I^2 + \Omega_3(t)\sigma_3 I^3, \tag{5.6}$$

where σ_2 and σ_3 are the effective 400 nm two-photon and three-photon ionization cross sections. In equation 5.6, the signal is expressed in terms of the time-dependent survival probabilities, $\Omega_2(t)$ and $\Omega_3(t)$, pertaining to the solvated electrons generated by 400 nm two-photon and three photon-ionization, respectively. These quantities correspond to the fraction of solvated electrons still being present at a time, t, following their initial generation through the primary matter field interaction at $t = 0$.[62–64]

We have previously reported experimental data on the time-dependent survival probability of solvated electrons generated through femtosecond 266 nm two-photon ionization of liquid-to-supercritical ammonia.[41,42] Since the combined energy of two 266 nm photons is equal to that of three 400 nm photons, this information can now be as independent experimental information for $\Omega_3(t)$ in equation (5.6). The procedure to unambiguously determine the central quantity of this work namely, the time-dependent survival probability, $\Omega_2(t)$, of solvated electrons generated at an ionization energy of 6.2 eV via 400 nm two-photon absorption, is outlined in great detail in the supporting information. The result of such an analysis is shown in Figure 5.2.

At first glance, the correction introduced by the subtraction of the independently measured 9.3 eV contribution might seem small. However, the correction introduces a significant reduction of the asymptotic absorption plateau. In Figure 5.2a, the absorption is $\sim 2 \times 10^{-3}$ $\Delta\Delta OD$ units at a delay of 200 ps. Together with the value of the peak value of $\Delta\Delta OD = 23 \times 10^{-3}$ this allows us to calculate an ultimate survival probability, Ω_∞, corresponding

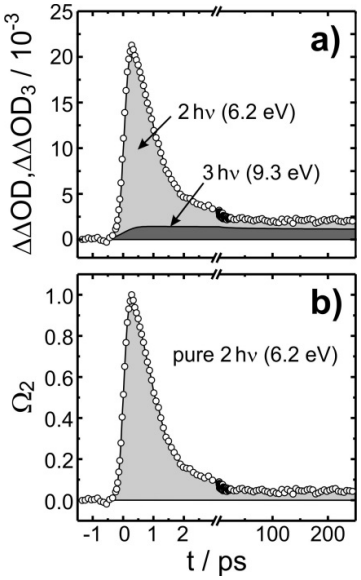

Figure 5.2: a) Decomposition of the experimentally obtained pump-probe signal recorded at $I = 82\,\mathrm{GW\,cm^{-2}}$ (open circles) into a two-photon (light gray) and three-photon (dark gray) contribution, the latter of which is adopted from Ref. 42. b) Geminate survival probability of solvated electrons that are exclusively produced by the 400 nm two-photon ionization (6.2 eV).

to the aforementioned fraction of solvated electrons that is able to avoid the geminate recombination altogether.[63] For the data in Figure 5.3a we obtain a value for Ω_∞ of roughly 9%. After correction for the 3-photon contribution, this value is lowered to 5% as is shown in Figure 5.2b.

5.4.2 Ultimate Survival Probability and Ionization Mechanism

Having disentangled the individual contributions to the optical pump-probe signal, it is now possible to compare the geminate dynamics resulting from the below-band gap ionization at 6.2 eV with those originating from the vertical ionization at an energy of 9.3 eV as reported earlier.[41,42] The time-dependent survival probabilities induced at these two ionization energies are shown in Figure 5.3a for the ammoniated electron at a temperature of 294 K and a density of $0.632\,\mathrm{g\,cm^{-3}}$. At 9.3 eV (cf. blue data) only about 20% of the initially generated solvated electrons are lost within the first 200 ps due to their reactive encounters with the molecular fragments. In stark contrast, the geminate dynamics following the 6.2 eV ionization are much more efficient and within less than 5 ps, more than 90% of all initially generated electrons

are completely annihilated. The acceleration and increased efficiency of the recombination upon lowering the ionization energy is a strong indication that the initial distribution of solvated electrons around the primary site of ionization becomes more compact.[10,11,14,19,65,66] While in the case of the vertical ionization, where the electrons are initially born as highly mobile charge carriers that can travel very large distances from the cationic hole even within the duration of the ionization pulse, this initial distribution is rather diffuse, the below-band-gap ionization produces electrons that must be localized in the immediate vicinity of their geminate molecular fragments. Quite naturally, a tighter initial distribution accounts for an enhanced encounter probability at significantly shorter encounter times.

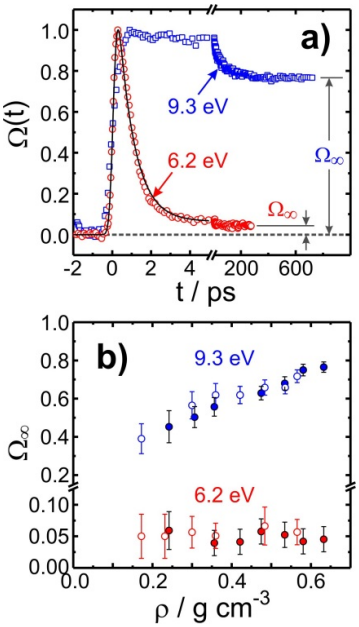

Figure 5.3: Comparison of the experimental survival probabilities of the solvated electron generated by photoionization of liquid NH_3 at 6.2 eV and at 9.3 eV. a) Time-dependent survival probability at a temperature of 294 K and a density of 0.632 g cm^{-3}. b) Ultimate escape probabilities, as a function of the solvent density. Closed circles represent data obtained along the 300 bar isobar and open circles data along the 423 K isotherm. The data at 9.3 eV is reproduced from Ref. 41.

The increased recombination efficiency is expressed more quantitatively in the ultimate survival probability,[63] Ω_∞, which is plotted in Figure 5.3b as a function of the solvent density (the density dependence of the full recombination kinetics is discussed in the next section). The data for the 9.3 eV

ionization were adopted from Ref. 41, where the pronounced reduction of Ω_∞ with decreasing density was attributed to a compaction of the initial spatial electron distribution as evidenced by a shrinking "thermalization distance", $\langle r_0 \rangle$. Monte-Carlo simulations of the diffusion-limited encounter dynamics revealed that the value of $\langle r_0 \rangle$ decreases gradually from 3.2 nm in the dense cryogenic liquid to only about 0.5 nm in the dilute supercritical phase.[42] Thus the average injection length slowly approaches the magnitude of the interparticle distances in the neat solvent as the system is isobarically heated or isothermally diluted.[67,68]

The ultimate escape probability from the 6.2 eV photoionization behaves vastly different (cf. Figure 5.3b). Firstly, it is about an order of magnitude smaller as compared to that resulting from vertical ionization and secondly, remaining at roughly 5% regardless of the temperature or the density, it appears to be entirely insensitive to the imposed thermodynamic conditions. Both findings suggest that the initial distribution of the geminate fragments has assumed a critical compactness with a mean thermalization distance perhaps even corresponding to the nearest neighbor distance in fluid ammonia. If this were indeed the case, the recombination dynamics should no longer be governed by the diffusional encounter of the geminate fragments. The diffusion-driven electron annihilation typically manifests itself in quasi-stretched exponential decays of the time-dependent escape probability (see Ref. 64 for analytic expressions of $\Omega(t)$ in this limit). However, as demonstrated in Figure 5.3a by the solid curve, the kinetic data obtained by the 400 nm two-photon ionization can be fitted satisfactorily by a single-exponential decay to which a finite offset signal is added (see below for a more detailed analysis). This further corroborates the idea of a recombination mechanism following below-band-gap ionization in which the diffusional dynamics are no longer rate-limiting.[69]

To follow up on the interpretation of the 400 nm data reflecting non-diffusive recombination within an initial spatial distribution of critical compactness, the reactive three-body system, ($e^-_{am} + NH_2 + NH_4^+$), composed of a solvated electron, an aminyl radical, and an ammonium cation is sketched simplistically for liquid-like densities. Under these conditions, the nitrogen-nitrogen radial distribution function of ammonia[68,70] indicates a coordination number of approximately 12 indicative of closest particle packing and reminiscent of simple monoatomic liquids lacking specific anisotropic interactions.[71] From early

radiolysis experiments it is known that the reaction of e^-_{am} with NH_2 is not hindered by an energy barrier such that every encounter leads inevitably to an annihilation of the electron.[50] Thus, we can depict the majority of negatively charged carriers as being generated by the primary matter-field interaction in immediate contact with the aminyl radical and thus, in an instantly reactive configuration with the NH_2 dipole belonging to the first solvation shell of the electron (see sketch in Figure 5.4, red arrows). In contrast, direct encounters between e^-_{am} and NH_4^+ do not destroy the spectroscopic signal but instead lead to the formation of stable contact ion-pairs whose absorption spectrum is practically indistinguishable from that of the solvated electron itself.[49,50,72–74] The spectroscopic data presented here strongly suggest that despite the very efficient ultrafast recombination there is still a fraction of ∼5% of electrons that is able to circumvent its annihilation. Therefore, this small fraction needs to be generated in an initially non-reactive configuration, e.g. one in which the ammonium cation becomes part of the electron's first solvation shell thereby spatially separating the two species whose direct encounter is ultimately required for the spectroscopic signal to decay (see blue arrows in Figure 5.4).

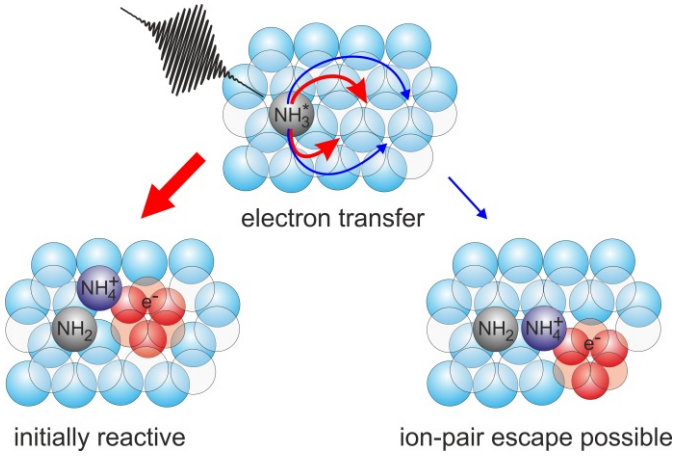

Figure 5.4: Sketch of the initial spatial distribution of the three geminate products produced upon 6.2 eV photoionization of fluid ammonia. Solvated electrons are generated in close proximity to the aminyl radicals and the ammonium cations. The majority of electrons are ejected into configurations that are instantly reactive (red arrows). However, a small fraction of solvated electrons is produced in configurations that allow for a geminate escape.

In the sketch of Figure 5.4, octahedral cavities within the solvent network are proposed as primary acceptor sites for the photo-ejected electron without having any conclusive evidence at this stage. At an excitation energy of

6.2 eV (which is about 2 eV below the optical valence-to-conduction band gap) a substantial stabilization of the nascent photolysis products by the surrounding ammonia molecules is required. The electrons cannot be ejected into a quasi-free state, but instead they must be trapped in a highly localized "pre-configured" environment.[7,15,19] The energetic stabilization associated with such states can be expected to be larger the more the local arrangement of solvent molecules around the primary trapping cavity resembles that of the fully thermalized solvated electron (provided the cavity notion of the solvated electron holds true). Using a dynamic temperature-jump simulation within the cavity model of the solvated electron[5,75–82] we derived from pump-probe studies on metal ammonia solutions an effective coordination number of the fully thermalized ammoniated electron of roughly six.[53,54] Note that an eightfold coordination was suggested by quantum-path integral Monte Carlo simulations.[83]

The close packing of the ammonia molecules at liquid-like densities offers quasi-tetrahedral and quasi-octahedral cavities, both of which should feature a strong dynamical disorder. If -as indicated in Figure 5.4- the octahedral cavities are the primary electron acceptor sites, the ionization mechanism should be heavily affected by the density of such voids within the solvent. This idea can be tested as follows. At any time, t, the induced absorption, $\Delta\Delta OD(t)$ is a direct measure of the number of solvated electrons. Prior to the onset of their geminate recombination, the number of solvated electrons generated by the ionization pulse should be proportional to the number of ionizable molecules in the pump focal volume, which in turn is simply proportional the density, ρ, of the neat solvent. Therefore, the peak induced absorption at early time delays divided by the density of ammonia, i.e. the expression $\Delta\Delta OD_{\text{max}}(t \approx 0)/\rho$, should be constant provided a primary acceptor site is available nearby for every molecule being ionized. However, if the number of electron accepting voids is significantly smaller than the number of ionizable molecules, then the ratio $\Delta\Delta OD_{\text{max}}(t \approx 0)/\rho$ can be expected to become density-dependent.

In this spirit, we have measured $\Delta\Delta OD_{\text{max}}(t \approx 0, \rho)$, at early delays along the supercritical isotherm at 423 K for various solvent densities ranging between 0.565 g cm^{-3} (1300 bar, liquid-like) and 0.172 g cm^{-3} (140 bar, gas-like). During this experiment, a pump intensity of 80 GW cm^{-2} was chosen. Recall that under supercritical conditions, the three-photon contribution is negligible

at this irradiance and that within the experimental accuracy, the induced absorption is exclusively due to solvated electrons from the 400 nm two-photon ionization. Furthermore, once the supercritical phase is reached, the spectral position of the stationary absorption spectrum of the solvated electron is relatively insensitive to variations of temperature and density.[60,61] Therefore, the experiment was conducted in a single very accurate series of measurements by varying only the pressure at constant temperature without ever changing the probe wavelength (here 1450 nm), the pump-probe spatial overlap, and/or the temporal delay between the ionization and detection pulse.

The results of this experiment are compiled in Figure 5.5 where the density-corrected peak absorption of the solvated electron is plotted as a function of the solvent density and the average coordination number of the ammonia molecules (top axis). The latter quantity was obtained from accompanying classical molecular dynamics simulations on an NVE ensemble of 512 rigid NH_3 molecules at the same set of temperatures and densities as in the experiment using the extended single point charge model for ammonia[84] and the M.Dynamix program package.[85] The radial distribution functions and coordination numbers obtained here are in satisfactory agreement with recent simulations based on the more sophisticated Heinzinger model for fluid ammonia.[67] It can be seen in Figure 5.5 that starting from the closest packing of the highly compressed liquid, the density corrected peak absorption remains more or less constant until a critical solvent density of 0.4 g cm^{-3} is reached. A further dilution of the system leads to an abrupt decrease of $\Delta\Delta OD_{\max}/\rho$ indicating that the system becomes more and more deficient of suitable trapping sites for the photo-ejected electrons as gas-like conditions are progressively approached.

It can furthermore be seen that the rapid fall-off of the data occurs for coordination numbers smaller than $N \approx 7$. This result guides us to the following, certainly oversimplifying but nonetheless highly intriguing lattice picture. Representing the randomly disordered fluid as a frozen crystalline matrix, the fall-off in the solvated electron yield occurs when the system formally transits from coordination numbers around $N \approx 8$ reminiscent of a body-centered cubic structure to coordination numbers of $N \approx 6$ suggestive of a primitive cubic structure. Whereas the former lattice offers a large number of octahedral cavities, the latter structure can only provide cubic voids. Thus, we are tempted to conclude that octahedral trapping sites are indeed required for

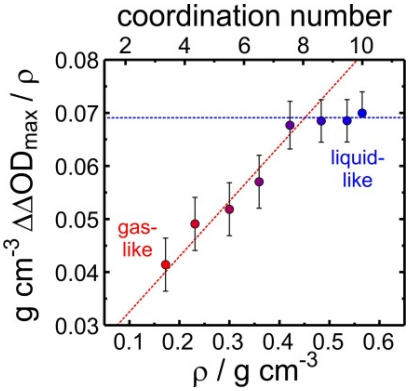

Figure 5.5: Density-normalized peak induced absorption of the solvated electron at various solvent densities and a temperature of 423 K. The mean coordination number was obtained from MD simulations. The dashed lines are meant to guide the eye.

ammoniated electrons to be efficiently generated by multi-photon ionization of the neat solvent with energies below the band gap. Once the solvent becomes deficient of such sites, the ionization efficiency is diminished and the density-corrected electron yield goes down. We reemphasize that portraying the fluid as structurally ordered lattice is a drastic oversimplification. Therefore, we will attempt in the future to quantify the number density of cavities with quasi-octahedral symmetry from temperature and density-dependent molecular dynamics simulations.

To conclude this discussion on the primary ionization mechanism we briefly review the electronic structure of ammonia at energies below the optical band gap. The extremely small ultimate survival probability is indicative of a highly compact initial electron distribution with a thermalization distance that is similar to the nearest-neighbor distances in the fluid. This suggests that just like in water a proton-coupled electron transfer (PCET) succeeds the primary matter-field interaction and localizes the electron in a suitable trap. The two 400 nm photons have a combined energy of 6.2 eV, which is very close to the lowest energy $\tilde{A} \leftarrow \tilde{X}$ transition of the NH_3 monomer in the gas phase.[86–88] This transition promotes an electron from the highest occupied lone-pair orbital centered on the nitrogen atom to a 3s-like Rydberg orbital. In the united atom approximation, this electronic transition can be formulated as $(a_1')^2(e')^4(a_2'')(3sa_1'), {}^1A_2'' \leftarrow (a_1)^2(e)^4(a_1)^2, {}^1A_1'$, which expresses the Rydberg character of the excited state and also accounts for the distortion of the

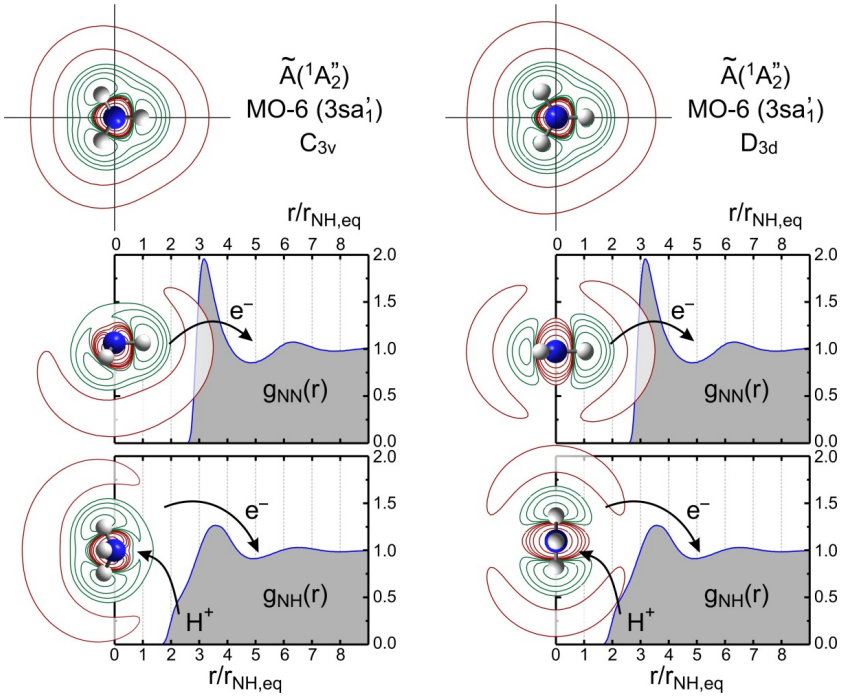

Figure 5.6: The $3sa_1'$ orbital of ammonia in C_{3v} (left column) and D_{3h} symmetry (right column) in comparison to the N–N (middle) and N–H (bottom) radial distribution functions ($T = 423\,\mathrm{K}$, $\rho = 0.565\,\mathrm{g\,cm^{-3}}$). The radial distance is normalized to the covalent N–H bond distance of 0.101 98 nm.

molecular frame from pyramidal (C_{3v}) to planar (D_{3h}) symmetry upon optical excitation.[89–91] The nuclear rearrangement in the $\tilde{A}$ state becomes evident through an extended Franck-Condon progression of the out-of-plane bending vibration (umbrella inversion) that modulates the UV-absorption $\tilde{A} \leftarrow \tilde{X}$.[86–88]

To visualize the spatial extension of this Rydberg excited state in relation to the molecular packing within the many-body system, three perpendicular cuts through the $3sa_1'$ orbital are shown in Figure 5.6 together with the radial distribution functions of the fluid. Whereas the latter was obtained from a classical MD-simulation and the above mentioned SPC/E model for ammonia,[84] the former was obtained from a CASSCF(8,9) calculation[92] and Dunning's aug-ccpVTZ basis set[93] (as implemented in Gaussian 09)[94] including a geometry optimization following the excited state gradient. At the level of theory used, the electronic structure calculation predicts a vertical $\tilde{A} \leftarrow \tilde{X}$ energy gap at the equilibrium geometry of the ground-state of 6.33 eV, which is in excellent agreement with the experimental gas phase value.[86–88]

The N–N radial distribution function has its first maximum at a distance

of 0.331 nm, which corresponds roughly to three times the equilibrium distance of the covalent N–H bond distance (0.102 nm for $\tilde{X}$). At the same time, the N–H radial distribution function is maximal at 0.37 nm and it has a pronounced shoulder around 0.23 nm. This feature is typically taken as an indicator for hydrogen bonded contacts, N$\cdots$H–N, between nearest neighbor particles of the fluid. It can be seen that in the direction of the N–H bond vector, the $3sa_1'$ wavefunction is tightly squeezed into the local solvation structure with the outer lobes even penetrating into the first coordination shell surrounding a tagged ammonia molecule. The resultant overlap with the electron density on the neighboring particles is expected to destabilize the $\tilde{A}$ state in the condensed phases of ammonia (Rydbergization effect[95,96]). The $3sa_1'$ orbital is also extended in the direction of the C_3 axis of the electronically excited NH_3 molecule reaching almost as far out as the donated H-atom of a hydrogen-bonded neighbor. Such a configuration immediately calls for a concerted electron and proton transfer (i.e. PCET mechanism)

$$NH_3 + 2\ h\nu \longrightarrow NH_3^* \tag{5.7}$$

$$NH_3^* + NH_3 \longrightarrow e_{am}^- + NH_2 + NH_4^+ \tag{5.8}$$

where the electronically excited $NH_3(\tilde{A})$ molecule ejects the electron from its diffuse $3sa_1'$ orbital into a suitable (presumably octahedral) void located somewhere between its first and second solvation shells while at the same time accepting the proton from a hydrogen-bonded donor molecule of its first solvation shell. This scenario is also sketched in Figure 5.4 (above) and generates the geminate fragments in an instantly reactive configuration that is ready to recombine without diffusion.

For the photoionization of liquid water, the so-called hot hydrogen atom (HHA) mechanism has also been proposed as an alternative scenario for electron injection.[8,38,39] Transferred to the photoionization of fluid NH_3, this scenario involves a homolytic N–H bond breakage that is facilitated by the predissociation of the Rydberg $\tilde{A}$ state.[97–99] Predissociation lifetimes in the gas phase have been estimated from vibrational linewidths[100] to be below 150 fs in agreement with recent femtosecond ionization experiments of jet-cooled NH_3 monomers.[101] The excited state decay produces an NH_2 radical and a translationally hot hydrogen-atom, which in turn can collisionally ionize and attach to a nearby ammonia molecule thereby producing the solvated electron

and an ammonium cation, i.e.

$$\mathrm{NH_3^*} \longrightarrow \mathrm{NH_2} + \mathrm{H_{hot}} \tag{5.9}$$

$$\mathrm{NH_3} + \mathrm{H_{hot}} \longrightarrow \mathrm{NH_4^+} + \mathrm{e_{am}^-}. \tag{5.10}$$

According to these equations, the PCET and the HHA mechanism yield the same side products namely, aminyl radicals and ammonium cations, and are therefore indistinguishable in terms of product distributions. In addition, the predissociation rate from the $\tilde{A}$ state is just a bit too fast compared to our time-resolution. Taken on their own, the data presented here are simply insufficient to discriminate either of the two mechanisms. However, whereas the initial solvated electron yield (i.e. prior to recombination) may be limited directly by the availability of suitable trapping sites, the HHA may also be influenced by the local density of collision partners for the departing hydrogen atom. Once again, detailed information regarding the number density of trapping sites as a function of the thermodynamic state variables are highly desirable to settle this issue.

5.4.3 Time-Dependent Survival Probability and Recombination Mechanism

Having discussed the ultimate survival probability and the mechanism for below band-gap ionization, we now turn our attention on the kinetics of electron annihilation. Figure 5.7 displays a selection of time-dependent survival probabilities representative of the wide range of temperature and density studied here. At a first glance, the kinetics appears to be rather insensitive to changes of the thermodynamic conditions, i.e. roughly 90% of the initially produced electrons are lost within the first 5 ps. Upon closer inspection however, a subtle acceleration of the recombination dynamics can be noticed with increasing temperature and decreasing density. It turns out that for delays up to 5 ps, the time-dependent survival probability can be very well described by a single-exponential decay

$$\Omega_2(t) = (1 - A) \cdot exp(-t/\tau) + A = (1 - A) \cdot \Omega_{\mathrm{exp}}(t) + A \tag{5.11}$$

with a time-constant, τ, to which a constant offset signal of relative amplitude, A, is added. The observation of simple exponential kinetics is in line with the

above conclusion that a diffusional encounter of the geminate fragments is not required for the annihilation of the electronic charge.

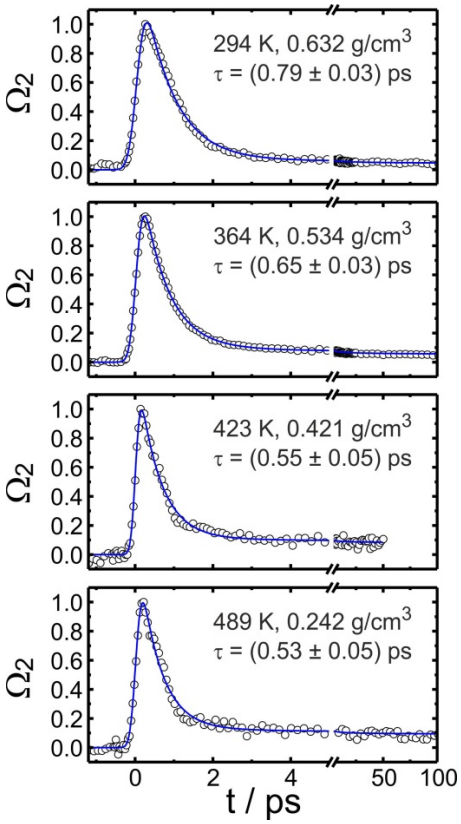

Figure 5.7: Experimentally determined time-dependent survival probabilities (circles) of the solvated electron pertinent to the pure 6.2 eV ionization of fluid ammonia for various thermodynamic conditions and a pump-beam irradiance of $\sim$80 GW cm^{-2}. The solid curves are fits to the data using equation (5.13).

As discussed above, the constant signal offset describes those electrons that are created in an initially unreactive configuration from which an ultimate escape is possible (see also Figure 5.4, right). To understand their recombination on time scales in excess of 5 ps the following conclusion from our recently published computer simulations of the vertical ionization/recombination in ammonia[42] proves useful: Solvated electrons that are formed at distances just outside the aminyl radical's solvent cage (i.e. within the 2nd solvation shell) escape as very long-lived ion-pairs ($e^-_{am} \cdot NH^+_4$). Provided the electrostatic attraction between the charged particles is sufficiently strong, it can be assumed that the ion-pair is formed instantly within duration of the ionization pulse. In

other words, all solvated electrons that are not formed in an initially reactive configuration must exist at $t = 0$ ps as ion-pairs ($e^-_{am} \cdot NH^+_4$) at a thermalization distance, r_0. In this case, the recombination dynamics of these species with the aminyl radical can be modeled as a neutral pair recombination where the dipolar interaction between the ion-pair and the aminyl radical is completely screened by the surrounding solvent dipoles. The electron's escape probability is then given by[102]

$$\Omega_{\text{neutral}}(t) = 1 - \frac{R_a}{r_0} \cdot \text{erfc}((r_0 - R_a)/\sqrt{4Dt}) \tag{5.12}$$

where R_a is the reaction distance for the reaction (5.5) and D is the sum of the temperature and density dependent diffusion coefficients of the ion-pair and the aminyl radical.[39,40] The total time-dependent escape probability is finally written as

$$\Omega_2(t) = (1 - A) \cdot \Omega_{\text{exp}} + A \cdot \Omega_{\text{neutral}}(t) \tag{5.13}$$

which can be used to model the experimental data for all time delays. The quantities, A, τ, and r_0, are adjustable fitting parameters while R_a and D can be taken from Refs. 49, 103, 104. The finite time-resolution of the experiment is taken into account by a convolution of Equation (5.13) with a Gaussian instrument response function having a full width at half maximum of 250 fs.

The fitting results are compared in Figure 5.7 with the experimental data for various thermodynamic conditions. The analysis reveals that regardless of temperature and density a fraction of ∼10% of all electrons recombine from initially non-reactive configurations. The thermalization distance for these electrons scatters around 0.7 nm, which is very close to the second minimum of the N–N radial distribution function (0.8 nm, see above). This provides further support for a localization of the initially non-reactive electron in a suitable trap between the second and third solvation shell around the photoexcited NH^*_3 as sketched on the right hand side of Figure 5.4.

The fitting procedure provides us also with a time constant of the exponential component to the overall decay of $\Omega_2(t)$. This quantity can be understood as a true lifetime of the instantaneously reactive configuration composed of the solvated electron, the aminyl radical, and the ammonium cation; all of which arranged in immediate spatial proximity. Its inverse is the rate $k(T) = 1/\tau(T)$ for the annihilation of the carrier of the spectroscopic signal

according to

$$(\mathrm{e}^-_{\mathrm{am}}\cdot\mathrm{NH}_4^+\cdot\mathrm{NH}_2) \longrightarrow (2\,\mathrm{NH}_3) \tag{5.14}$$

where the parentheses indicate that all three species share a joint solvation shell as indicated in Figure 5.4, left. The question arises as to whether this process occurs in a sequential or a concerted fashion. In a stepwise mechanism, the electron attaches first to the radical to form an amide anion

$$(\mathrm{e}^-_{\mathrm{am}}\cdot\mathrm{NH}_4^+\cdot\mathrm{NH}_2) \longrightarrow (\mathrm{NH}_2^-\cdot\mathrm{NH}_4^+) \tag{5.15}$$

which can subsequently accept a proton from the cation to yield two ammonia molecules

$$(\mathrm{NH}_2^-\cdot\mathrm{NH}_4^+) \longrightarrow (\mathrm{NH}_3\cdot\mathrm{NH}_3) \tag{5.16}$$

The sequential sequence consisting of a charge neutralization between the electron and the ammonium cation

$$(\mathrm{e}^-_{\mathrm{am}}\cdot\mathrm{NH}_4^+\cdot\mathrm{NH}_2) \longrightarrow (\mathrm{NH}_4\cdot\mathrm{NH}_2) \tag{5.17}$$

and a secondary hydrogen atom transfer from the intermediate ammonium radical to the aminyl radical

$$(\mathrm{NH}_4\cdot\mathrm{NH}_2) \longrightarrow (\mathrm{NH}_3\cdot\mathrm{NH}_3) \tag{5.18}$$

must be dismissed because the charge recombination is known to be highly endergonic[105] and hence, very slow. In a concerted mechanism, the transfer of the electron and the hopping of proton occur simultaneously in which case we must speak of a proton-coupled back electron transfer (PCBET).

To address this question, we first inspect the temperature dependence of the rate constant, $k(T)$, obtained at a constant pressure of 300 bar. The results are shown in Figure 5.8 in an Arrhenius representation, where the rate constant is plotted logarithmically as a function of the inverse temperature. The data follow nicely a straight line with a slope of 2.8 kJ/mol but it seems to level off for temperatures above 450 K. The slope corresponds to an activation energy that is equal to or even less than the thermal energy in the temperature range being studied. Therefore, we conclude that the recombination of solvated electrons from initially reactive configuration is a barrierless process. Provided the sequential mechanism indeed prevails and reaction (5.15) is rate limiting,

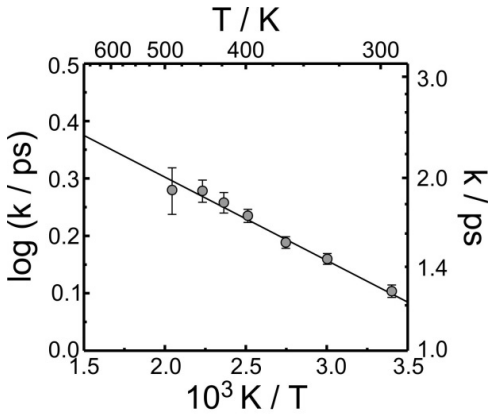

Figure 5.8: Arrhenius plot of the rate constant for geminate recombination of solvated electrons ejected into instantly reactive configurations upon 6.2 eV ionization of liquid-to-supercritical ammonia. A linear regression provides an activation energy of $E_a = (2.8 \pm 0.2)$ kJ/mol from the slope and suggests that the recombination is essentially a barrierless process.

such a conclusion would be in accord with early radiolysis studies where the recombination between e^-_{am} and NH_2 was found to occur at a diffusion-limited rate.[50,106]

However, before settling on such an interpretation, the role of the proton needs to be elucidated in more detail. To this end, the 400 nm two-photon ionization of fully deuterated fluid ammonia, ND_3, was also studied under similar thermodynamic conditions as before. Once again, the signals have been corrected for the three-photon contribution and whenever it was necessary the window artifact was also removed.

Figure 5.9 shows a comparison of the time-dependent survival probabilities of the solvated electron obtained in normal and in heavy ammonia under otherwise exactly identical thermodynamic conditions. Regardless of temperature and density, a pronounced deceleration of the recombination dynamics upon deuteration of the solvent can be noticed. This is in stark contrast to our previous findings on the vertical 9.3 eV-photoionization where no such isotope effect was observed. Interestingly, qualitatively similar results were reported by Elles et al. for the photoionization of liquid water where an isotope effect was only observed for ionization energies below the optical band gap.[11] However, whereas for water the deuteration results in a decrease of the ultimate survival probability (because of a diminishing thermalization distance), the values of $\Omega_2(t \to \infty)$ in light and heavy ammonia are identical

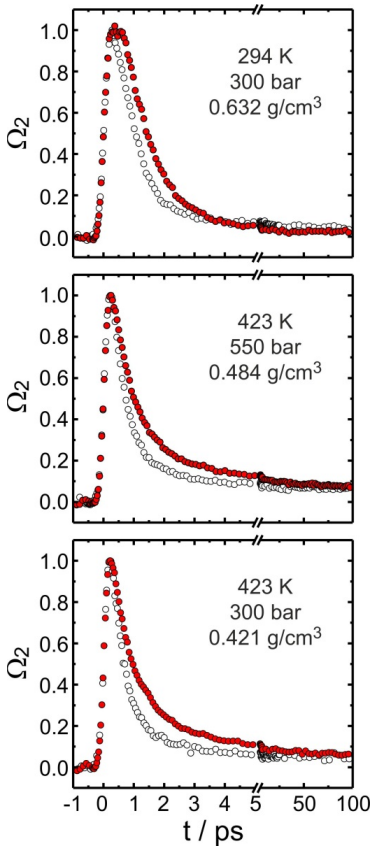

Figure 5.9: Time-dependent survival probability of the solvated electron produced by 6.2 eV photoionization of light ammonia (NH_3, open symbols) and heavy ammonia (ND_3, filled symbols) at various thermodynamic conditions.

within the signal to noise ratio.

What is truly affected upon deuteration of the ammonia solvent is the recombination kinetics. Elles et al. have discussed the isotope dependence of the various factors influencing the ionization mechanism such as energetic shifts due to the vibrational zero-point energy or the dissipation of excess energy through inelastic scattering.[11] For the experiments presented here, we need to explain the deceleration of the recombination events (rather than the ultimate electron yield) upon introduction of the heavy deuterons. The isotope effect observed here provides rather strong evidence for a recombination mechanism whose rate is limited by the motion of only the light protons. At the same time, the temperature-dependence of the rate suggests a barrierless recombination of the electron with aminyl radical. Taken together, both findings can be brought into harmony by invoking the concerted PCBET

mechanism. Thus, we conclude that the below band-gap photoionization and geminate recombination can best be thought of as a proton-coupled electron transfer followed by a proton-coupled back electron transfer.

5.5 Concluding Remarks

In summary, we have presented results on the electron injection and recombination dynamics from femtosecond 400 nm two-photon ionization experiments on fluid ammonia. The total ionization energy in these experiments amounts to only 6.2 eV, which is about 2 eV below the conduction band of the solvent. Hence, electron injection must involve nuclear rearrangements within the local environment of the primary site of ionization. Because of the diffuse character of the first excited Rydberg state of ammonia in relation to the molecular packing within the local solvation structure, a proton-coupled electron-transfer similar to that suggested for the ionization of liquid water is likely. As evidenced by the time-dependent escape probability, the below-band-gap ionization injects electrons into two distinct local configurations. In one of which, the electron finds itself somewhere between the second and third solvation shell, which enables an escape from the aminyl radical and which should be considered as an initially non-reactive configuration. In contrast, the other configuration can be considered as instantly reactive, because it facilitates an annihilation of the charge that is not hindered by an activation barrier. In these reactive configurations, the electron partially shares its solvation shell with the aminyl radical or alternatively, the aminyl is contributing to the electron's cavity. A pronounced kinetic isotope effect suggests the involvement of protonic motion during charge annihilation, which is why we call this process a proton-coupled back-electron transfer (PCBET). More experimental and theoretical work is required to verify the PCET as the mechanism that is responsible for the primary electron injection. In particular, a detailed analysis of the abundance of suitable trapping sites and its dependence on the thermodynamic state variable might prove highly valuable. We are currently in the process of investigating the ionization energy dependence of the recombination dynamics to characterize more precisely the electronic structure of the liquid as a function of density and temperature. Finally, we very much hope that these experiments inspire more sophisticated computational studies of the dynamics of electron recombination such as those recently conducted

for the hydrated electron.[107]

ACKNOWLEDGEMENTS

Financial support by the Deutsche Forschungsgemeinschaft through the Collaborative Research Center SFB 813 "Chemistry at Spin Centers" is gratefully acknowledged.

EXTRACTION OF THE SOLVATED ELECTRON SIGNAL FROM A PURE 400-NM 2-PHOTON IONIZATION

To understand the underlying photo-physical processes responsible for this peculiar irradiance dependence, we accurately established the number of photons involved in the primary matter field interaction leading to the generation of solvated electrons. Note that owing to our choice of the probing wavelength, thermalization/solvation dynamics are entirely suppressed and the signal, $\Delta\Delta OD(t)$, is only proportional to the number density of solvated electrons. Since the solvated electrons result from a multi-photon ionization of the solvent, the amplitude of the signal should follow a simple power law,[8] $\Delta\Delta OD(t, I) \propto I^n$, where n is the number of photons simultaneously interacting with the sample regardless of the pump-probe time-delay.

Figure 5.10 displays a double-logarithmic plot of $\Delta\Delta OD(t, I)$ at two different delay times, t, as a function of the pump irradiance normalized to the maximum value of $I_{\text{max}} = 82\,\text{GW cm}^{-2}$ attainable with the experimental setup. Inspecting first the intensity dependence of the peak induced absorption, $\Delta\Delta OD_{\text{max}}$, at early delays ($t \approx 0\,\text{ps}$), it can be noticed that in the log-log representation the data follow nicely a straight line with a slope that is very close to $n = 2$. This result leads immediately to the conclusion that electron injection into the solvent relies on a two-photon ionization process. However, performing the same analysis on the induced absorption at very late delays (i.e. the plateau at $t \approx 200\,\text{ps}$) yields a slope that is somewhere in between $n = 2$ and $n = 3$. This result can be interpreted qualitatively with two different types of solvated electrons. A major fraction of electrons originates from a two-photon ionization and recombines rather fast while a minor fraction of electrons is generated through a three-photon ionization of the solvent and recombines rather slowly. At a delay of about 200 ps, the two types of electrons are present in comparable amounts thereby giving rise to the power law $\Delta\Delta OD(200\,\text{ps}, I) \propto I^{2.5}$ with a non-integer exponent.

In this notion, the measured signal has to be regarded as a superposition of a two-photon and a three-photon contribution, i.e. $\Delta\Delta OD_2(t, I)$ and $\Delta\Delta OD_3(t, I)$, respectively. In the limit of $t = 0$ and prior to any recombination losses, the total solvated electron signal as a function of the irradiance can be

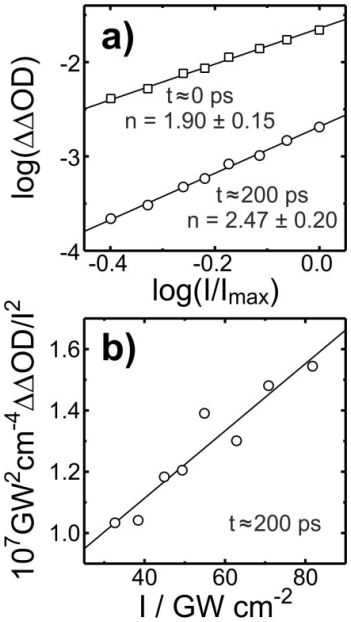

Figure 5.10: a) Dependence of the solvated electron's induced absorption on the normalized pump-pulse irradiance in a double logarithmic plot. b): Plot of $\Delta\Delta OD(t \approx 200ps)$ divided by the squared pump irradiance as a function of the pump irradiance. The straight line represents a linear fit of the data.

written as

$$\Delta\Delta OD(0\,\mathrm{ps}, I) = \Delta\Delta OD_2(0\,\mathrm{ps}, I) + \Delta\Delta OD_3(0\,\mathrm{ps}, I) = \sigma_2 I^2 + \sigma_3 I^3 \quad (5.19)$$

where σ_n is the effective cross-section for the n-photon ionization process. It should be noted that these quantities contain not only the n-photon absorption coefficient of the solvent, but they also depend on the pump-probe overlap inside the sample.

For later delay times, i.e. $t > 0$, it is necessary to explicitly account for the loss of solvated electrons due to geminate recombination with the aminyl radical (cf. Eq. 5.3 and 5.5, main paper). To this end, the time-dependent survival probability, $\Omega(t)$, is introduced, which corresponds to the fraction of solvated electrons still present at a time, t, following their initial generation through the primary matter field interaction at $t = 0$.[62–64] The complement, $1 - \Omega(t)$, can be regarded as a time-dependent recombination yield. The fate of the solvated electrons strongly depends on the history of their preparation. This is because electrons generated at ionization energies well above the

solvent's optical band gap can be considered as highly mobile carriers that are characterized by much larger thermalization distances as compared to electrons created at very low ionization energies close to or even below the band gap.[11,17] As a result, the former species are much more likely to avoid a reactive encounter with a geminate fragment than the latter. This important distinction can be taken into account by defining survival probabilities, $\Omega_n(t)$, that pertain specifically to electrons originating from the n-photon ionization processes.

Inserting these ionization-specific escape probabilities into equation (5.19) gives the full temporal evolution of the total intensity-dependent pump-probe signal

$$\begin{aligned}\Delta\Delta OD(t,I) &= \Delta\Delta OD_2(t,I) + \Delta\Delta OD_3(t,I) \\ &= \Omega_2(t)\sigma_2 I^2 + \Omega_3(t)\sigma_3 I^3. \end{aligned} \tag{5.20}$$

Since at $t = 0$, $\Omega_2(t) = \Omega_3(t) = 1$, the power law exponent becomes $n = 2$ provided that $\sigma_2 I^2 \gg \sigma_3 I^3$. Owing to the increasing recombination efficiency with decreasing ionization energy, $\Omega_2(t)$ decays much faster with time than $\Omega_3(t)$. Thus, with increasing delay, the second term in equation (5.20) becomes increasingly important thereby producing a non-integer power law. In the limit $\Omega_2(t) \to 0$ and $\Omega_3(t)$ still being finite, an exponent of $n = 3$ should even be observed.

The energy of two 400 nm photons amounts to 6.2 eV. Furthermore, the energy of three 400 nm photons is equal to 9.3 eV, which corresponds exactly to the energy of two photons having a wavelength of 266 nm each. We have previously reported experimental data on the time-dependent survival probability of solvated electrons generated through femtosecond 266 nm two-photon ionization of liquid-to-supercritical ammonia.[41,42] This information can now be used as an independent input for $\Omega_3(t)$ in equation (5.20), which reads upon rearranging

$$\Delta\Delta OD(t,I)/I^2 = \Omega_2(t)\sigma_2 + \Omega_3(t)\sigma_3 \cdot I. \tag{5.21}$$

Thus, by plotting the differential optical density of the solvated electron divided by I^2 as a function of the pump irradiance for a fixed pump-probe time delay (say e.g. 200 ps), a linear correlation should be obtained. Such a correlation is demonstrated in Figure 5.10b for a representative time delay of

200 ps and for the same thermodynamic conditions as in Fig. 5.1, main paper. While the intercept represents an entangled quantity, the slope together with $\Omega_3(200\text{ps})$ from Refs. 41,42 give immediate access to the effective 3-photon ionization cross section, σ_3.

As shown in Figure 5.11a, this quantity can now be used to reconstruct the pure contribution resulting exclusively from the 2-photon ionization with 400 nm-pulses. We find

$$\Delta\Delta OD_2(t, I) = \Delta\Delta OD(t, I) - \Omega_3(t)\sigma_3 \cdot I^3 \tag{5.22}$$

for all pump-probe time delays. After normalization to its peak value (cf. Figure 5.11b), the time-dependent survival probability pertaining to electrons from the photoionization at 6.2 eV is finally obtained, i.e. $\Omega_2(t) = \Delta\Delta OD_2(t, I)/\Delta\Delta OD_2(0, I) = \Delta\Delta OD_2(t, I)/(\sigma_2 \cdot I^2)$.

At first glance, the correction introduced by the subtraction of the independently measured 9.3 eV contribution might seem small. However, the correction introduces a significant reduction of the asymptotic absorption plateau. In Figure 5.11a, the absorption is $\sim 2 \times 10^{-3}$ $\Delta\Delta OD$ units at a delay of 200 ps. Together with the value of the peak value of $\Delta\Delta OD = 23 \times 10^{-3}$ this allows us to calculate an ultimate survival probability, Ω_∞, corresponding to the aforementioned fraction of solvated electrons that is able to avoid the geminate recombination altogether.[63] For the data in Figure 5.11a we obtain a value for Ω_∞ of roughly 9%. After correction for the 3-photon contribution, this value is lowered to $\sim$5% as is shown in Figure 5.11b.

Interestingly, it was noticed that the relative importance of the 9.3 eV component decreases as the supercritical phase was gradually approached, i.e. the ratio, σ_2/σ_3, decreases with increasing temperature and decreasing density, respectively. In fact, for $T > 405$ K and for $I \geq 80$ GW cm^{-2}, the three-photon signal became undetectable. This finding can be understood in light of our previous experiments on the two-photon 266 nm ionization of ammonia, which revealed a pronounced shift of the optical valence-to-conduction band gap to higher energies as the temperature is raised and the density is decreased.[41,42] At ionization energies below the band gap, as is the case for the 400 nm 2-photon ionization, lower lying Rydberg states are believed to be involved in the primary matter-field interaction.[108] These very diffuse excited Rydberg states are known to overlap with core excitations on neighboring particles

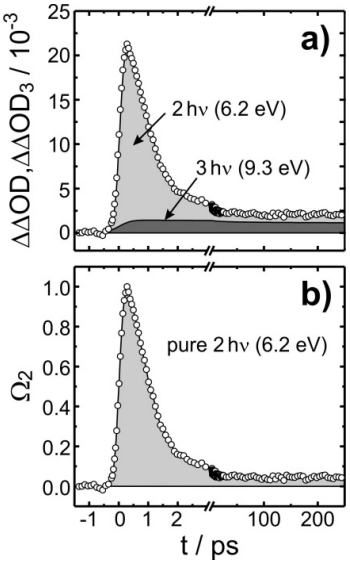

Figure 5.11: a) Decomposition of the experimentally obtained pump-probe signal recorded at $I = 82\,\mathrm{GW\,cm^{-2}}$ (open circles) into a two-photon (light gray) and three-photon (dark gray) contribution, the latter of which is adopted from Ref. 42. b) Geminate survival probability of solvated electrons that are exclusively produced by the 400 nm two-photon ionization (6.2 eV).

thereby lading to a Pauli repulsion that can be expected to be much stronger in the dense liquid as compared to the dilute supercritical fluid (cf. also Section 5.4.2, main paper). Due to this Rydbergization effect, we can expect the relevant states below the conduction band to experience an energetic downshift as the system is isobarically heated or isothermally diluted. The thermally induced energetic shifts of the conduction band and the Rydberg excited states are qualitatively sketched in Figure 5.12, which rationalizes in an intuitive fashion why the generation of ammoniated electrons with 400 nm femtosecond pulses shifts from an apparent mixed multi-photon ionization in the densely packed cryogenic liquid to a pure two-photon ionization in the dilute supercritical fluid.

It should also be stressed at this stage that some inaccuracies of the 2-photon survival probability, $\Omega_2(t)$, arise at early delay times. This is because $\Omega_2(t)$ is computed from the difference between two independently measured signals. One of which was recorded with an excitation wavelength of 400 nm while the other had used a pump wavelength of 266 nm. Therefore, because of their different inherent group velocity mismatches between the pump and probe pulses, these two experiments must have a different temporal instrument

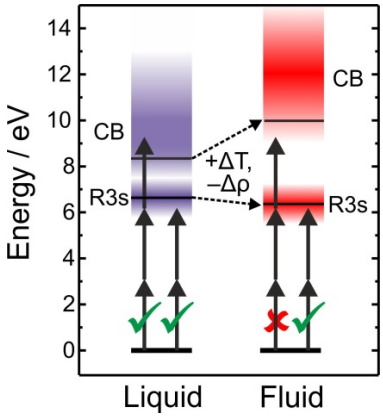

Figure 5.12: Schematic diagram showing the thermally induced shifts of the electronic energy levels pertinent to the 6.2 eV and 9.3 eV photoionization of ammonia.

response function even if the pulse durations were the same. With an optical path length of our sample cell of 1 mm, the group delay is approximately 500 fs for the 266 nm pump / 1760 nm probe experiment while it is slightly below 200 fs for the experiment utilizing a 400 nm pump and a 1450 nm probe. Therefore, the data below 0.5 ps have to be analyzed with special care while for longer delays it can safely be assumed that they are unaffected by the mismatched temporal pump-probe walk-off.

[1] Mozumder, A. *Fundamentals of Radiation Chemistry;* Academic Press: San Diego, 1999.

[2] Chen, X.; Bradforth, S. E. *Annu. Rev. Phys. Chem.* **2008**, *59*, 203.

[3] Lee, I.-R.; Lee, W.; Zewail, A. H. *ChemPhysChem* **2008**, *9*, 83.

[4] Ehrler, O. T.; Neumark, D. M. *Acc. Chem. Res.* **2009**, *42*, 769.

[5] Larsen, R. E.; Glover, W. J.; Schwartz, B. J. *Science* **2010**, *329*, 65.

[6] Abel, B.; Buck, U.; Sobolewski, A. L.; Domcke, W. *Phys. Chem. Chem. Phys.* **2012**, *14*, 22.

[7] Sander, M. U.; Luther, K.; Troe, J. *Ber. Bunsenges. Phys. Chem.* **1993**, *97*, 953.

[8] Crowell, R. A.; Bartels, D. M. *J. Phys. Chem.* **1996**, *100*, 17940.

[9] Hertwig, A.; Hippler, H.; Unterreiner, A.; Vöhringer, P. *Ber. Bunsenges. Phys. Chem.* **1998**, *102*, 805.

[10] Madsen, D.; Thomsen, C. L.; Thogersen, J.; Keiding, S. R. *J. Chem. Phys.* **2000**, *113*, 1126.

[11] Elles, C. G.; Jailaubekov, A. E.; Crowell, R. A.; Bradforth, S. E. *J. Chem. Phys.* **2006**, *125*, 044515.

[12] Kratz, S.; Torres-Alacan, J.; Urbanek, J.; Lindner, J.; Vöhringer, P. *Phys. Chem. Chem. Phys.* **2010**, *12*, 12169.

[13] Torres-Alacan, J.; Kratz, S.; Vöhringer, P. *Phys. Chem. Chem. Phys.* **2011**, *13*, 20806.

[14] Thomsen, C. L.; Madsen, D.; Keiding, S. R.; Thogersen, J.; Christiansen, O. *J. Chem. Phys.* **1999**, *110*, 3453.

[15] Sander, M. U.; Luther, K.; Troe, J. *J. Phys. Chem.* **1993**, *97*, 11489.

[16] Iglev, H.; Fischer, M. K.; Rossmadl, H. *J. Chem. Phys.* **2011**, *134*, 214507.

[17] Elles, C. G.; Shkrob, I. A.; Crowell, R. A.; Bradforth, S. E. *J. Chem. Phys.* **2007**, *126*, 164503.

[18] Elles, C. G.; Rivera, C. A.; Zhang, Y.; Pieniazek, P. A.; Bradforth, S. E. *J. Chem. Phys.* **2009**, *130*, 084501.

[19] Bartels, D. M.; Crowell, R. A. *J. Phys. Chem. A* **2000**, *104*, 3349.

[20] Goulet, T.; Jay-Gerin, J.-P. *J. Phys. Chem.* **1988**, *92*, 6871.

[21] Cobut, V.; Frongillo, Y.; Patau, J. P.; Goulet, T. andFraser, M. J.; Jay-Gerin, J. P. *Radiat. Phys. Chem.* **1998**, *51*, 229.

[22] Frongillo, Y.; Goulet, T.; Fraser, M.; Cobut, V.; Patau, J.; Jay-Gerin, J. *Radiat. Phys. Chem.* **1998**, *51*, 245.

[23] Goulet, T.; Pepin, C.; Houde, D.; Jay-Gerin, J.-P. *Rad. Phys. Chem.* **1999**, *54*, 441.

[24] Hervé du Penhoat, M.-A.; Goulet, T.; Frongillo, Y.; Fraser, M.-J.; Bernat, P.; Jay-Gerin, J.-P. *J. Phys. Chem. A* **2000**, *104*, 11757.

[25] Clifford, P.; Green, N. J. B.; Pilling, M. J. *J. Phys. Chem.* **1984**, *88*, 4171.

[26] Green, N. J. B.; Pilling, M. J.; Pimblott, S. M.; Clifford, P. *J. Phys. Chem.* **1990**, *94*, 251.

[27] Pimblott, S. M. *J. Phys. Chem.* **1991**, *95*, 6946.

[28] Green, N. J. B.; Pilling, M. J.; Pimblott, S. M.; Clifford, P. *J. Phys. Chem.* **1989**, *93*, 8025.

[29] Wu, G.; Katsumura, Y.; Muroya, Y.; Li, X.; Terada, Y. *Chem. Phys. Lett.* **2000**, *325*, 531.

[30] Bartels, D. M.; Takahashi, K.; Cline, J. A.; Marin, T. W.; Jonah, C. D. *J. Phys. Chem. A* **2005**, *109*, 1299.

[31] Baldacchino, G.; De Waele, V.; Monard, H.; Sorgues, S.; Gobert, F.; Larbre, J. P.; Vigneron, G.; Marignier, J. L.; Pommeret, S.; Mostafavi, M. *Chem. Phys. Lett.* **2006**, *424*, 77.

[32] Muroya, Y.; Lin, M. Z.; de Waele, V.; Hatano, Y.; Katsumura, Y.; Mostafavi, M. *J. Phys. Chem. Lett.* **2010**, *1*, 331.

[33] Jay-Gerin, J. P.; Lin, M. Z.; Katsumura, Y.; He, H.; Muroya, Y.; Meesungnoen, J. *J. Chem. Phys.* **2008**, *129*, 114511.

[34] Bernas, A.; Ferradini, C.; Jay-Gerin, J.-P. *J. Photochem. Photobiol. A* **1998**, *117*, 171.

[35] Bernas, A.; Ferradini, C.; Jay-Gerin, J.-P. *Chem. Phys.* **1997**, *222*, 151.

[36] Schinke, R. *Photodissociation dynamics;* Cambridge University Press: Cambridge, 1993.

[37] Engel, V.; Schinke, R.; Staemmler, V. *J. Chem. Phys.* **1988**, *88*, 129.

[38] Han, P.; Bartels, D. M. *J. Phys. Chem.* **1992**, *96*, 4899.

[39] Nikogosyan, D. N.; Görner, H. *J. Photochem. Photobiol. B* **1992**, *13*, 219.

[40] Bernas, A.; Grand, D. *J. Phys. Chem.* **1994**, *98*, 3440.

[41] Urbanek, J.; Dahmen, A.; Torres-Alacan, J.; Königshoven, P.; Lindner, J.; Vöhringer, P. *J. Phys. Chem. B* **2012**, *116*, 2223.

[42] Urbanek, J.; Vöhringer, P. *J. Phys. Chem. B* **2013**, *117*, 8844.

[43] Krohn, C. E.; Antoniewicz, P.; Thompson, J. *Surf. Sci.* **1980**, *101*, 241.

[44] Krohn, C. E.; Thompson, J. C. *Phys. Rev. B* **1979**, *20*, 4365.

[45] Lindblad, A.; Bergersen, H.; Pokapanich, W.; Tchaplyguine, M.; Ohrwall, G.; Bjorneholm, O. *Phys. Chem. Chem. Phys.* **2009**, *11*, 1758.

[46] Harima, Y.; Sato, H.; Suga, K. *J. Phys. Chem.* **1989**, *93*, 6418.

[47] Bennett, G. T.; Coffman, R. B.; Thompson, J. C. *J. Chem. Phys.* **1987**, *87*, 7242.

[48] Huntress, W. T.; Mosesman, M. M.; Elleman, D. D. *J. Chem. Phys.* **1971**, *54*, 843.

[49] Belloni, J.; Cordier, P.; Delaire, J. A.; Delcourt, M. O. *J. Phys. Chem.* **1978**, *82*, 537.

[50] Kieffer, F.; Klein, J.; Lapersonne-Meyer, C.; Magat, M.; Belloni, J.; Billiau, F.; Cordier, P.; Delaire, J.; Delcourt, M. O. *Faraday Discuss. Chem. Soc.* **1977**, *63*, 55.

[51] Zurek, E.; Edwards, P. P.; Hoffmann, R. *Angew. Chem. Int. Edt.* **2009**, *48*, 8198.

[52] Kambhampati, P.; Son, D. H.; Kee, T. W.; Barbara, P. F. *J. Phys. Chem. A* **2002**, *106*, 2374.

[53] Lindner, J.; Unterreiner, A.-N.; Vöhringer, P. *ChemPhysChem* **2006**, *7*, 363.

[54] Lindner, J.; Unterreiner, A.-N.; Vöhringer, P. *J. Chem. Phys.* **2008**, *129*, 064514.

[55] Schäfer, T.; Schwarzer, D.; Lindner, J.; Vöhringer, P. *J. Chem. Phys.* **2008**, *128*, 064502.

[56] Schäfer, T.; Lindner, J.; Vöhringer, P.; Schwarzer, D. *J. Chem. Phys.* **2009**, *130*, 224502.

[57] Hertwig, A.; Hippler, H.; Unterreiner, A.-N. *Phys. Chem. Chem. Phys.* **1999**, *1*, 5633.

[58] Tuttle, T. R.; Golden, S.; Hurley, I. *J. Phys. Chem.* **1982**, *86*, 1801.

[59] Tuttle, T. R.; Golden, S.; Lwenje, S.; Stupak, C. M. *J. Phys. Chem.* **1984**, *88*, 3811.

[60] Olinger, R.; Hahne, S.; Schindewolf, U. *Ber. Bunsenges. Phys. Chem.* **1972**, *76*, 349.

[61] Olinger, R.; Schindewolf, U.; Gaathon, A.; Jortner, J. *Ber. Bunsenges. Phys. Chem.* **1971**, *75*, 690.

[62] Tachiya, M. *J. Chem. Phys.* **1988**, *89*, 6929.

[63] Onsager, L. *Phys. Rev.* **1938**, *54*, 554.

[64] Goulet, T.; Jay-Gerin, J.-P. *J. Chem. Phys.* **1992**, *96*, 5076.

[65] Kloepfer, J. A.; Vilchiz, V. H.; Lenchenkov, V. A.; Germaine, A. C.; Bradforth, S. E. *J. Chem. Phys.* **2000**, *113*, 6288.

[66] Lian, R.; Oulianov, D. A.; Shkrob, I. A.; Crowell, R. A. *Chem. Phys. Lett.* **2004**, *398*, 102.

[67] Tassaing, T.; Soetens, J.-C.; Vyalov, I.; Kiselev, M.; Idrissi, A. *J. Chem. Phys.* **2010**, *133*, 214505.

[68] Feng, H.; Liu, X.; Gao, W.; Chen, X.; Wang, J.; Chen, L.; Ludemann, H.-D. *Phys. Chem. Chem. Phys.* **2010**, *12*, 15007.

[69] Zhang, T.; Lee, Y. J.; Kee, T. W.; Barbara, P. F. *Chem. Phys. Lett.* **2005**, *403*, 257.

[70] Tassaing, T.; Danten, Y.; Besnard, M. *J. Mol. Liq.* **2002**, *101*, 149.

[71] Hansen, J.-P.; McDonald, I. R. *Theory of simple liquids;* 3rd ed.; Academic Press: London, 2009.

[72] Rubinstein, G.; Tuttle, T. R.; Golden, S. *J. Phys. Chem.* **1973**, *77*, 2872.

[73] Jou, F.-Y.; Freeman, G. R. *J. Phys. Chem.* **1981**, *85*, 629.

[74] Belloni, J.; Billiau, F.; Cordier, P.; Delaire, J. A.; Delcourt, M. O. *J. Phys. Chem.* **1978**, *82*, 532.

[75] Tuttle, T. R.; Golden, S. *J. Phys. Chem.* **1991**, *95*, 5725.

[76] Kevan, L. *Acc. Chem. Res.* **1981**, *14*, 138.

[77] Rossky, P. J.; Schnitker, J. *J. Phys. Chem.* **1988**, *92*, 4277.

[78] Shkrob, I. A.; Glover, W. J.; Larsen, R. E.; Schwartz, B. J. *J. Phys. Chem. A* **2007**, *111*, 5232.

[79] Jortner, J. *J. Chem. Phys.* **1959**, *30*, 839.

[80] Barnett, R. N.; Landman, U.; Cleveland, C. L.; Kestner, N. R.; Jortner, J. *Chem. Phys. Lett.* **1988**, *148*, 249.

[81] Nicolas, C.; Boutin, A.; Levy, B.; Borgis, D. *J. Chem. Phys.* **2003**, *118*, 9689.

[82] Turi, L.; Gaigeot, M. P.; Levy, N.; Borgis, D. *J. Chem. Phys.* **2001**, *114*, 7805.

[83] Deng, Z.; Martyna, G. J.; Klein, M. L. *J. Chem. Phys.* **1994**, *100*, 7590.

[84] Gao, J.; Xia, X.; George, T. F. *J. Phys. Chem.* **1993**, *97*, 9241.

[85] Lyubartsev, A. P.; Laaksonen, A. *Comp. Phys. Commun.* **2000**, *128*, 565.

[86] Walsh, A. D.; Warsop, P. A. *Trans. Faraday Soc.* **1961**, *57*, 345.

[87] Burton, G. R.; Chan, W. F.; Cooper, G.; Brion, C. E. *Chem. Phys.* **1993**, *177*, 217.

[88] Vaida, V.; McCarthy, M. I.; Engelking, P. C.; Rosmus, P.; Werner, H.-J.; Botschwina, P. *J. Chem. Phys.* **1987**, *86*, 6669.

[89] Walsh, A. D. *J. Chem. Soc.* **1953**, page 2301.

[90] Douglas, A. E. *Discuss. Faraday Soc.* **1963**, *35*, 158.

[91] Rianda, R.; Frueholz, R. P.; Goddard, W. A. *Chem. Phys.* **1977**, *19*, 131.

[92] Rosmus, P.; Botschwina, P.; Werner, H. J.; Vaida, V.; Engelking, P. C.; Mccarthy, M. I. *J. Chem. Phys.* **1987**, *86*, 6677.

[93] Kendall, R. A.; Dunning, T. H.; Harrison, R. J. *J. Chem. Phys.* **1992**, *96*, 6796.

[94] Frisch, M. J.; Trucks, G. W.; Schlegel, H. B.; Scuseria, G. E.; Robb, M. A.; Cheeseman, J. R.; Scalmani, G.; Barone, V.; Mennucci, B.; Petersson, G. A.; Nakatsuji, H.; Caricato, M.; Li, X.; Hratchian, H. P.; Izmaylov, A. F.; Bloino, J.; Zheng, G.; Sonnenberg, J. L.; Hada, M.; Ehara, M.; Toyota, K.; Fukuda, R.; Hasegawa, J.; Ishida, M.; Nakajima, T.; Honda, Y.; Kitao, O.; Nakai, H.; Vreven, T.; Montgomery, Jr., J. A.; Peralta, J. E.; Ogliaro, F.; Bearpark, M.; Heyd, J. J.; Brothers, E.; Kudin, K. N.; Staroverov, V. N.; Kobayashi, R.; Normand, J.; Raghavachari, K.; Rendell, A.; Burant, J. C.; Iyengar, S. S.; Tomasi, J.; Cossi, M.; Rega, N.; Millam, J. M.; Klene, M.; Knox, J. E.; Cross, J. B.; Bakken, V.; Adamo, C.; Jaramillo, J.; Gomperts, R.; Stratmann, R. E.; Yazyev, O.; Austin, A. J.; Cammi, R.; Pomelli, C.; Ochterski, J. W.; Martin, R. L.; Morokuma, K.; Zakrzewski, V. G.; Voth, G. A.; Salvador, P.; Dannenberg, J. J.; Dapprich, S.; Daniels, A. D.; Farkas, .; Foresman, J. B.; Ortiz, J. V.; Cioslowski, J.; Fox, D. J. *Gaussian 09;* Gaussian Inc. Wallingford CT, 2009.

[95] Mulliken, R. S. *Acc. Chem. Res.* **1976**, *9*, 7.

[96] Bursulaya, B. D.; Jeon, J.; Yang, C.-N.; Kim, H. J. *J. Phys. Chem. A* **2000**, *104*, 45.

[97] Tannenbaum, E.; Coffin, E. M.; Harrison, A. *J. Chem. Phys.* **1953**, *21*, 311.

[98] Groth, W. E.; Schurath, U.; Schindler, R. N. *J. Phys. Chem.* **1968**, *72*(11), 3914.

[99] Ashfold, M.; Bennett, C.; Dixon, R. *Chem. Phys.* **1985**, *93*, 293.

[100] Ziegler, L. D. *J. Chem. Phys.* **1985**, *82*, 664.

[101] Zhang, J. Y.; Liu, H. P.; Ying, S. H.; Jiang, B.; Xu, D. L.; Wang, L.; Lou, N. Q. *Chin. Sci. Bull.* **2002**, *47*, 1523.

[102] Collins, F. C.; Kimball, G. E. *J. Colloid Sci.* **1949**, *4*, 425.

[103] Vogelsgesang, R.; Schindewolf, U. *Ber. Bunsenges. Phys. Chem.* **1971**, *75*, 651.

[104] Buchhauser, J.; Gross, T.; Karger, N.; Ludemann, H.-D. *J. Chem. Phys.* **1999**, *110*, 3037.

[105] Schindewolf, U. *Ber. Bunsenges. Phys. Chem.* **1982**, *86*, 887.

[106] Belloni, J.; Billiau, F.; Delaire, J.; Delcourt, M.; Marignier, J. *Radiat. Phys. Chem.* **1983**, *21*, 177.

[107] Uhlig, F.; Marsalek, O.; Jungwirth, P. *J. Phys. Chem. Lett.* **2012**, *3*, 3071.

[108] Marin, T. W.; Takahashi, K.; Bartels, D. M. *J. Chem. Phys.* **2006**, *125*, 104314.

Part III

Conclusions and Outlook

Femtosecond multi-photon ionization and solvated electron geminate recombination in neat fluid ammonia was studied as a function of the thermodynamic state variables temperature and density covering the liquid and supercritical phase of the solvent. The excitation was carried out with a total energy of 9.3 eV and 6.2 eV, i.e above and below the optical valence-to-conduction band-gap of ammonia which is located around 8.2 eV[1–4] in the dense liquid. At both excitation energies strongly different temperature and density-dependencies of the recombination dynamics were observed, thereby confirming that the primary matter-field interaction produces distinctive initial spatial distributions of the geminate photolysis fragments e^-_{am}, NH_2 and NH_4^+.

At a total ionization energy of 9.3 eV the formation of the solvated electron is vertical in nature, i.e. initially quasi-free electrons are created in the conduction band of the solvent and only subsequently become solvated and thereby well-localized by the liquid network. A pronounced dependence of the ammoniated electron's survival probability on the thermodynamic state variables temperature, density, and the dielectric constant was analyzed based on a full Monte Carlo analysis of the diffusional encounters between geminate reactants. The model explicitly accounted for the two known recombination pathways of the ammoniated electron with the NH_2 radical, namely, a direct and an indirect, ion-pair mediated annihilation.[5] The latter of which is due to the transient appearance of electron-cation pairs ($e^-_{am} \cdot Na^+$), which diffusively migrate through the solution in a correlated manner.

A comparison between the experimental and simulated geminate recombination dynamics revealed a strong decrease of the ammoniated electron's average thermalization distance form 3.2 nm in the cryogenic, high density liquid to roughly 0.5 nm in the dilute supercritical fluid. This finding was attributed to an increasing threshold for vertical photo-emission into the polar, protic solvent, which results in a gradual decrease of the excess energy initially imparted on the conduction band electron. Qualitatively speaking, increasing the temperature or decreasing the density at a constant excitation energy above the band-gap has that same effect as raising the total photoionization energy at constant thermodynamic conditions.

At 6.2 eV the conduction band of the solvent is bypassed by about 2 eV,

thus the ionization mechanism is not vertical in nature, but must involve nuclear rearrangements within the local environment of the primary site of excitation. Compared to the excitation at 9.3 eV, geminate recombination is much more efficient and within less than 5 ps after the action of the UV-laser pulse, more than 90% of all initially created electrons are lost. This observation indicates that the distribution of solvated electrons around the primary site of ionization is tight, i.e. the electron is initially photo-injected into suitable trapping sites located between the first and third solvation shell of the initially ionized ammonia molecules. Because of the diffuse character of the first excited Rydberg state of ammonia in relation to the molecular packing within the local solvation structure, a proton-coupled electron-transfer (PCET) similar to that suggested for the ionization of liquid water is suggested.

A detailed analysis of the geminate recombination dynamics revealed that the below-band-gap ionization injects electrons into two distinct local configurations. One of which can be considered as instantly reactive, because the electron partially shares its solvation shell with the aminyl radical and the annihilation of the charge is not hindered by an activation barrier. In contrast, the other configuration, where electron finds itself somewhere between the second and third solvation shell, enables a diffusional escape from the NH_2 radical and should be considered as an initially non-reactive. A pronounced kinetic isotope effect suggests the involvement of protonic motion during charge annihilation consistent with a proton-coupled back-electron transfer (PCBET).

Summed up, the results presented in this thesis show that temperature and density-dependent femtosecond multiphoton ionization experiments in fluid ammonia provide new insight into the complex dependence of the ionization process on structural and electronic properties of the solvent network. Additional experimental work is highly desirable to further explore the pathways leading to the formation of the solvated electron in polar and protic fluids, including the following issues:

- At excitation energies below the optical valence-to-conduction band-gap multiple competing ionization mechanisms were suggested,[6] some of which still require experimental verification.
- It is still not finally clarified which ionization mechanism is responsible for the formation of solvated electrons in polar, protic liquids at excitation energies just below the band-gap, i.e. whether a proton-coupled

electron transfer or a hot hydrogen atom mechanism prevails?

- At excitation energies above the band-gap the identified notion of thermally induced energy level shifts of the optical band-gap[4] requires further testing.
- Are the ionization mechanisms identified in liquid water[6–9] generic for the multi-photon ionization of all polar, protonated solvents?

To resolve these questions it is highly desirable to further explore the photoionization in fluid ammonia as the analysis of geminate recombination is facilitated by the simple reaction pathways of the ammoniated electron. In particular, an experiment systematically mapping the electron's temperature and density-dependent average thermalization distance for various excitation energies, E, i.e. $\langle r_0(E,T,\rho)\rangle$, above and below the band gap, should provide valuable new insight into the electronically excited states involved in the photoemission process. Finally, it is interesting to explore the multiphoton ionization of liquid-to-supercritical aprotic solvents like amines and aminoalcohols to address in detail the role of hydrogen-bonding for the recombination dynamics of the solvated electron.

[1] Lindblad, A.; Bergersen, H.; Pokapanich, W.; Tchaplyguine, M.; Ohrwall, G.; Bjorneholm, O. *Phys. Chem. Chem. Phys.* **2009**, *11*, 1758.

[2] Bennett, G. T.; Coffman, R. B.; Thompson, J. C. *J. Chem. Phys.* **1987**, *87*, 7242.

[3] Harima, Y.; Sato, H.; Suga, K. *J. Phys. Chem.* **1989**, *93*, 6418.

[4] Urbanek, J.; Vöhringer, P. *J. Phys. Chem. B* **2013**, *117*, 8844.

[5] Belloni, J.; Cordier, P.; Delaire, J. A.; Delcourt, M. O. *J. Phys. Chem.* **1978**, *82*, 537.

[6] Sander, M. U.; Luther, K.; Troe, J. *Ber. Bunsenges. Phys. Chem.* **1993**, *97*, 953.

[7] Crowell, R. A.; Bartels, D. M. *J. Phys. Chem.* **1996**, *100*, 17940.

[8] Bartels, D. M.; Crowell, R. A. *J. Phys. Chem. A* **2000**, *104*, 3349.

[9] Elles, C. G.; Jailaubekov, A. E.; Crowell, R. A.; Bradforth, S. E. *J. Chem. Phys.* **2006**, *125*, 044515.

Completing my dissertation is so far probably the most challenging venture of my life. To continue the footsteps of generations of distinguished scientists and to unlock some of nature's remaining secrets has proven to be a highly satisfying task. Thus, my first debt of gratitude goes to my advisor, Prof. Dr. Vöhringer who provided me the opportunity to study an intriguing chemical species, that although being known for more than 200 years still provides many unresolved questions. Our numerous discussions guided and encouraged my research. I could not have imagined having a better advisor and mentor during that time. Additionally, I would like to thank the rest of my dissertation committee, Priv. Doz. Dr. Unterreiner, Prof. Dr. Bredow and Prof. Dr. Weitz.

Moreover, I would particularly like to thank Dr. Lindner for valuable suggestions regarding the time-resolved experiments and his support in mastering the alignment of our home-built laser system. A special thanks to all my colleagues in the Vöhringer work group, in particular, Annika Gehrmann and Dr. Stephan Kratz for the constructive collaboration relating to our mutual light house, the solvated electron. Additionally, I am in debt to the precision engineering workshop led by Peter Königshoven for the construction of many customized opto-mechanical components for new experiments.

I would also like to show my appreciation to Alexander Paulheim and Anna Uritzki for introducing me into the joy of exploring south-east Asia. Last but not the least, I would like to thank my parents, my brother and my sister for their continuous support throughout my life.